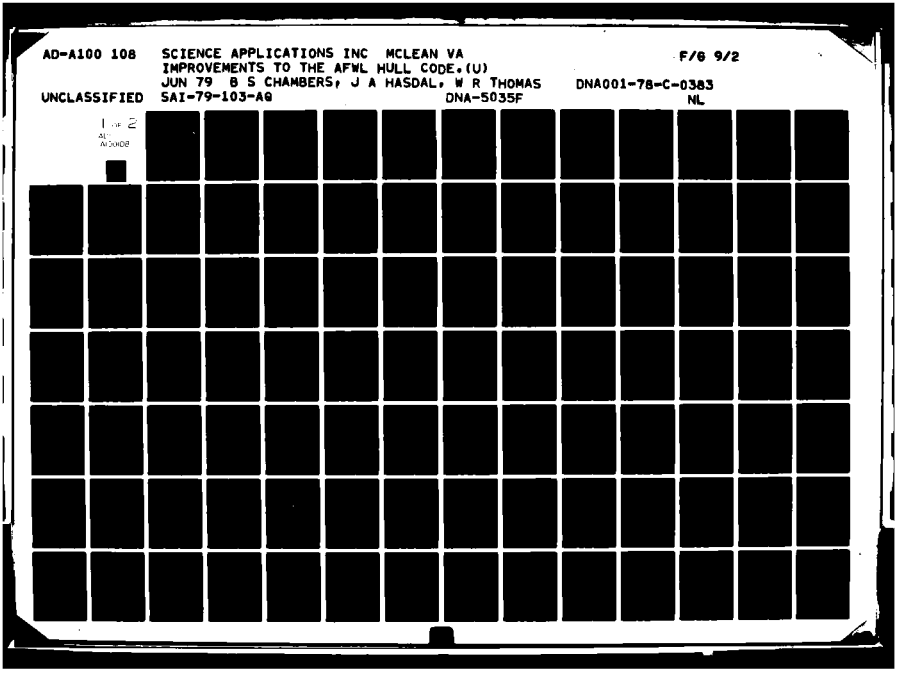
AD-A100 108
SCIENCE APPLICATIONS INC MCLEAN VA
IMPROVEMENTS TO THE AFWL HULL CODE.(U)
F/G 9/2
JUN 79 B S CHAMBERS, J A HASDAL, W R THOMAS
DNA001-78-C-0383
UNCLASSIFIED
SAI-79-103-AQ
DNA-5035F
NL

LEVEL II

12

DNA 5035F

AD A100108

IMPROVEMENTS TO THE AFWL HULL CODE

Burton S. Chambers, III
John A. Hasdal
Willard R. Thomas
Science Applications, Inc.
P.O. Box 1303
McLean, Virginia 22102

1 June 1979

Final Report for Period 21 August 1978 — 31 March 1979

CONTRACT No. DNA 001-78-C-0383

APPROVED FOR PUBLIC RELEASE;
DISTRIBUTION UNLIMITED.

THIS WORK SPONSORED BY THE DEFENSE NUCLEAR AGENCY
UNDER RDT&E RMSS CODE B342078464 N99QAXAG11110 H2590D.

DTIC FILE COPY

Prepared for
Director
DEFENSE NUCLEAR AGENCY
Washington, D. C. 20305

Destroy this report when it is no longer needed. Do not return to sender.

PLEASE NOTIFY THE DEFENSE NUCLEAR AGENCY, ATTN: STTI, WASHINGTON, D.C. 20305, IF YOUR ADDRESS IS INCORRECT, IF YOU WISH TO BE DELETED FROM THE DISTRIBUTION LIST, OR IF THE ADDRESSEE IS NO LONGER EMPLOYED BY YOUR ORGANIZATION.

UNCLASSIFIED

SECURITY CLASSIFICATION OF THIS PAGE (When Data Entered)

REPORT DOCUMENTATION PAGE	READ INSTRUCTIONS BEFORE COMPLETING FORM
1. REPORT NUMBER: DNA 5035F	2. GOVT ACCESSION NO.: AD-A100 208
	3. RECIPIENT'S CATALOG NUMBER
4. TITLE (and Subtitle): IMPROVEMENTS TO THE AFWL HULL CODE	5. TYPE OF REPORT & PERIOD COVERED: Final Report for Period 21 August 1978—31 March 1979
	6. PERFORMING ORG. REPORT NUMBER: SAI-79-103-AQ
7. AUTHOR(s): Burton S. Chambers, III; John A. Hasdal; Willard R. Thomas	8. CONTRACT OR GRANT NUMBER(s): DNA 001-78-C-0383
9. PERFORMING ORGANIZATION NAME AND ADDRESS: Science Applications, Inc., P.O. Box 1303, McLean, Virginia 22102	10. PROGRAM ELEMENT, PROJECT, TASK AREA & WORK UNIT NUMBERS: Subtask N99QAXAG111-10
11. CONTROLLING OFFICE NAME AND ADDRESS: Director, Defense Nuclear Agency, Washington, D. C. 20305	12. REPORT DATE: 1 June 1979
	13. NUMBER OF PAGES: 134
14. MONITORING AGENCY NAME & ADDRESS(if different from Controlling Office)	15. SECURITY CLASS. (of this report): UNCLASSIFIED
	15a. DECLASSIFICATION/DOWNGRADING SCHEDULE

16. DISTRIBUTION STATEMENT (of this Report)

Approved for public release, distribution unlimited.

17. DISTRIBUTION STATEMENT (of the abstract entered in Block 20, if different from Report)

18. SUPPLEMENTARY NOTES

This work sponsored by the Defense Nuclear Agency under RDT&E RMSS Code B342078464 N99QAXAG11110 H2590D.

19. KEY WORDS (Continue on reverse side if necessary and identify by block number)

HULL Code
Flux Corrected Transport
Aircraft Survivability
Air Blast
Overpressures
Peak Overpressures
Hydrodynamics
High Explosive Tests

20. ABSTRACT (Continue on reverse side if necessary and identify by block number)

Two problems were addressed during this effort: (1) numerical diffusion, which exists in HULL, significantly affects the calculations of nuclear air bursts a low overpressure, and (2) some HULL calculations being performed are of phenomena that have large regions of relatively little hydrodynamic activity in them and to efficiently perform these types of calculations, modifications to HULL were needed.

Modifications were made to the HULL code in an attempt to reduce numerical diffusion at low overpressure by employing a version of Flux Corrected

DD FORM 1 JAN 73 1473 EDITION OF 1 NOV 65 IS OBSOLETE
S/N 0102-LF-014-6601

UNCLASSIFIED

SECURITY CLASSIFICATION OF THIS PAGE (When Data Entered)

20. ABSTRACT (Continued)

Transport (FCT). A version of FCT was provided by the AFWL and this was implemented in HULL and tested for a simulation of a spherically symmetric explosion. The modifications to HULL were made in the AFWL two-dimensional version.

The low overpressure shocks were sharpened by the FCT approach for a given cell size. The improvement is not considered to be sufficient to justify the additional cost incurred as a result of the more complex numerical differencing in this particular version of FCT.

In the second area, a technique was developed for avoiding computing within certain regions of the mesh, which was also implemented in the two-dimensional version, and additional quantitative criteria were established as the basis for subsequent development of better rezone techniques.

An implementation of a computational subgrid was developed and is recommended for use in HULL to obviate the need for rezone in many problems. In addition, it was found that numerical errors in HULL associated with zone size changes are less pronounced than the effects introduced with different artificial viscosity prescriptions. Furthermore, it was observed that pulse dispersion introduced by propagation through regions of coarse zoning will lead to reductions in peak overpressure, which in regions of low overpressure will never be regained as is the case at high overpressure.

PREFACE

The research reported herein was directed towards making some improvements to the HULL code. An AFWL version of the Flux Corrected Transport (FCT) was implemented in HULL and compared with the usual HULL difference technique for an explosion of a high pressure isothermal sphere into air. In addition, algorithms for treating only a portion of the computational mesh, a computational subgrid, were developed. One dimensional HULL calculations were performed for use in the development of improved rezone techniques.

The principal investigator for this effort was Mr. Burton S. Chambers, III. Dr. John A. Hasdal implemented FCT in HULL and designed the computation subgrid technique. Dr. Willard R. Thomas supervised the one-dimensional HULL calculations. The authors especially thank Ms. Caroline Peerson-Reeves, who provided technical assistance to Drs. Hasdal and Thomas.

Mr. James Moulton was the DNA technical monitor for this effort. Capt. Leon Chandler of AFWL provided the FCT method, developed at AFWL for inclusion in HULL.

TABLE OF CONTENTS

TABLE OF CONTENTS
(continued)

LIST OF ILLUSTRATIONS

LIST OF ILLUSTRATIONS
(continued)

LIST OF ILLUSTRATIONS
(continued)

LIST OF ILLUSTRATIONS
(continued)

LIST OF ILLUSTRATIONS
(continued)

SECTION 1

INTRODUCTION

The effort reported herein was performed to complement the Defense Nuclear Agency (DNA)/Air Force Weapons Laboratory (AFWL) program addressing aircraft survivability during base escape. The AFWL was sponsored by DNA to perform fine-zoned HULL calculations in order to provide an improved representation of air blast at ground level for low overpressures (several psi) as well as air blast environments at different heights-of-target. These data are required for higher confidence assessments of aircraft survivability while aircraft (bombers and/or tankers) are escaping the effects of a hostile nuclear attack. The principal requirement for the AFWL calculations is to reduce the uncertainties in air blast at low overpressures. Although much work has been done in this area considerable uncertainty still exists. In particular, the uncertainties in range to which certain overpressures extend are making base escape assessments difficult.

SAI conducted two tasks in support of the above program. The first was to implement an AFWL version of the Flux Corrected Transport (FCT) technique developed by Boris, et al (Reference 1-3) into HULL to allow better treatment of low overpressure shocks. The second was to develop improved rezone techniques to be used in HULL. A rezone capability is used to maintain adequate resolution of shocks without requiring many zones in regions where little hydrodynamic activity is occurring.

SECTION 2

THE HULL HYDROCODE

HULL is the acronym for a computational hydrodynamics code used to solve the nonlinear hyperbolic conservation laws for an ideal inviscid fluid. It exists in many versions (references 4,5), any one of which may be invoked when a calculation is to be performed. The three-dimensional version of HULL, for example, solves finite difference representations of a closed system of partial differential equations. These equations describe nondisippative continuum fluid flow in the absence of electric and magnetic fields. The equations include the conservation law for mass, momentum, and energy, written in a Lagrangian frame, as well as the fluid equation of state, and are listed here for direct reference.

$$\frac{d\rho}{dt} + \rho\nabla\cdot\vec{u} = 0 \tag{1}$$

$$\rho\frac{d\vec{u}}{dt} + \nabla P = \vec{\rho g} \tag{2}$$

$$\rho\frac{dE}{dt} + \nabla\cdot\vec{Pu} = \vec{\rho u\cdot g} \tag{3}$$

$$P = P(\rho, I) \tag{4}$$

where ρ is material density, P is pressure, $\vec{u}$ is fluid velocity, E is total specific energy, I is internal specific energy, $\vec{g}$ is acceleration due to gravity, and t is time. Although the equations are written in a Lagrangian frame, during one phase of the hydrocode calculation, masses,

momentum, and energy are transported across a fixed calculational grid making HULL an Eulerian code. A first order donor cell technique is used; this introduces artificial increases in entropy that usually permit the calculation of strong shock waves without the introduction of a physical representation for fluid viscosity.

Although additional information on HULL are available in the references cited above, Appendix A is provided to acquaint the reader with the capability of HULL to accurately predict airblast from HE detonations. HULL has been demonstrated to be very accurate for many HE events, however considerable uncertainty still exists for the low overpressure regime. For example, in the Appendix the discussion of Figure 27 (comparisons of overpressure measurements on Dial Pack with SHELL results) points out that results from SHELL below 10 psi fall below the data. The use of HULL improved this result somewhat; however, there exists considerable room for improvement for the several psi regime. From the figures in Appendix A it is clear that there can exist differences between 40 and 80% in range to a given low overpressure.

This large uncertainty in range leads to significant differences in aircraft system survivability assessments. This effort addressed two areas where Chandler and Needham of AFWL felt improvement in HULL was desirable and would help reduce these large uncertainties. Chandler felt improvements could be gained by including FCT methods, originally developed at NRL (references 1-3), in the HULL code. He performed some work in one-dimension (reference 6) which demonstrated that FCT techniques can improve shock definition when used with the HULL difference technique. SAI implemented the AFWL FCT technique in HULL in two dimensions and then tested it.

The second task was performed because of a need for improving the rezone techniques identified by Needham. Rezone techniques, for the purposes of this effort, attempt to provide fine zoning where

shocks exist and coarse zoning where little hydrodynamic activity is occurring. The intent is to reduce the number of zones used in the calculations to an optimum value, thereby obtaining the most information for the least cost. However, if used improperly, a rezone technique may reduce the number of zones in regions that in fact have significant hydrodynamic activity.

SECTION 3

IMPLEMENTATION OF FCT IN HULL

To support implementation of a flux corrected transport (FCT) method, SAI obtained the FCT difference equations from AFWL, designed the architectural modifications to HULL, wrote the software to implement these modifications, tested the software in a simplified version of HULL, and then provided the coding to AFWL.

The small, self-contained version of HULL developed by SAI for timing studies on the CRAY-1 computer (reference 7) was chosen as the version for the initial implementation of FCT for several reasons, the more important of which are: (1) the code architecture is similar to production versions of HULL, thus the FCT code will not be unique to this version, (2) execution is significantly faster, thereby minimizing cost and turnaround; also most of the HULL system bookkeeping overhead is absent for this in-core version, (3) this version will execute on the CDC machines available at AFWL. The method of FCT implementation employed is presented following a short discussion of the computational phases concept used in HULL.

3.1 HULL PHASES

The fundamental variables computed and stored in HULL two-dimensional airblast calculations are pressure, two components of velocity, internal energy, and mass of each cell of the mesh of cells which represent the physical conditions simulated by a calculation. In many calculations, the total of the mesh variables exceeds central memory allocations of most machines for which HULL is implemented, e.g., a 100 by 200 cell single material mesh requires 100,000 storage

locations just for the mesh variables. Therefore, mesh variables must generally be placed in auxiliary storage, currently on-line disk or extended core. The mesh variables are stored in these media in an array which corresponds to a geometric image of the physical conditions. In two dimensional calculations, cell indexes (I,J) correspond to geometric coordinates (X,Y). A row of a two dimensional mesh is that set of variables for which J = constant (Y = constant) and $1 \leq I \leq IMAX$ ($XMIN \leq X \leq XMAX$). In this storage mode, contiguous rows of the mesh are sequentially accessible.

The computational phases in HULL are distinct, independent numerical operations. A complete set of these phases operating in sequence will advance the mesh from time t to time t + dt. This is called a *time step*. Repetitive operation of this set upon the mesh produces the time evolution of the hydrodynamic variables (mesh) in a calculation. The computational phases are independent in the sense that no intermediate communication occurs between the phases other than by means of the mesh variables.

Combining these storage and phasing methods, a successful code structure would be that of operating upon the entire mesh in turn with each phase. This structure requires complete input/output processing of the mesh for each phase, unless the mesh can be contained in central memory. The actual numerical computations used in the HULL differencing require at most two rows for a phase plus space for temporary storage which is internal to the phase. Figure 1 illustrates the phase set operation structure used in HULL which, in contrast to the above mentioned structure, requires one input/output processing of the mesh per time step. The description of the phases indicated in Figure 1 is:

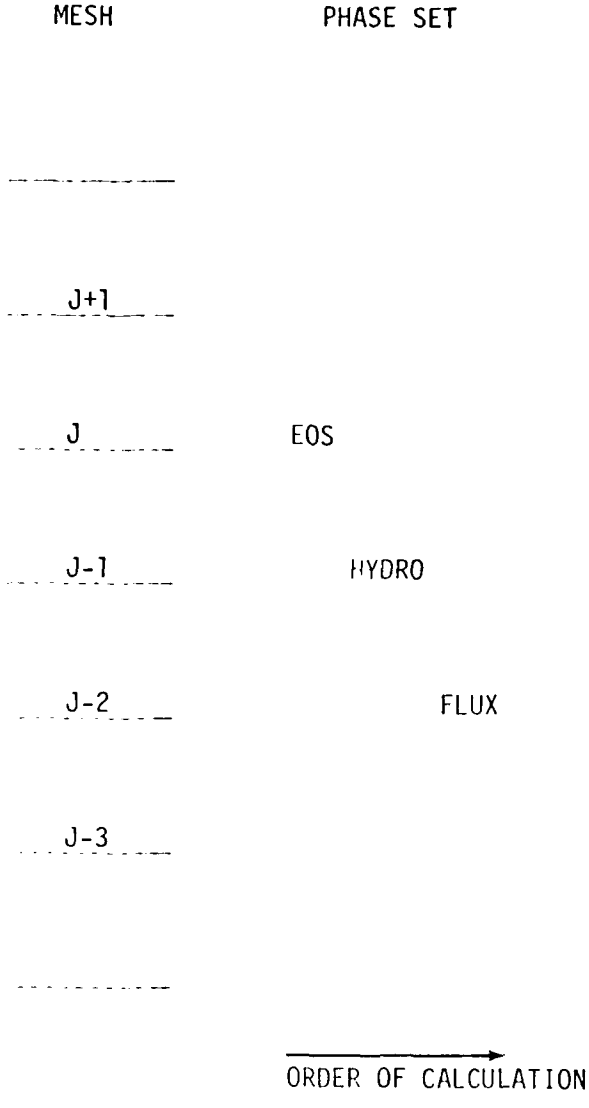

Figure 1. HULL phases and phase operation sequence.

- EOS - Equation of State, updates cell pressure to time t value.

- HYDRO - Lagrangian phase, computes intermediate internal energy and velocity component values on a Lagrangian mesh at time t + dt.

- FLUX - Transport phase, fluxes mass and internal energy between cells to obtain final mesh variable values at time t + dt.

The separate phases are provided a pointer index indicating the row to be processed by each. The phases are executed in the order - EOS, HYDRO, FLUX - which has the effect that each phase in effect requires one row of the mesh in core; i.e., that row updated by that phase. In particular, in terms of Figure 1, after the EOS operation upon row J, the HYDRO phase can update row J-1 variables using mesh values at time t from rows J and J-1. Upon completion of HYDRO, FLUX can produce the time t + dt value of the variables in row J-2 using the intermediate mesh values from rows J-1 and J-2. Rows J+1 to JMAX, and rows 1 to J-3 are not involved in this phase set operation and need not be in central memory. Prior to the next phase set operation the pointer indexes are advanced one row, row J-2 now at time t + dt is output, and row J + 1 at time t is input. After each row has been operated upon by each phase, the entire mesh has been advanced to time t + dt.

It is evident that this structure is independent of the particular storage used for those rows of the mesh not currently designated by the phase row pointer indexes. It is compatible with central memory, extended core, or disk storage of the mesh.

3.2 FLUX CORRECTED TRANSPORT PHASING

The Flux Corrected Transport (FCT) algorithm as it is currently configured by AFWL, can be separated into two independent numerical operations, termed diffusion (DIFF) and anti-diffusion (ADIFF). Further, these operations can be designated as operational phases, which are quite similar in structure to the HULL phases. This approach is the one which has been taken for implementation of FCT in HULL, in which the advantages of the HULL phasing structure are apparent in minimization of storage requirements.

The FCT algorithm operates upon the mesh variables in conserved quantity form; i.e., mass, individual momentum components, and total energy. The available algorithm is constructed for two spatial dimension calculations, which is the only form implemented during this effort. There are then, four conserved quantities per cell to consider.

The FCT phases are independent of each other in the sense that the HULL phases of Figure 1 are independent. However, the FCT phases are not independent of the HULL phases in this sense. They are not independent, because each one requires information other than that contained in the mesh variables. The effects of non-independence are minimized, in terms of required extra variable storage, by sequencing the combined HULL and FCT phase set as is illustrated in Figure 2. When ADIFF is completed upon row J-5, this row can be output; it is not needed for the ADIFF operation upon row J-4 to be done in the next operation of the phase set. Therefore, FCT when included in HULL requires six rows of mesh in central memory. The extra storage requirements arising from the non-independence are defined in the following discussion of the FCT phases.

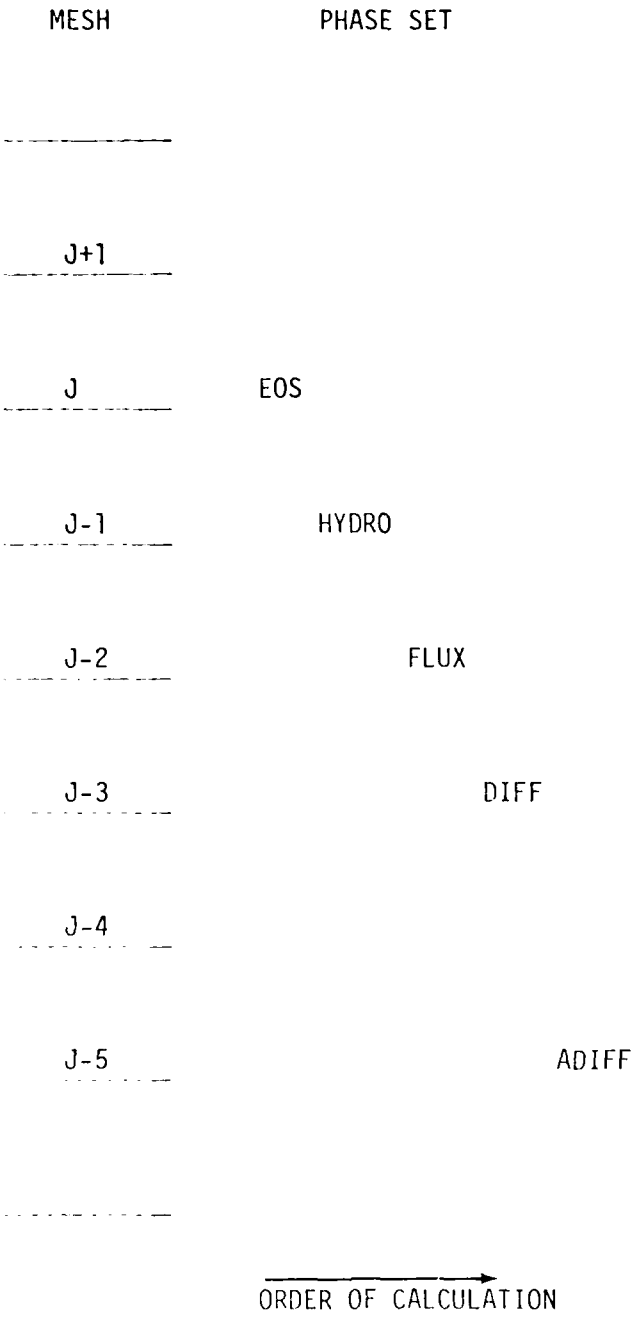

Figure 2. HULL and FCT phases, and phase operation sequence.

3.3 FCT DIFFUSION PHASE - DATA STORAGE REQUIREMENTS

The diffusion of the conserved quantity variables of a cell requires the following:

- The conserved quantities of the subject cell and those of its four adjacent cells at time t,
- The volumes of these five cells,
- The boundary velocities on the four boundaries of the subject cell,
- The conserved quantities of the subject cell at time t + dt.

Figure 3 illustrates the geometric arrangement of the cells of the mesh involved, when the center cell (C) is undergoing diffusion. In terms of Figure 2, cell C in Figure 3 is in row J-3 and cells A and B are in rows J-2 and J-4 respectively. The HYDRO phase indicated in Figure 2 will alter the mesh variables of row J-1 from their values at time T. Therefore, it is apparent that separate storage of four rows of the mesh in conserved quantity form is required containing the values of rows J-1 through J-4 at time T. This will satisfy the first data requirement listed above. It is to be noted that the EOS phase affects only the pressure variables in the mesh, which are not used in FCT; and row J is not required in separate storage.

The volume of each cell can be computed from the cell geometry arrays DX(I), DY(J), and TAU(I).

TAU(I) contains the area between the concentric circles bounding each cell in cylindrical geometry, of which the mesh is a vertical cross-section of a right cylinder. These arrays are extant in HULL and additional storage is not required. The second data requirement is then satisfied.

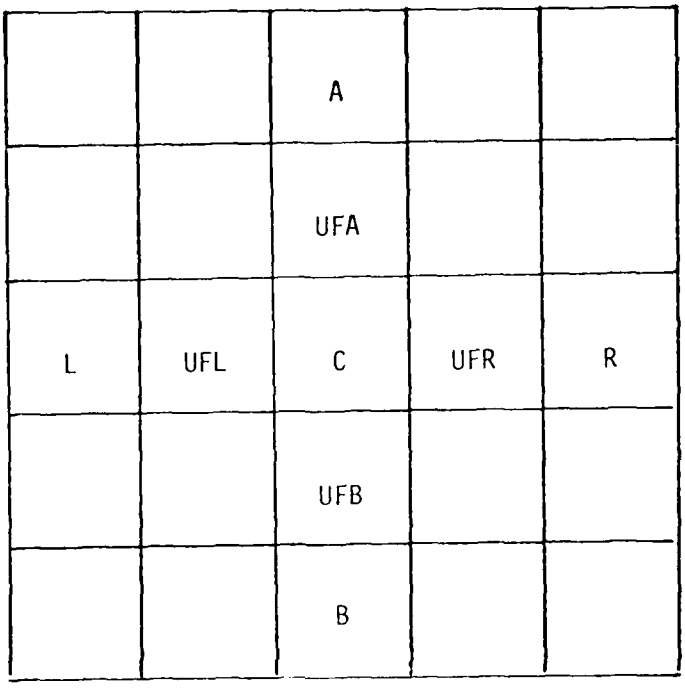

VOLUME OR CONSERVED QUANTITY OF CELL - C - CENTER (I,J), A - ABOVE, B - BELOW, L - LEFT, R - RIGHT

BOUNDARY VELOCITY FUNCTION - UF*

Figure 3. DIFF phase mesh and velocity configuration.

The third data requirement - boundary velocities - will require separate storage. These velocities are computed as temporary variables internal to the FLUX phase. The velocities are extracted as each is computed in FLUX, and placed in storage by rows. These same velocities are used in the anti-diffusion phase of FCT and the total storage requirements are established in the discussion of ADIFF.

The center cell conserved quantity variables at time t + dt can be computed directly from the mesh. After the FLUX phase, the mesh variables (mass, velocity components, and internal energy) are the time t + dt values. Therefore, no additional storage is necessary for the fourth data requirement of the DIFF phase.

The diffused row of the mesh produced by DIFF can be stored in the four corresponding variables, cell by cell in row J-3 of the mesh. However, this would result in the situation wherein the ADIFF phase must access its input variables from two different storage structures - an awkward situation at best. Thus the DIFF phase results are placed in a temporary storage array, which contains the five rows of diffused conserved quantity variables required in ADIFF.

3.4 FCT DIFFUSION PHASE - ALGORITHM

Figure 4 contains the form of the velocity function used in the diffusion phase. The functions in this exhibit are in terms of the representative storage array of Figure 3, in which the velocity function values are assigned indexable locations between their related cells. The form of the boundary velocities (i.e., E in Figure 4) is the same in DIFF and ADIFF; therefore, each velocity is converted to the variable form E as it is extracted to storage from the FLUX phase.

In terms of Figure 3, if C ≡ (I,J) and
L ≡ (I-2,J), etc.

UFL = UF(I-1,J) UFR = UF(I+1,J)

UFB = UF(I,J-1) UFA = UF(I,J+1)

where

$$UF(i,j) = (1/6)-(1/2)E(i,j) + (1/3)(E(i,j))^2$$

$$E(i,j) = | DT \cdot VELOCITY\ (i,j)/DR(i,j) |$$

DT = (T+dT)-T (TIME STEP ADVANCE)

DR = AVERAGE DISTANCE BETWEEN CELL CENTERS

VELOCITY = BOUNDARY VELOCITY FROM FLUX PHASE

THUS:

$$E(I-1,J) = \left| \frac{2 \cdot DT \cdot VELOCITY\ ((I-2,J) \rightarrow (I,J))}{DX(I-2,J) + DX(I,J)} \right|$$

$$E(I+1,J) = \frac{|2 \cdot DT \cdot VELOCITY\ ((I,J) \rightarrow (I+2,J))|}{DX(I,J) + DX(I+2,J)}$$

$$E(I,J-1) = \frac{|2 \cdot DT \cdot VELOCITY\ ((I,J-2) \rightarrow (I,J))|}{DY(I,J-2) + DY(I,J)}$$

$$E(I,J+1) = \frac{|2 \cdot DT \cdot VELOCITY\ ((I,J) \rightarrow (I,J+2))|}{DY(I,J) + DY(I,J+2)}$$

Figure 4. DIFF phase velocity function.

Figure 5 contains the computational form of the diffusion phase of the FCT algorithm. The quantity DQC of the figure (diffused conserved quantity) is obtained for each conserved quantity of every cell in the row upon which DIFF is operating, row J-3 of Figure 2.

The boundary conditions for diffusion are relatively straightforward. The guiding principle in establishing the computational rules at the boundaries is that the diffusion flux of the conserved quantity is zero across the mesh boundaries, and is zero at the limits of the (I,J) index range which is being processed by FCT. The particular computational method chosen is to set the appropriate velocity function equal to zero. A zero velocity does not yield this result, as is apparent from the form of UF (i,j) in Figure 4.

3.5 FCT ANTI-DIFFUSION PHASE DATA STORAGE REQUIREMENTS

The anti-diffusion of the diffused quantity variables of a cell requires the following:

- The diffused conserved quantities of the subject cell and those of the twelve third-nearest neighbor cells,
- The volumes of these thirteen cells,
- The boundary velocities of the sixteen common cell boundaries of the thirteen cells.

Figure 6 illustrates the geometric arrangement of the above quantities, when the center cell (C) is undergoing anti-diffusion. In terms of Figure 2, cell C in Figure 6 is in row J-5 and cells AA and BB are in rows J-3 and J-7 respectively. Recall that rows J-3 through J-7 are rows of diffused conserved quantities which are in a storage area separate from the mesh, thus ADIFF has already processed mesh rows J-6 and J-7 which are not required by ADIFF and need not be in central memory. The five rows of diffused conserved quantity variables satisfy the first data requirement listed above.

In terms of Figure 3, if C ≡ (I,J) and

L ≡ (I-2,J), etc.

DQC = QC + (GFR-GFL) + (GFA-GFB)

where

DQC - DIFFUSED CONSERVED QUANTITY OF CELL (I,J)

QC - CONSERVED QUANTITY OF CELL (I,J) AT TIME T+DT

GF* - DIFFUSION FLUX OF QC ACROSS CELL (I,J) BOUNDARIES, WHERE * IS L, R, A, B.

and

GF* = GF (UF*, QC, Q*)

GFL = (VOLUME (I-2, J) + VOLUME (I,J))(1/2)·UFL·(RC-RL)

GFR = (VOLUME (I,J) + VOLUME (I+2,J))(1/2)·UFR·(RR-RC)

GFA = (VOLUME (I,J+2) + VOLUME (I,J)) (1/2)·UFA·(RA-RC)

GFB = (VOLUME (I,J-2) + VOLUME (I,J)) (1/2)·UFB·(RC-RB)

where

UF* - ARE AS SPECIFIED IN FIGURE 4

R* - CONSERVED QUANTITY DENSITY - Q*/VOLUME(*) WHERE * IS C,A,B,L,R; AND Q* IS THE CONSERVED QUANTITY AT TIME T.

Figure 5. DIFF phase - conserved quantity diffusion computation.

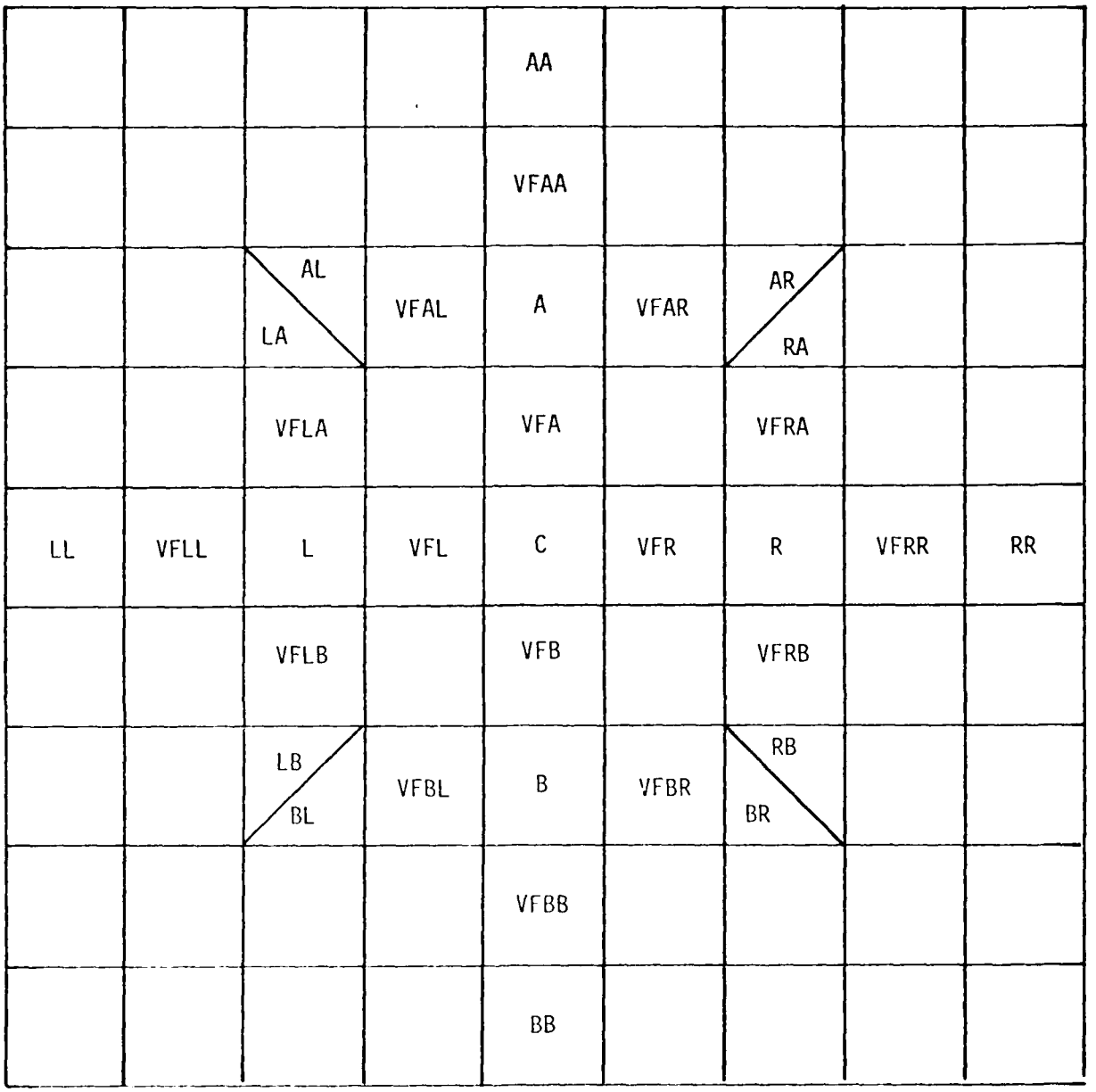

REFER TO FIGURE 3 FOR NOTATION CONVENTION: NOTING THAT LL - LEFT LEFT.

VF**IS THE BOUNDARY VELOCITY FUNCTION, * is L,A,R,B.

Figure 6. ADIFF phase mesh and velocity configuration.

The boundary velocity array storage convention is that the velocities found with index set (I,J) for example for cell B, are in the relation to B as are VFBL and VFBB of Figure 6. Therefore, the number of rows of boundary velocities required in storage is six, because the Y-direction velocities obtained from FLUX operating upon row J-2 of Figure 2 are associated with the below boundary of row J-1. There are two boundary velocities per cell, so that the six rows of storage are equivalent to three rows of conserved quantity storage. The cell volumes, as in DIFF, can be computed from the existing cell geometry arrays and require no additional storage.

The resultant conserved quantities of FCT produced at the end of ADIFF, on a cell by cell basis are converted to the standard representations of the hydrodynamic variables and replace the time t + dt values of mass, velocity components, and internal energy in row J-5. Thus, no additional storage is required to hold the fully corrected conserved quantities. Also, if the calculation is multi-material, the individual material masses can be updated by ADIFF to sum to the new corrected mass of each cell.

3.6 FCT ANTI-DIFFUSION - ALGORITHM

Figure 7 contains the form of the velocity function used in the anti-diffusion phase. The functions in this exhibit are in terms of the storage array of Figure 6, in which the velocity functions are assigned locations capable of being indexed. The storage array of Figure 6 was incorporated into the coding of the ADIFF phase subroutine. As will be seen from the description of the corrector functions, this type of array is accessible by each part of the corrector functions directly under indexing control.

In terms of Figure 6, if C ≡ (I,J) and

LL ≡ (I-4,J), etc.

VFL = VF(I-1,J) VFRR = VF(I+3,J)

VFA - VF(I,J+1) VFBL = VF(I-1,J-2)...

where

$$VF(i,j) = (1/6)(1-(E(i,j))^2)$$

$$E(i,j) = |DT \cdot VELOCITY(i,j)/DR(i,j)|, \text{ c.f. Figure 4.}$$

Thus:

$$E(I-1,J-2) = \frac{|2 \cdot DT \cdot VELOCITY\ ((I-2,J-2) \rightarrow (I,J-2))|}{DX(I-2,J-2) + DX(I,J-2)}$$

$$E(I+2,J+1) = \frac{|2 \cdot DT \cdot VELOCITY\ ((I+2,J) \rightarrow (I+2,J+2))|}{DY(I+2,J) + DY(I+2,J+2)}$$

The remaining fourteen values of E are constructed in a similar manner.

Figure 7. ADIFF phase velocity function.

Figure 8 contains the computational form of the anti-diffusion phase of the FCT algorithm. The quantity FQC (flux corrected conserved quantity) is obtained for each conserved quantity of every cell in the row upon which ADIFF is operating, row J-5 of Figure 2. The formalism of DIFF and ADIFF is quite similar with the exception of operation of the corrector function (K of Figure 8) upon the diffused conserved quantity fluxes before a corrected conserved quantity is computed. The corrector function is presented in the following discussion.

The corrector function is a function of the value and of the sign of the flux upon which it is operating. This dependence separates the functional form into three routines which are presented in the order of operation employed in the coding. Figure 9 contains the computational form of the part of the corrector function termed Test 1. This test employs the values of the conserved quantities of cells (I-4,J) to (I+4,J) and (I,J-4) to (I,J+4) in terms of Figure 6, or the in-line third and first nearest neighbor cells. This test of itself requires that five rows of diffused conserved quantities be available to ADIFF. Step 1 of Test 1 is self-evident from the form of the GF* function of Figure 8 and Figure 5 ; it is the result of the fact that the adjacent cells have identical values of the conserved quantity being corrected. Parts 2 and 3 of Test 1 occur in pairs and involve two cells to each side of the cell boundary under consideration. From Figure 9, Test 11 on the above boundary includes this flux (GFA) and cells AA and A, Test 12 includes GFA and cells B and C. If one of the Test 1 conditions is true for a boundary, the corrector function provides a zero value of the corrected diffused conserved quantity flux for that boundary. If the result of Test 1 is false, the form of the corrector function is determined by the sign of the boundary flux function.

In terms of Figure 6, if C ≡ (I,J), and
LL ≡ (I-4,J), etc.

FQC = DQC -(HFR-HFL)-(HFA-HFB)

where

FQC - FLUX CORRECTED CONSERVED QUANTITY OF CELL (I,J)

DQC - DIFFUSED CONSERVED QUANTITY OF CELL (I,J)

HF* - CORRECTED ANTI-DIFFUSED FLUX OF CONSERVED QUANTITY ACROSS CELL (I,J) BOUNDARIES, WHERE * IS L,R,A,B

and

HF* = K*(GF*)

GF* = GF(VF*,DQC,DQ*)

GFL = (VOLUME (I-2,J) + VOLUME (I,J))(1/2)·VFL·(DRC-DRL)

GFR = (VOLUME (I,J) + VOLUME (I+2,J))(1/2)·VFR·(DRR-DRC)

GFA = (VOLUME (I,J+2) + VOLUME (I,J))(1/2)·VFA·(DRA-DRC)

GFB = (VOLUME (I,J) + VOLUME (I,J-2))(1/2)·VFB·(DRC-DRB)

where

VF* - ARE AS SPECIFIED IN FIGURE 7.

K* - CORRECTOR FUNCTIONS

DR* - DIFFUSED CONSERVED QUANTITY DENSITY

Figure 8. ADIFF phase - corrected anti-diffused conserved quantity flux computation.

In terms of Figure 6, if C ≡ (I,J) and
LL ≡ (I-4,J), etc.

THE VALUE OF HF* IS ZERO IF ANY OF THE FOLLOWING IS TRUE.

1. GF* = 0.0, * = A,B,L,R => HF* = 0.0

2. TEST 11

|GFA·(DRAA-DRA)| < 0.0 => HFA = 0.0

|GFB·(DRA-DRC)| < 0.0 => HFB = 0.0

|GFL·(DRR-DRC)| < 0.0 => HFL = 0.0

|GFR·(DRRR-DRR)| < 0.0 => HFR = 0.0

3. TEST 12

|GFA·(DRC-DRB)| < 0.0 => HFA = 0.0

|GFB·(DRB-DRBB)| < 0.0 => HFB = 0.0

|GFL·(DRL-DRLL)| < 0.0 => HFL = 0.0

|GFR·(DRC-DRL)| < 0.0 => HFR = 0.0

where GF* - DIFFUSED CONSERVED QUANTITY FLUX

DR** - DIFFUSED CONSERVED QUANTITY DENSITY

Figure 9. ADIFF phase part 1 of the corrector function - K.

Figure 10 contains the form of the corrector function if GF* > 0.0, and Figure 11 the form for GF* < 0.0. Use of the asterisk character, *, is a shorthand notation for the appropriate index of the cell designated when the C,L,R,A,B letters are substituted for the asterisk. Use of a double asterisk, **, implies that the second character substituted indicates the direction relative to the first character, in which the appropriate variable is to be found. If ** is set to LL this implies left of a position to the left of center, and if ** is set to LR, it implies a position right of a position to the left of center which results in the center position. From this, the W and P functions can be readily interpreted in terms of their independent variables; i.e., WP* operates upon the four diffused conserved quantity densities adjacent to the cell *. In terms of Figure 6, WPL = WP (DRLA,DRLB,DRLL,DRC). The GF* and HF*, fluxes are the indexable boundary flux positions and correspond to the VF** positions in the array of Figure 6.

Figure 12 contains the functional forms for the functions of Figures 10 and 11 which are as yet undefined. A presentation of the invariant properties of the various parts of the corrector function will introduce some order into what is a rather large collection of variables and functions. First it must be noted that the basic three kinds of independent variable are:

- The cell diffused conserved quantity densities (DR**)
- The cell volumes (Volume**)
- The cell boundary diffused flux functions (GF**).

All other quantities are composed of a set of these variables. Each corrector function (Test 1 is not included in the subsequent discussion), is a function of the center cell, the four adjacent cells, and the four central velocity functions, i.e., C,A,B,L,R,GFA,GFB,GFL,GFR. It is then

In terms of Figure 6, if C ≡ (I,J) and
LL ≡ (I-4,J), etc.

HF* = MAX (0.0, MIN (GF*, PPLUS*, PMINUS*))

where

HF* - CORRECTED DIFFUSED CONSERVED QUANTITY FLUX

GF* - DIFFUSED CONSERVED QUANTITY FLUX

PPLUS* = PPLUS (GF*, VOLUME*, DR*, WP*, PP*)

PMINUS* = PMINUS (GF*, VOLUMEC, DRC, WMC, PMC)

and

VOLUME* - VOLUME OF CELL, * IS L,R,A,B

DR* - DIFFUSED CONSERVED QUANTITY DENSITY

WP* = WP (DR*A, DR*B, DR*L, DR*R)

WM* = WM (DR*A, DR*B, DR*L, DR*R)

PP* = PP (GF*A, GF*B, GF*L, GF*R)

PM* = PM (GF*A, GF*B, GF*L, GF*R)

WHERE * IS C,L,R,A,B, c.f. FIGURE 12

(NOTE THAT C* = * ic CA = A, and AB = C)

Figure 10. ADIFF phase corrector function for GF* > 0.0

In terms of Figure 6, if C ≡ (I,J) and
LL ≡ (I-4,J), etc.

HF* = (S*) MAX (0.0, MIN (|GF*|, MPLUS*, MMINUS*))

where

HF* - CORRECTED DIFFUSED CONSERVED QUANTITY FLUX

GF* - DIFFUSED CONSERVED QUANTITY FLUX

MPLUS* = MPLUS (GF*, VOLUMEC, DRC, WP*, PP*)

MMINUS* = MMINUS (GF*, VOLUME*, DR*, WM*, PM*)

S* = S(DR*, DRC), AND IS POSITION DEPENDENT

AND THE REMAINING FUNCTIONS AND VARIABLES ARE AS DEFINED IN FIGURE 10; i.e.,

VOLUME*, DR*, WP*, WM*, PP*, PM*

WHERE * IS C,L,R,A,B

Figure 11. ADIFF phase corrector function for GF* < 0.0

In terms of Figure 6, if C ≡ (I,J) and
LL ≡ (I-4,J), etc.

$$WP^* = MAX\ (DR^*A,\ DR^*B,\ DR^*L,\ DR^*R)$$

$$WM^* = MIN\ (DR^*A,\ DR^*B,\ DR^*L,\ DR^*R)$$

$$PP^* = MAX\ (0.0,\ GF^*L) - MIN\ (0.0,\ GF^*R) + MAX\ (0.0,\ GF^*B) - MIN\ (0.0,\ GF^*A)$$

$$PM^* = MAX\ (0.0,\ GF^*R) - MIN\ (0.0,\ GF^*L) + MAX\ (0.0,\ GF^*A) - MIN\ (0.0,\ GF^*B)$$

$$\left.\begin{aligned} SA &= SIGN\ (1.,\ (DRA-DRC)) \\ SB &= SIGN\ (1.,\ (DRC-DRB)) \\ SL &= SIGN\ (1.,\ (DRC-DRL)) \\ SR &= SIGN\ (1.,\ (DRR-DRC)) \end{aligned}\right\} = \pm\ 1.$$

$$PPLUS^* = (GF^*)\cdot(VOLUME^*)\cdot(WP^*-DR^*)/PP^*$$

$$MPLUS^* = (GF^*)\cdot(VOLUMEC)\cdot(DRC-WPC)/PPC$$

$$PMINUS^* = (GF^*)\cdot(VOLUMEC)\cdot(DRC-WMC)/PMC$$

$$MMINUS^* = (GF^*)\cdot(VOLUME^*)\cdot(WM^*-DR^*)/PM^*$$

Figure 12. ADIFF phase functions used for corrector function.

additionally only a function of the three independent variables in the direction of the flux it is correcting. That is the corrector for GFR includes the central quantities and the quantities RA, RB, RR, GFRA, GFRB, GFRR. The exceptions are the cell quantities (I$\pm$2, J$\pm$2), each of which is involved in two flux corrections; the diffused conserved quantity DRAR is the same quantity as DRRA. The double notation convention which produces this seeming irregularity, is helpful when the effects of the mesh boundaries is considered. It is seen that the central cell must be at least two cells distant from any boundary to apply the corrector without regard to boundary conditions. This implies that for a considerable number of cells, the mesh boundary effect must be included in ADIFF computations: specifically any cell with a mesh index of i = 1,2,IQ-1, IQ, or J = 1,2,JQ-1,JQ, where IQ and JQ are the index limits within which FCT is applied.

One more property of the various corrector function is to be noted. This is that the directional sense of each function is independent of the direction of the cell (from the central cell) upon which its operation is centered. Any difference relation has the same direction, e.g., (right-most)-(left-most) and (above-most)-(below-most) for PM*, regardless of the reference cell denoted by the *. Another interpretation of this property is that the functions can be translated along an index direction; they do not rotate their sense of operation about the central cell. Unfortunately, the mesh boundaries impress a reflective effect upon the operation of ADIFF when the center cell is in the boundary rows and/or columns of the mesh.

3.7 FCT ANTI-DIFFUSION - BOUNDARY CONDITIONS

The guiding principles for treatment of ADIFF when the subject cell is proximate to a mesh boundary are:

- The flux of diffused conserved quantities is zero across a mesh boundary
- The cells which are outside the mesh, in the structure of Figure 6, shall have no effect upon the correction of cell boundaries which are not mesh boundaries.

The functions of Figures 10, 11, and 12 do not explicitly represent boundary condition forms except by imposition of the two principles listed above.

The form of the functions implies that by assignment of special, chosen values to the virtual cell and cell boundary quantities; then the functions may operate correctly when a mixture of virtual and existing cells and cell boundaries is to be referenced. This is almost the case; however, Test 1 requires a value of the virtual cells which conflicts with the value required by the GF* greater than 0.0 and less than 0.0 forms of the corrector function, nonetheless this method was incorporated in the implementation with functions of the indexes used in the coding which remove these conflicts.

For Test 1 parts 2 and 3, of Figure 9, coefficient functions for Test 11 and Test 12 were developed which multiply the relations by a value of +1.0 if both cells of the relation are mesh cells, and multiply +0.0 if one (or both) of the cells is virtual, i.e., outside the mesh. This method removes the conflict regarding specified values for virtual cells. For example, application of Test 12 is invalid for cell R when the left boundary of cell C is a mesh boundary, c.f. Figure 6; cell L is virtual, and can contain a specified value compatible with the corrector functions of Figures 10, 11 and 12.

There are sixteen possible boundary flux functions (GF**). The first boundary principle requires that the GF** functions be zero when a mesh boundary is represented. Again a conflict is encountered in the specified value of a virtual cell. To insure that a zero value of GFL occurs when cell L is virtual, the conserved quantity value of cells L and C must be identical. This specification is not compatible with the corrector function operation on GFR, which requires cell L to be identical to cell R. To relieve this conflict, the index range of the routine which can compute all sixteen GF** values is restricted to the computation of GF** values which are not virtual nor mesh boundary fluxes. This index range restriction is a function of the index values relating to cell C.

The above two procedures allow specification of all values of virtual cells and virtual and mesh cell boundary flux values, so that the more complex forms of the corrector function may operate in the given functional forms regardless of the location of cell C in the mesh. When one of the boundaries of cell C is a mesh boundary, specification of the GF* flux of that boundary as zero, will cause Test 1 - Step 1 (Figure 9) to be true and the correction of that flux is complete. This allows specification of the virtual diagonal cells in this direction from cell C, to those values which are appropriate to correctors of the adjacent cell C boundaries. To illustrate, if the indexes of cell C are (I = 1; J = 4, <JQ-1), then setting GFL = 0.0 determines that HFL = 0. Note that cells AL and BL are not used in this determination. If cell AL is set equal to cell AR, cell BL is set equal to cell BR, and GFAL = GFBL = 0.0; then the corrector for fluxes GFA and GFB can operate with the virtual cells AL and BL, and the zero mesh boundary fluxes GFAL and GFBL. Inspection of WP, WM, PP, and PM functions will show that these specifications result in no effect from the virtual cell. Note that when cell C indexes are (I = 4, <IQ-1; J = 1) that cell BL is appropriately termed cell LB and is set equal to

cell LA, to not contribue to correction of GFL. When the cell C indexes are (I = 2, IQ-1; J = 2, JQ-1) then the extreme cells are virtual and must be set equal to cell C, to insure no effect, and the extreme boundary flux GF** is a mesh boundary and is set to zero. It can also be shown that the diagonal cells will not conflict in their required specified values in the mesh corners; the diagonal cell is used in only one direction of flux correction, in these cases.

3.8 FCT ALGORITHM IN HULL

The foregoing discussion contains concepts and methods developed in the process of FCT implementation; some items became apparent in retrospect. Thus, not all of the items are reflected in the coding. Several storage structures and data movement procedures though quite inefficient, have been included to allow flexibility in the code. This facilitates debugging, and inclusion of other than major changes in the form of the algorithm, which may be changed for improved results or simplifications which are warranted. The FCT code as it is currently constituted is debugged and operational, and its absolute effectiveness can begin to be evaluated. The execution time overhead cannot be evaluated with this form owing to the inefficiencies which exist.

Evaluation of the absolute effectiveness is only one consideration for inclusion of this form of FCT. If FCT in a fully efficient form were to provide numerical results comparable to a HULL run with smaller cell size of the same cost; the conclusion would be against inclusion of additional code which did not provide any improvement at reasonable cost. Thus, FCT if it proves to be effective must also prove to be cost effective.

To improve the efficiency of the coding of the algorithm requires the elimination of extra data movement. This is readily done in the present form. Such a process also results in the addition of more index directed code, to which the current form of the code is amenable as was designed. The negative aspect of this type of coding is that the indexing is several levels deep and becomes quite obscure. Note that the accessing implied in Figure 6 is two-dimensional, for example to use the same line of code to compute the velocity functions, the indexes (I,J) must be biased as (I+IB, J+JB) where IB and JB are unequal and have values $\pm$ 1 or 0.

The version of HULL used in this implementation is managed with the CDC-UPDATE system, and therefore the evaluation and coding efficiency efforts may proceed independently of each other.

SECTION 4

SUMMARY OF RESULTS OF FCT IN HULL

This section presents a summary of results for a set of two-dimensional HULL calculations performed to demonstrate that the chosen FCT technique had been implemented in such a fashion so as not to affect the operational integrity of HULL. These calculations also provide a test case to compare with if AFWL chooses to implement the FCT technique in the AFWL version of HULL. Furthermore, the existence of the calculations allows a comparison between HULL with and without FCT to be made.

The test calculation chosen was a hypothetical hot sphere of 2 meters initial radius. The density of the sphere was the same as the cold air outside, or 1.225 milligrams per cubic centimeter. The sphere was initially at rest and at an elevated specific internal energy, which was 2×10^{10} ergs/gm. Therefore, the initial pressure within the hot sphere was about 1 MPa. The surrounding cold air was slightly above 2×10^{9} ergs/gm. These initial conditions produced a shock that was about 0.4 MPa (i.e., about 60 psi) at 4 milliseconds after "detonation." Figure 13 summarizes the initial conditions, and Appendix B presents various snapshots of the pressure and density profiles for various times. Because of the spherical symmetry of the chosen case, it is expected that the results for any given technique will be essentially the same along any radial line. Any sizable error in the difference technique in one direction should show up as an asymmetry. Although agreement would not prove that the coding has been validated, i.e., it is not sufficient, it is necessary.

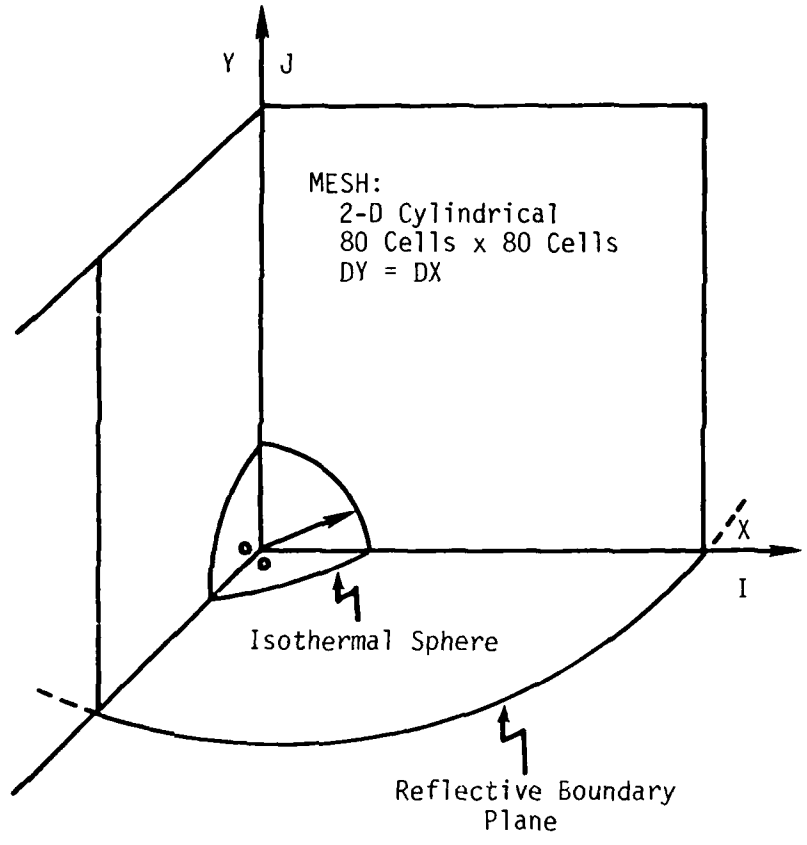

Figure 13. Cylindrical mesh geometry, initial state, time = 3.355×10^{-3} sec.

The results show excellent agreement along the x and y (radial and altitude respectively) directions as can be seen by a purusal of Appendix B. An example of a representative case is shown in Figure 14 showing the results along the y-direction in the first column of cells. The results along the x-direction in the first row are essentially the same. The results differ along the line where I=J, i.e., along the radial which is 45 degrees in elevation. However, these differences are small and the largest difference is seen to be at the peak. The large dot, labeled - see text, is the peak along the line where I=J. In order to compare the I=J radial with other radials, the index I has been multiplied by the square root of 2 so that the cell indices are proportional to the length along the radial. (Each calculation used constant zoning, therefore, the ratio of length to cell number is a constant.)

The primary conclusions of the comparison of the HULL results with the HULL/FCT results are: (1) the implementation did not degrade the operational status of HULL, (2) the implementation was accomplished with no sizable errors in any one direction (agreement with the HULL without FCT implies correctness as well), and (3) the two-dimensional results with FCT are similar to the AFWL 1-D results, where the FCT technique seemed to improve spatial resolution of shock fronts about a factor of two.

Although only a few results are shown in this report for the smaller zone size calculation performed with HULL (i.e., problem number 1.0005, $\Delta x = \Delta y = 5$ cm), the results suggest that although FCT improves shock front and contact surface resolution, it may not improve the solution elsewhere any better than can be done with the same size cell HULL calculation. Basically, the 2-D HULL/FCT results for the 10 cm-zoned calculation were close to the 2-D HULL results for the same zoned calculation. The differences between the 2-D HULL results for the 5 cm-zoned calculation and the 2-D HULL results for the 10 cm-zoned calculation were generally larger than the differences between the two 10 cm. calculations (HULL and HULL/FCT).

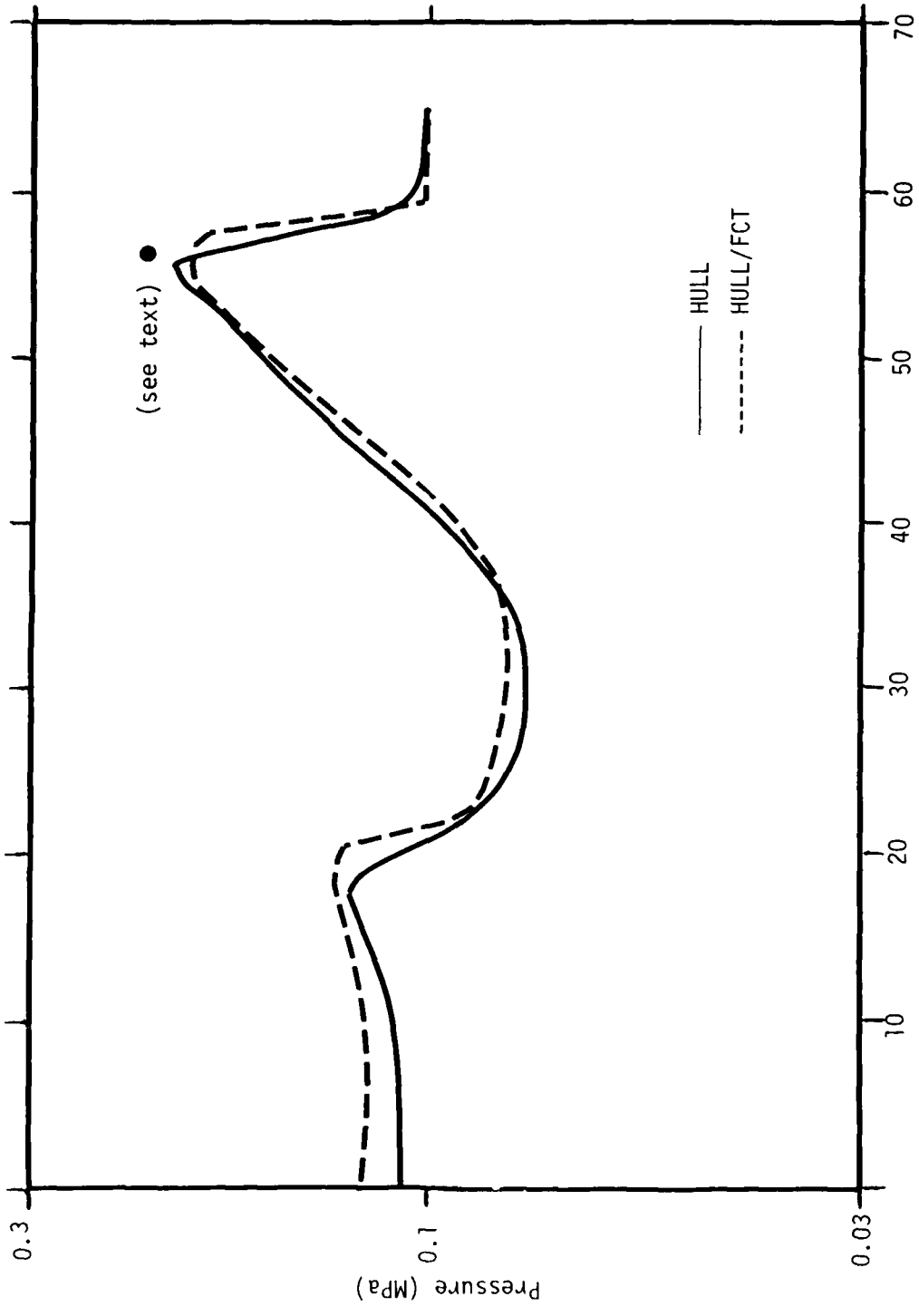

Figure 14. Pressure at 10 ms

One final observation is in order. At the time of this writing the AFWL implementation of FCT was not able to work at much higher overpressures. The reasons are not known. Possibly an error exists in the manner the equations were formulated, or conceivably there exists other more basic problems. Clearly, more work needs to be done in formulating an acceptable way of using FCT with the HULL difference scheme. It may be more rewarding to use the fully multidimensional FCT approach, (see reference 8), without trying to tailor the FCT technique for use with the HULL difference scheme. Since it has been demonstrated that FCT can be added to HULL in the form recommended by AFWL, it follows that it is possible to implement in the simpler form as used at NRL.

SECTION 5

IMPROVING REZONE TECHNIQUES

After a review of certain AFWL calculations, SAI chose to implement a computational subgrid technique to obviate the need for most rezones. The computational subgrid is essentially a region that is recognized by the code to be hydrodynamically active, thus allowing it to skip calculations elsewhere in the mesh. Because of the complex architecture which is partially a result of the many options available in HULL, care is required in the use of this technique just as with most rezone routines. The computational subgrid technique is discussed in some detail in Section 5.1.

The remainder of the effort addressing this task quantified the effects of using various zoning algorithms. In order to develop rezone algorithms, a quantitative understanding is needed of effects caused by changes in zone size. A rezone usually attempts to reduce the number of zones in a given problem by gradually increasing zone size. This is done to reduce large errors from use of mismatch in zone size. These results are discussed in Section 5.2.

5.1 COMPUTATIONAL SUBGRIDS

Most rezone procedures in HULL were introduced as economy measures, wherein the majority of the cells in the mesh are maintained in the hydrodynamically active region of a calculation. Then when the active region approaches the mesh boundaries, the cell dimensions are increased in size, the hydrodynamic variables are averaged geometrically into the expanded mesh, and the calculation continued. This method attempts to minimize the cost and execution time needed by avoiding the overhead of processing excessive numbers of ambient cells.

If the HULL computations can be confined to a subgrid of the mesh which contains the hydrodynamically active cells, then the need for frequent rezones in a calculation can be avoided. With this method a much larger mesh can be used initially with little overhead, and when the mesh is maximally active, one of the existing specialized shock following rezones can be invoked, e.g., rezones 3 or 4.* Many of the calculations performed at AFWL are amenable to this computational subgrid form of processing, e.g., shock tubes, axially centered bursts, applied left or bottom boundary condition problems. Figure 15 illustrates the form this algorithm takes in typical two dimensional calculations. In the shock tube example, the shock enters across the bottom boundary ($J = 1$, $1 \leq I \leq IMAX-1$). Three rows of the mesh are hydrodynamically active, and two rows are allowed for propagation in the current cycle. Therefore, the computations are limited to the first five rows J = 1 to JQ in this cycle; rows JQ + 1 to JMAX-1 are ambient and do not change. If JMAX = 100 rows, this cycle costs nominally 5% of the cost without this computational limitation. The ground burst example in Figure15 illustrates the computational subgrid limitations in two dimensions; only four cells in four rows are processed in this cycle.

5.1.1 Computational Subgrid Algorithm

The algorithm is constructed to include cell (I = 1, J = 1) in the subgrid in all cases. This greatly reduces the overhead and intrusion of the algorithm coding in HULL. Four new variables are required; two variables (IQUIET, JQUIET) specify the computational limits in the current cycle, and two variables are updated during the cycle to force extension of the subgrid in the next cycle (IREZQ, JREZQ). Figures 16 through 20 contain the change deck for the algorithm in terms of the SAI HULL version managed with CDC UPDATE.

*These are specific options available in HULL. Details can be found in reference 9.

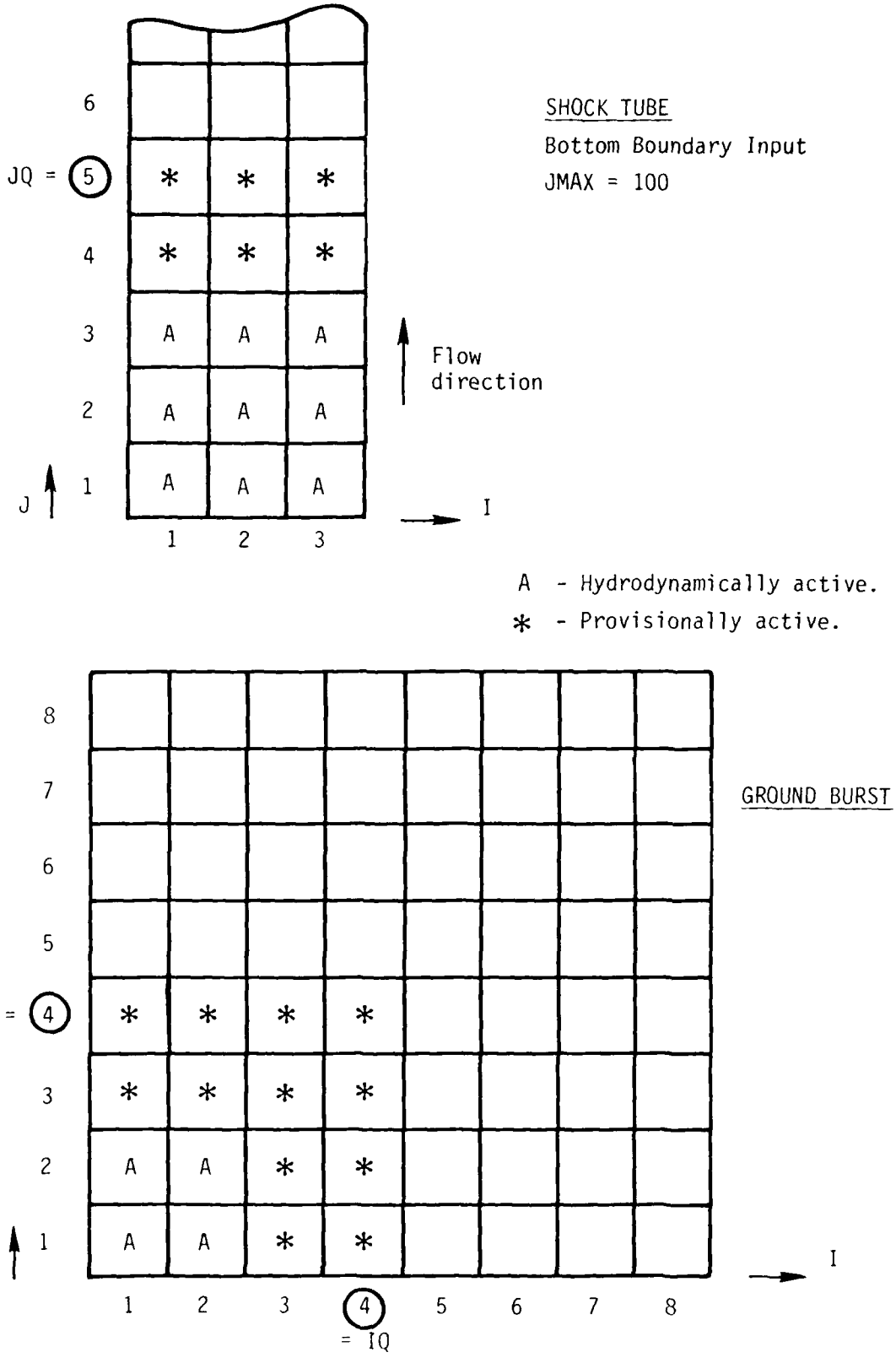

Figure 15. Computational subgrid examples, limits of HULL computations.

```
100=*DELETE   NULL.751
110=      COMMON /INDEX/ I, J, IREZQ, JREZQ, IQUIET, JQUIET
120=*INSERT   NULL.1759
130=*KEEPIQ   *2   ACTIVE  .EQ.  1
140=      IQUIET=MINO(IMAXM1,MAXO(IQUIET,((IREZQ+3)/2)*2))
150=      JQUIET=MINO(JMAXM1,MAXO(JQUIET,JREZQ+2))
160=      ==========MAIN - H1
170=*INSERT   NULL.1978
180=*KEEPIQ   *1   ACTIVE  .EQ.  1
190=      IF(J1.GT.JQUIET) GO TO 200
200=*INSERT   NULL.2003
210=*KEEPIQ   *1   ACTIVE  .EQ.  1
220=      IF(I.GT.IQUIET) GO TO 200
230=*INSERT   NULL.2017
240=*KEEPIQ   *1   ACTIVE  .EQ.  1
250=      IF(I.GT.IQUIET) GO TO 200
260=      ==========MAIN - H3
270=*INSERT   NULL.2106
280=*KEEPIQ   *1   ACTIVE  .EQ.  1
290=      IF(J3.GT.JQUIET) GO TO 400
300=*INSERT   NULL.2129
310=*KEEPIQ   *1   ACTIVE  .EQ.  1
320=      IF(I.GT.IQUIET) GO TO 400
330=*INSERT   NULL.2156
340=*KEEPIQ   *1   ACTIVE  .EQ.  1
350=      IF(I.GT.IQUIET) GO TO 400
360=      ==========MAIN - H4
370=*DELETE   NULL.2176
380=*SKIPIQ   ENDMAX   NM  .EQ.  1
390=*KEEPIQ   *1   ACTIVE  .EQ.  1
400=      IF(J4.GT.JQUIET) GO TO 500
410=*INSERT   NULL.2177
420=*KEEPIQ   *1   ACTIVE  .EQ.  1
430=      DO 450 I=1,IQUIET
440=*KEEPIQ   *1   ACTIVE  .NE.  1
450=*INSERT   NULL.2180
460=*LABEL    ENDMAX
470=      ==========SUBR - H3
480=*INSERT   NULL.3684
490=*KEEPIQ   *2   ACTIVE  .EQ.  1
500=      IF(ABS(H(N3+2)).GT.VMIN) IREZQ=MAXO(I,IREZQ)
510=      IF(ABS(H(N3+3)).GT.VMIN) JREZQ=J
```

Figure 16. Computational subgrid coding, insertions into main and subroutine H3.

```
==========================================SUBR - HULLIN.INIT
*INSERT   HULL.7882
*KEEPTO    *4   ACTIVE  .EQ.  1
      IREZQ =0
      JREZQ =0
      IQUIET=4
      JQUIET=4
      VMIN  =1.E-4
==========================================SUBR - HULLIN.HYDRO.PRESSURE
*DELETE   HULL.6560.6580
      IF(IVT.EQ.1) JAH=0
      NN=0
      DO 66 JAH1=1,NROWFB
      JAH=JAH+1
      DO 67 IAH=1,IMAX
*KEEPTO    *1    ISLAND
      IF(H(NN+4).EQ.0.0) GO TO 67
      CALL STATE(TAU(IAH)+DT(JAH),H(NN+1),TEMP)
      IF(IAH.LT.IMAX) GO TO 67
      GA(JAH)=H(NN+1)
      GF(JAH)=H(NN+5)/(TAU(IAH)+DT(JAH))
   67 NN=NN+NH
   66 CONTINUE
==========================================SUBR - HULLIN.ACTIVE.FLAGS
*KEEPTO   ENDACTX   ACTIVE  .EQ.  1
      IF(IVT.EQ.1) JAHX=0
      NN=0
      NI=-NH
      DO 68 JAH1=1,NROWFB
      JAHX=JAHX+1
      NI=NI+NVAREFR
      DO 69 IAH=1,IMAXM1
*KEEPTO    *1    ISLAND
      IF(H(NN+4).EQ.0.0) GO TO 69
      IWSA=0
*KEEPTO    *2    NM  .EQ.  1
      DO 65 INM=2,NM
   65 IF(H(NN+NHM+INM).GT.0.0) IWSA=1
      IF(ABS(H(NN+1)-H(NI+1)).GT.1.E-6) IWSA=1
      IF(IWSA.GT.0.OR.ABS(H(NN+2)).GT.VMIN) IREZQ=MAX0(IREZQ,IAH)
      IF(IWSA.GT.0.OR.ABS(H(NN+3)).GT.VMIN) JREZQ=MAX0(JREZQ,JAHX)
   69 NN=NN+NH
   68 CONTINUE
*LABEL    ENDACTX
```

Figure 17. Computational subgrid coding, subroutine HULLIN initialization of IQUIFT, JQUIET.

```
 960=C*************************************************SUBR - BB1
 970=*DELETE   HULL.10523,10527
 980=*INSERT   HULL.10534
 990=*KEEPTO   *1   ACTIVE  .EQ.  1
1000=      DO 15 I=1,IQUIET
1010=*KEEPTO   *1   ACTIVE  .NE.  1
1020=*DELETE   HULL.10562
1030=*DELETE   HULL.10609,10610
1040=*DELETE   HULL.10618
1050=*DELETE   HULL.10625
1060=    5 CN=0
1070=C
1080=*INSERT   HULL.10640
1090=C
1100=*KEEPTO   *1   ACTIVE  .EQ.  1
1110=      DO 10 I=1,IQUIET
1120=*KEEPTO   *1   ACTIVE  .NE.  1
1130=*DELETE   HULL.10645
1140=*DELETE   HULL.10651
1150=*DELETE   HULL.10695
1160C************************************************SUBR - BB1
1170=*DELETE   HULL.11068
1180C=
1190=*KEEPTO   *1   ACTIVE  .EQ.  1
1200=      DO 10 I=1,IQUIET
1210=*KEEPTO   *1   ACTIVE  .NE.  1
1220=*DELETE   HULL.11074
1230=   10 CONTINUE
1240C************************************************SUBR - IBB1
1250=*INSERT   HULL.11112
1260C=
1270=*KEEPTO   *1   ACTIVE  .EQ.  1
1280=      DO 10 I=1,IQUIET
1290=*KEEPTO   *1   ACTIVE  .NE.  1
```

Figure 18. Computational subgrid coding, phase 1 boundary routines.

```
1300=*****************************************SUBR - BB3
1310=*INSERT    HULL.11714
1320=*KEEPIO    *1    ACTIVE  .EQ.  1
1330=       DO 50 I=1,IQUIET
1340=*KEEPIO    *1    ACTIVE  .NE.  1
1350=*DELETE    HULL.11723
1360=*DELETE    HULL.11731
1370=*DELETE    HULL.11746
1380=*DELETE    HULL.11755,11756
1390=*DELETE    HULL.11765
1400=*DELETE    HULL.11768
1410=*DELETE    HULL.11774
1420=*****************************************SUBR - IB3
1430=*INSERT    HULL.12040
1440=*KEEPIO    *1    ACTIVE  .EQ.  1
1450=       DO 20 I=1,IQUIET
1460=*KEEPIO    *1    ACTIVE  .NE.  1
1470=*****************************************SUBR - IBB3
1480=*INSERT    HULL.12102
1490=*KEEPIO    *1    ACTIVE  .EQ.  1
1500=       DO 10 I=1,IQUIET
1510=*KEEPIO    *1    ACTIVE  .NE.  1
```

Figure 19. Computational subgrid coding, Phase 2 boundary routines.

```
1520=============================================SUBR - REMESH
1530=*INSERT   HULL.12387
1540=*KEEPIO   *2   ACTIVE  .EQ.  1
1550=       XREZQ=X(IQUIET)
1560=       YREZQ=Y(JQUIET)
1570=*INSERT   HULL.13027
1580=*KEEPIO   ENDALIV   ACTIVE  .EQ.  1
1590=       DO 2183 ILEFT=1,IMAXM1
1600=       IQUIET=ILEFT
1610=       IF(X(ILEFT).GE.XREZQ) GO TO 2184
1620= 2183 CONTINUE
1630= 2184 DO 2185 ILEFT=1,JMAXM1
1640=       JQUIET=ILEFT
1650=       IF(Y(ILEFT).GE.YREZQ) GO TO 2186
1660= 2185 CONTINUE
1670= 2186 JQUIET=JQUIET+1
1680=       IQUIET=((IQUIET+3)/2)*2
1690=       IREZQ=4
1700=       JREZQ=4
1710=*LABEL   ENDALIV
```

Figure 20. Computational subgrid coding, rezone compatibility.

Figure 16 contains the algorithm coding inserts and changes in the MAIN subprogram of program HULL. It is seen that simple branches are taken when a cell index exceeds one of the subgrid limits. A cycle is allowed to complete the row (5) loop for all rows of the mesh. Thereby, the particular method used for mesh storage (disk, extended core, incore) and mesh input/output has no interaction with the algorithm, and extra coding is not required to ensure that mesh transfer from old mesh storage to new mesh storage is complete. The only phase which can be performed in rows - for which J > JQUIET, is Phase H4, and in particular only the particle routines are active. The multi-material routines in Phase H4 are executed only within the subgrid limits.

Lines 470 through 510 of Figure 16, contain the intermediate variable update procedure. This code is extractive, and does not change any of the computations in HULL.

Figure 17 contains the algorithm inserts into subroutine HULLIN of Program HULL. The coding in lines 600 through 740 is also required by the cell by cell activity flag code and the "*KEEPTO" SAIL directive for this code is to be set to be compatible for values of the option "ACTIVE" other than one and zero. Lines 760 through 950 contain the IREZQ, JREZQ initializing code which is performed at each calculation restart; therefore, the four algorithm variables are local to program HULL and need not be in the "ZBLOCK". The activating conditions shown are:

1. Presence of material other than air
2. A non-ambient pressure (H(1))
3. A non-minimum absolute velocity.

These conditions are sufficient for most calculations although other conditions may be necessary in some circumstances including an absolute specification of the subgrid limits.

Figures 18 and 19 contain the coping inserts for the bottom (J = 1) and top (J = JMAX) boundary routines. The primary change is substitution of IQUIET for IMAXM1 (IMAX-1) in the "DO-LOOPS". The IMAXM1 limit of the loops is required for the cell based activity flags and for no computation limiting code at all.

Figure 20 contains the IQUIET, JQUIET variable reset coding to be entered into subroutine REMESH of program HULL. This is the only place where the subgrid limits can be reduced in value. The new limits are placed at the geometrically equivalent cell in the rezoned mesh. Some extension is allowed because a rezoned mesh usually contains larger cells, and a two cell boundary between the hydrodynamically active cells and the cells beyond the subgrid is to be maintained.

The coding in Figures 16 through 20 is untested at this date. It has been provided to AFWL with the understanding that the initial testing will be done in one of the two-dimensional calculations AFWL will be running. However, the modifications in the figures should not, even if incorrect, degrade the operational status of the code due to the way they are implemented.

5.1.2 Limitations of the Computational Subgrid Algorithm

The algorithm as presented in this memorandum is incompatible with the following HULL calculation options:

DIMEN = 3 (three dimensional mesh)
CODE = 2* (interactive dust)
RAD = 0 (radiation diffusion)
REZONE= 7 (continuous rezone)
STRESS = 0 (elastic-plastic stress)
SURF = 0* (thermal layer bottom boundary).

The options marked with an asterisk (*) may or may not be compatible. * the [illegible] particles which are outside the subgrid have [illegible] algorithm is likely to be compatible. However, [illegible] affected by gravity and will in general [illegible]. Therefore only if all such particles are [illegible] subgrid at each cycle is CODE = 2 [illegible] and ACTIVE = 1 is not recommended [illegible] monitored. The SURF options generate [illegible] energy into several rows of cells at the [illegible]. Therefore, if JQUIET is always equal to [illegible] always greater than the uppermost row where the [illegible] affect, then SURF = 0 and ACTIVE = 1 are compatible options. In general, a fireball top will force JQUIET to indicate a row well above the rows affected by the SURF routines, and the option pair is compatible.

SAI recommends that inclusion of DEEP-SIX or calls to SINK be included for the case where the option ACTIVE is equal to 1 and incompatible options are likely to be accidentally run. In this manner, nonsense will not be generated from some inadvertent attempt to run incompatible options.

5.2 QUANTIFYING THE REQUIREMENTS FOR PROPER REZONES

A series of one-dimensional HULL (Cartesian geometry) calculations were performed to study the effects caused by changes in zone sizes and zoning configurations for use in developing rezone techniques. Each run had a reflective right-hand boundary and identical initial conditions. The initial conditions consisted of air at a density of 1.225 milligrams per cubic centimeter and a specific internal energy of 2.08×10^9 ergs/gm, which are approximately sea level conditions for a gamma of 1.4. The air was initially at rest. Mass, momentum and energy were fluxed into the mesh from the inlet left-hand boundary.

The boundary conditions were from LAMB (reference 10) and represented the air blast from a 1 megaton nuclear surface burst (2 megaton free-field) at either of two ground ranges, 569 meters or 8.5 kilometers. The corresponding peak overpressures are about 4 MPa and 16 KPa.

The waveforms selected are meant to approximately bound the overpressure region of interest. However, since there exists interest in investigating interacting waveforms, a reflective boundary was included at the right hand side of the mesh which is equivalent to the case of two equal shocks running head-on into each other. The overall grid length (50m) and physical locations of observers were essentially the same from run to run for each given overpressure. Table 1 provides a summary of the zoning and observer locations for each calculation.

The results from each run were processed with a computer program which plotted observer time histories of various quantities of interest (such as overpressure). Figure 21 shows the observer locations and cell boundaries for each calculation listed in Table 1. Each observer is located at the center of the cell closest to the corresponding observer location in the uniform grid calculation. The symbol V within parentheses indicates that the calculation employed artificial viscosity, otherwise no viscosity was used in HULL. The donor cell technique in HULL will numerically generate some viscous dissipation. Although the treatment of the incident shock seems to be handled nicely without artificial viscosity, the reflected wave will exhibit a considerable overshoot.

Figure 22 extracted from reference 6 shows three 1-D HULL calculation similar to those in Table 1 except that the reflective wall is at about 625 m. The ones shown were run with a uniform grid, one without any artificial viscosity, one with the new AFWL artificial viscosity (reference 11), and finally one with the usual choice of

Table 1. XO = 56900 cm

Nominal Length of Mesh = 5000 cm.
(V) - Denotes Visc Option with Cl = .6

RUN	ZONING	OBSERVERS & LOCATIONS (10^4 cm)
101	DX = 100 cm Length of mesh = 5000.0	1,10,20,30,40,50; 5.695, 5.785, 5.885, 5.985, 6.085, 6.185
102	DX = 50 cm Length of mesh = 5000.0	1,20,40,60,80,100 same positions within 0.25 m
130,131 (V)	DX(1) → DX(11) = 100 cm DX = 1.1124*DX previous for zones 12-26 Length of mesh = 5001.5 cm	1,10,17,21,24,26; 5.695, 5.785, 5.879, 5.974, 6.076, 6.165
135,136 (V)	DX(1) = 494.2136 cm DX = (1/1.1124)*DX previous for zones 2-15 DX(16) → DX(26) = 100 cm Length of mesh = 5001.5 cm	1,3,5,9,16,26; 5.715, 5.804, 5.876, 5.981, 6.085, 6.185
140,141 (V)	DX(1) → DX(11) = 100 cm DX = 1.0532*DX previous for zones 12-32 Length of mesh = 4999.6 cm	1,10,18,24,29,32; 5.695, 5.785, 5.879, 5.981, 6.093, 6.175
145,146 (V)	DX(1) = 296.98 cm DX = (1/1.0532)*DX previous for zones 2-21 DX(22) → DX(32) = 100 cm Length of mesh = 4999.6 cm	1,4,8,14,22,32; 5.705, 5.787, 5.879, 5.986, 6.085, 6.185
150,151 (V)	DX = 100 cm Length of mesh = 5000.0 cm	1,10,20,30,40,50; 5.695, 5.785, 5.885, 5.985, 6.085, 6.185

TABLE 1. XO = 850000 cm
(continued)

NOMINAL LENGTH OF MESH = 100000 cm
(V) - DENOTES VISC OPTION WITH C1 = .6

RUN	ZONING	OBSERVERS & LOCATIONS (10^5 cm)
132,133 (V)	DX(1) → DX(11) = 2000 cm DX = 1.1124*DX previous for zones 12-26 DX(27) = DX(26) IMAX = 27 Length of mesh = 100029 cm	1,10,17,21,24,26 8.510, 8.690, 8.878, 9.067, 9.273, 9.451
137,138 (V)	DX(1) = 9884.272 cm DX = (1/1.1124)* DX previous for zones 2-15 DX(16) = DX(27) = 2000 cm IMAX = 27 Length of mesh = 100029 cm	1,3,5,9,16,26 8.549, 8.728, 8.872, 9.082, 9.290, 9.490
142,143 (V)	DX(1) → DX(11) = 2000 cm DX = 1.0532*DX previous for zones 12-32 DX(33) = DX(32) IMAX = 33 Length of mesh = 999923 cm	1,10,18,24,29,32 8.510, 8.690, 8.879, 9.081, 9.305, 9.470
147,148 (V)	DX(1) = 5939.6 cm DX = (1/1.0532)*DX previous for zones 2-21 DX(22) → DX(33) = 2000 cm IMAX = 33 Length of mesh = 999923 cm	1,4,8,14,22,32 8.530, 8.695, 8.878, 9.092, 9.290, 9.490
152,153 (V)	DX = 2000 cm IMAX = 51 Length of mesh = 100000 cm	1,10,20,30,40,50 8.510, 8.690, 8.890,9.090, 9.290, 9.490

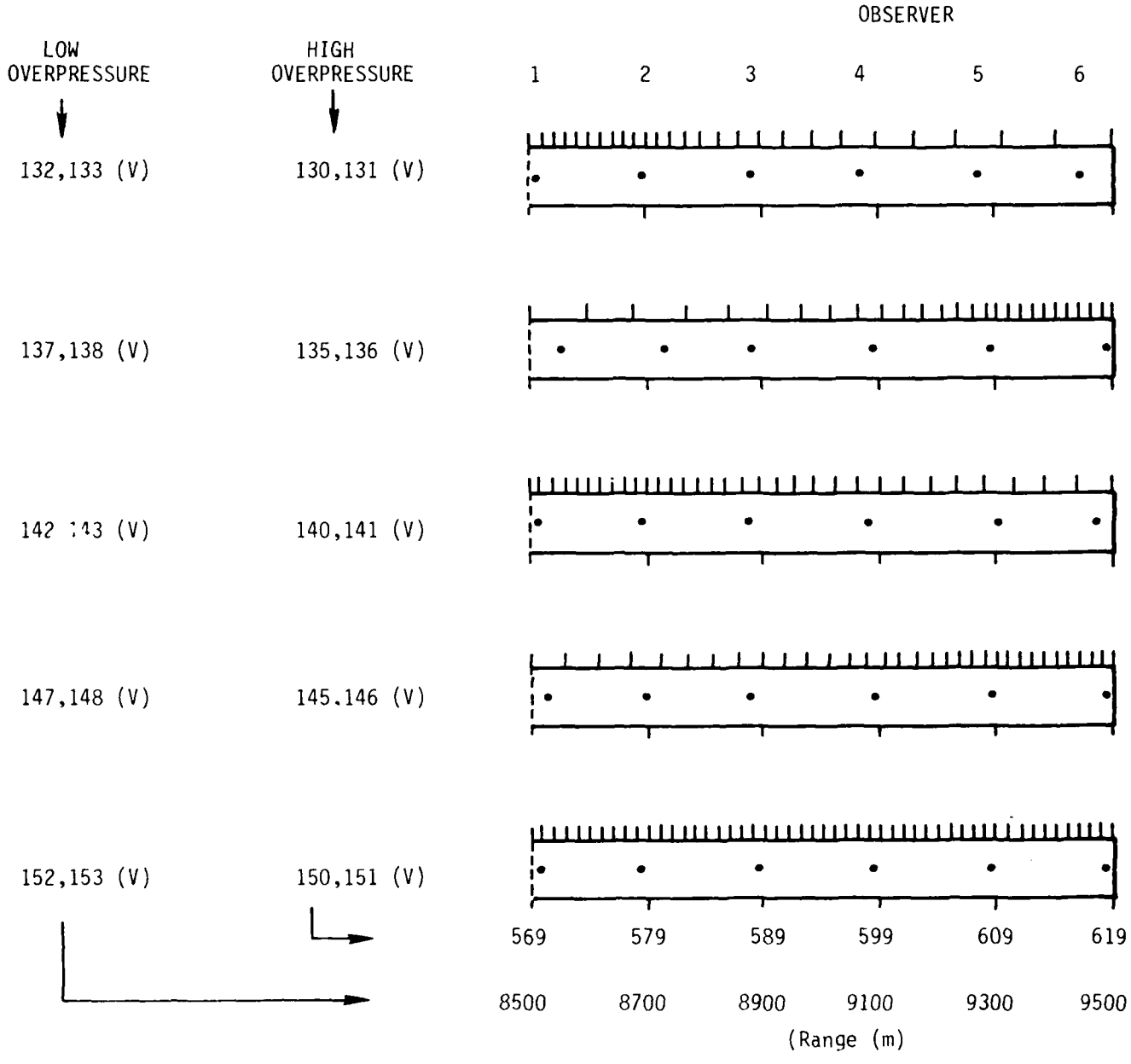

Figure 21. Observer and cell locations for low and high overpressure 1-D HULL calculations.

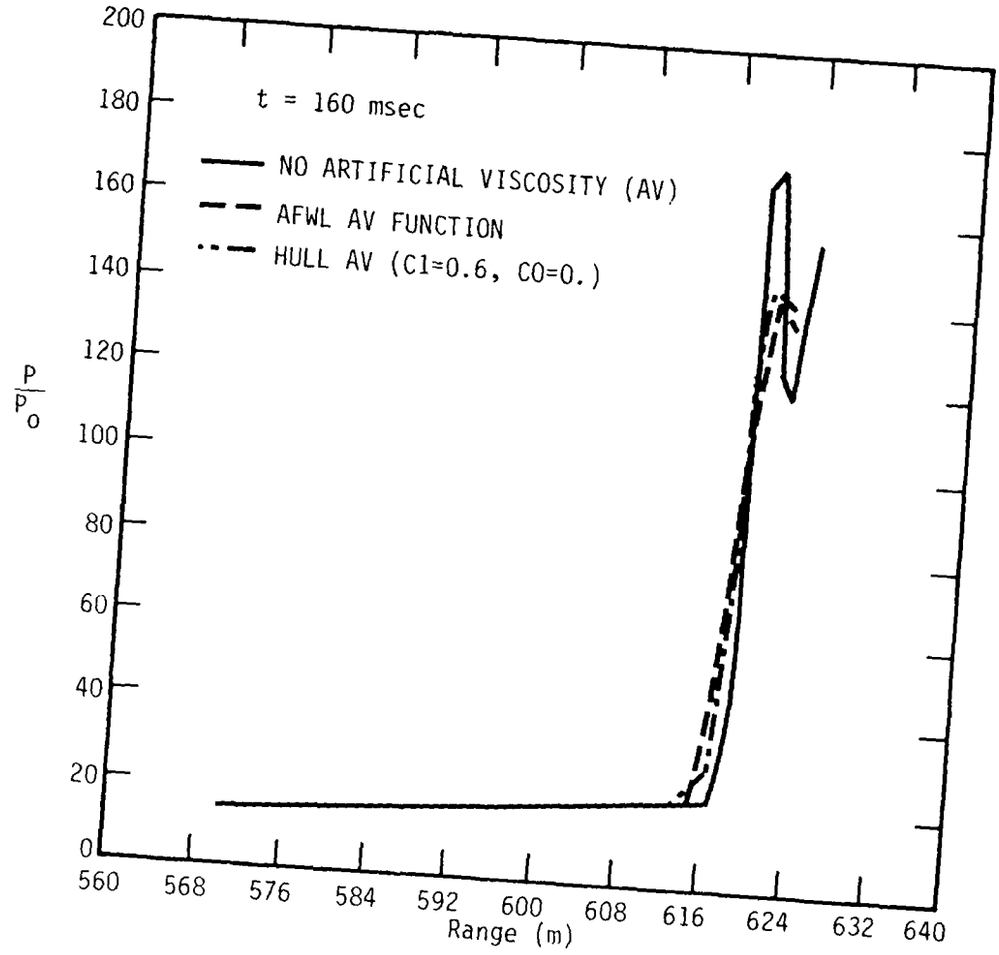

Figure 22. SAI one-dimensional calculations of relative pressure at 160 milliseconds.

viscosity in HULL. The effect induced by the use of artificial viscosity is to increase the numerical diffusion as expected with the results that oscillations due to the second order differencing are damped, however, resolution between physical peaks may be lost if they are sufficiently close together.

Appendix C presents overpressure history for some of the runs and observers shown in Table 1 and Figure 22. To aid in interpretation of the data, Figures 23A and 23B are included here which show the path of the various pressure peaks for the low overpressure and high overpressure uniform grid runs with no artificial viscosity. The dots at the bottom show the locations of the observers for convenience. The following conclusions were made by comparing the appropriate overpressure histories that are presented in Appendix C:

1) The pulses are generally sharper and higher in regions of finer zoning, and broaden and reduced in regions of coarse zoning.

2) The toe of the incident pulse arrives at a given observer slightly earlier in runs which include the viscosity, and is especially noticeable in the runs made at low overpressure. However, the arrival time of the peak, when the usual approach is taken for defining peak arrival time, does not depend on whether artificial viscosity is used at either overpressure.

3) The presence of artificial viscosity lowers and widens the reflected pulse.

Other conclusions can also be drawn from careful comparison of various runs in the data base represented by the few examples shown in Appendix C. For example, consider the comparison of low overpressure runs 133, 138, and 153 at observer 6. Each run included artificial viscosity, and the uniformily zoned run (153) produced the highest peak and the fastest rise time. It would seem that the peak was reduced more by propagating from small zones to larger zones than vice versa, but the rise times were almost equal for the non-uniform grid no matter what the direction of propagation. Since the peak measured at this

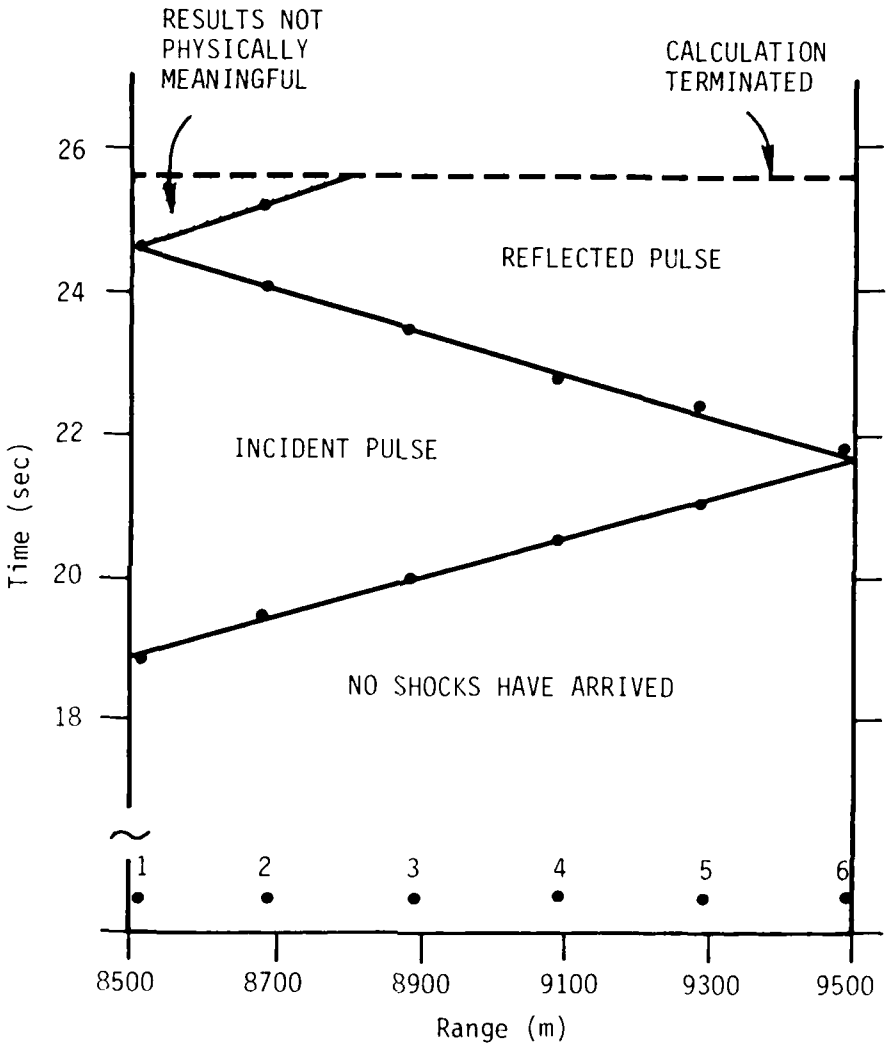

Figure 23A. Low overpressure peak pressure path. Run 152.

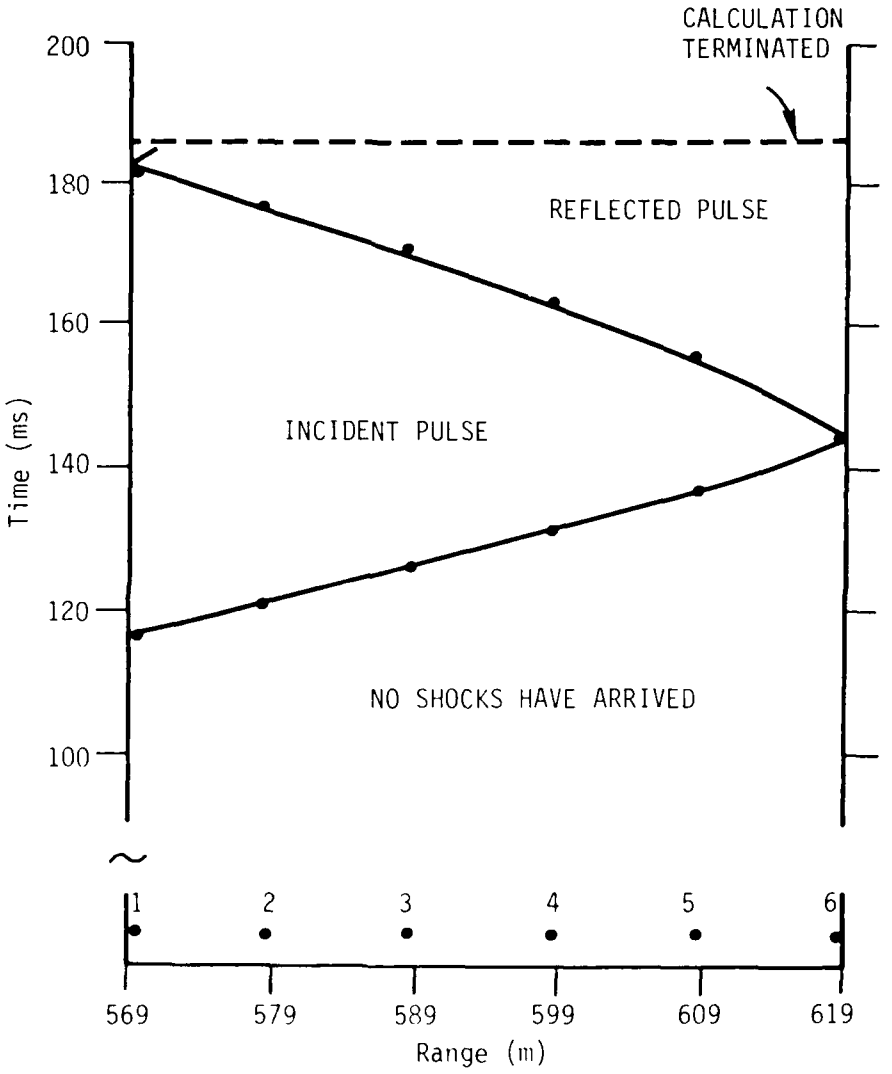

Figure 23B. High overpressure peak pressure path. Run 150.

observer for run 133 is contained in a cell over four times as large as that containing observer 6 in both runs 138 and 153, the result is not surprising. An indication of the effect of the cell size difference on the peak can be seen by comparing the incident wave peak at observer 1 for runs 133 and 138 where the observer is in the small cell for run 133, instead of 138. The incident peak has been reduced by a factor of 0.83. This is comparable with the reduction at observer 6 of 0.88. Therefore, except for the fact that the distribution of pressure is over a larger cell area, it is expected that essentially the same dispersive effect is seen when propagating from a region of small zone to larger zone and vice versa.

The zoning change leads to pulse dispersion, which can be thought of as a filtering effect where the largest zones filter out frequencies higher than it is capable of passing. This manner of explanation (i.e., use of linear theory) is not appropriate for the high overpressure, where the non-linear effects are large.

Now consider the comparison of high overpressure runs 131, 136, and 151 at observers 1 and 6. These also were run with artificial viscosity. The uniformily zoned run (151) produced the highest peak and quickest rise time. Although the rise time for run 136 at observer 1 was about four times that for run 151 at the same observer, the pulse in run 136 at observer 6 has sharpened up again by the time it arrived due to the non-linearity of hydrodynamics. Essentially the dispersed pulse can shock up since the characteristics within the pulse will tend to cross (reference 12).

This leads to a significant and suggestive observation about the problem associated with calculating low overpressure waveforms. The majority of experience in this country in the field of air blast calculations has been gained at the AFWL. Generally the bulk of the AFWL experience has been in either computing fireball development (rise, growth, etc.) or shock propagation. In the latter category, the low

overpressure regime is the last to be calculated. Just suppose that in the process of learning how to do calculations at low overpressure, the experience gained at high overpressures guided the subsequent effort. It has been demonstrated in this effort, that shocks can resharpen at high overpressure if the shock has experienced some dispersion as a result of propagating through regions of coarse zoning. This will not happen at low overpressure. Simply stated, what did work as a reasonable zoning technique in high overpressure, will not necessarily work at low overpressure. The implication is important to the present issues being raised in the air blast community, and therefore, warrants additional and more careful attention than received to date. Figures 24 and 25, obtained by tracing the appropriate curves found in Appendix C, are provided to show the result for low and high overpressure. The solid curves are for the uniformily zoned (1m) grid, and the dashed lines are for the grid where the zoning was coarse near the inlet boundary (about 4m), and gradually (11% change) became finer as the reflective boundary was approached. At observer 6 they were 1m wide.

An analysis of 1-D HULL calculations performed early in this effort had resulted in the following interesting observations for high overpressures: The waveforms at observer 6 for the runs where this observer was contained in a 1 m cell were essentially the same whether the pulse has propagated through a region which increased by 5 or 11% from $\frac{1}{2}$ m to 1 m cells or even abruptly, i.e., the entire factor of 2. Furthermore, the waveforms at observer 6 for the runs where observer 6 is contained in a $\frac{1}{2}$ m cell were essentially the same whether the pulse had propagated through a region where the zone size had been decreased smoothly (by either 5 or 11%) or abruptly. The implication (at high overpressure) was that the results are fairly insensitive to zoning variations. As was just shown however, the same was not true of low overpressures. The waveforms at observer 6 are shown in Figure 26 for the two uniformily zoned cases where observer 6 is in either the small ($\frac{1}{2}$ m) or large (1 m) cell. The input conditions are the same as those

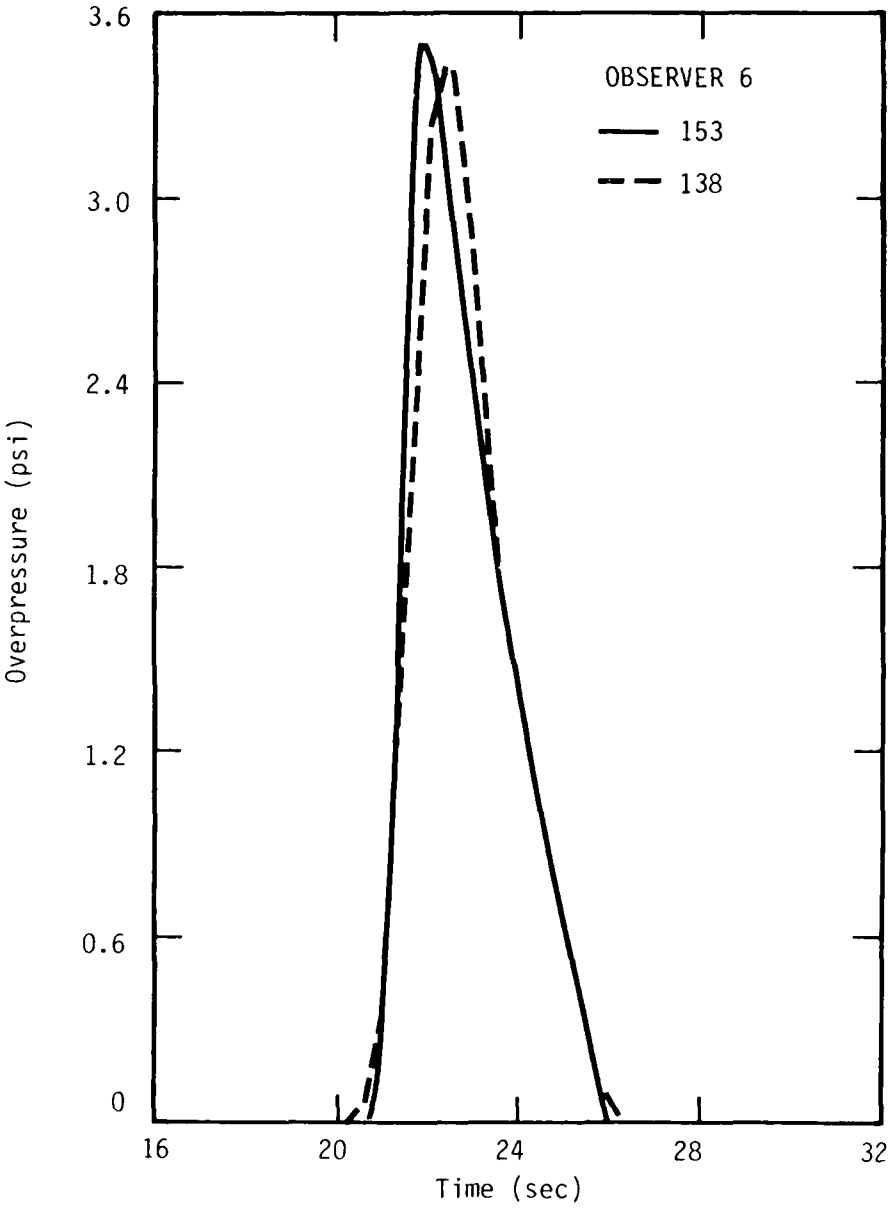

Figure 24. Effect of propagation through large zones (low overpressure).

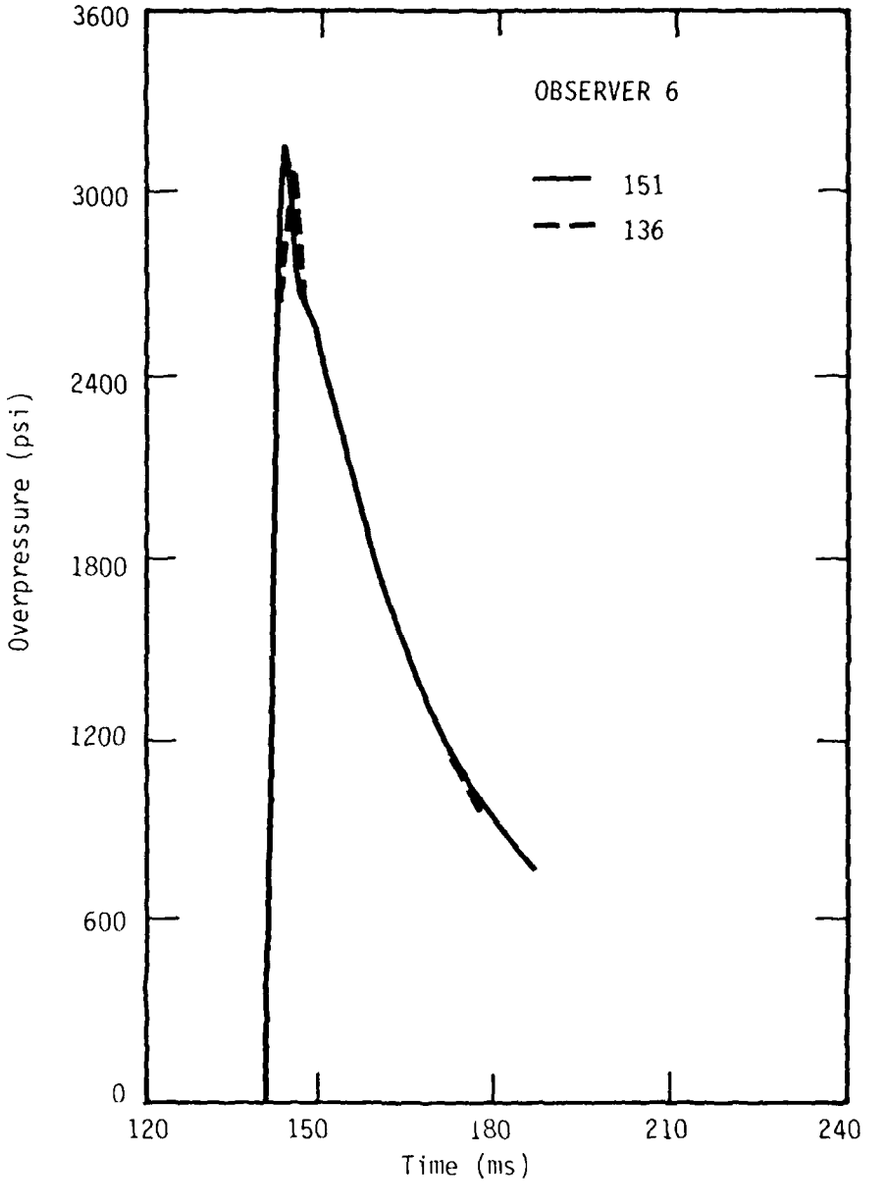

Figure 25. Effect of propagation through large zones (high overpressure).

that were discussed and shown earlier. In the figure oscillations can be seen which result from using the second order HULL diferencing (in the Lagrangian phase) without any artificial viscosity. The period of the oscillation is proportional to the zone size at the observer location. Furthermore, the rise time to the peak is approximately equal to the period of this oscillation. The rise time is 2 ms for the $\frac{1}{2}$ m cell and about 4 ms for the 1 m case. The rise time to the pressure of the incident pressure (about 500 psi) is about 0.6 ms for the $\frac{1}{2}$ m cell, and since the shock velocity at the incident pressure is about 1.9m/ms the rise to the incident pressure is occurring over 2-3 cells.

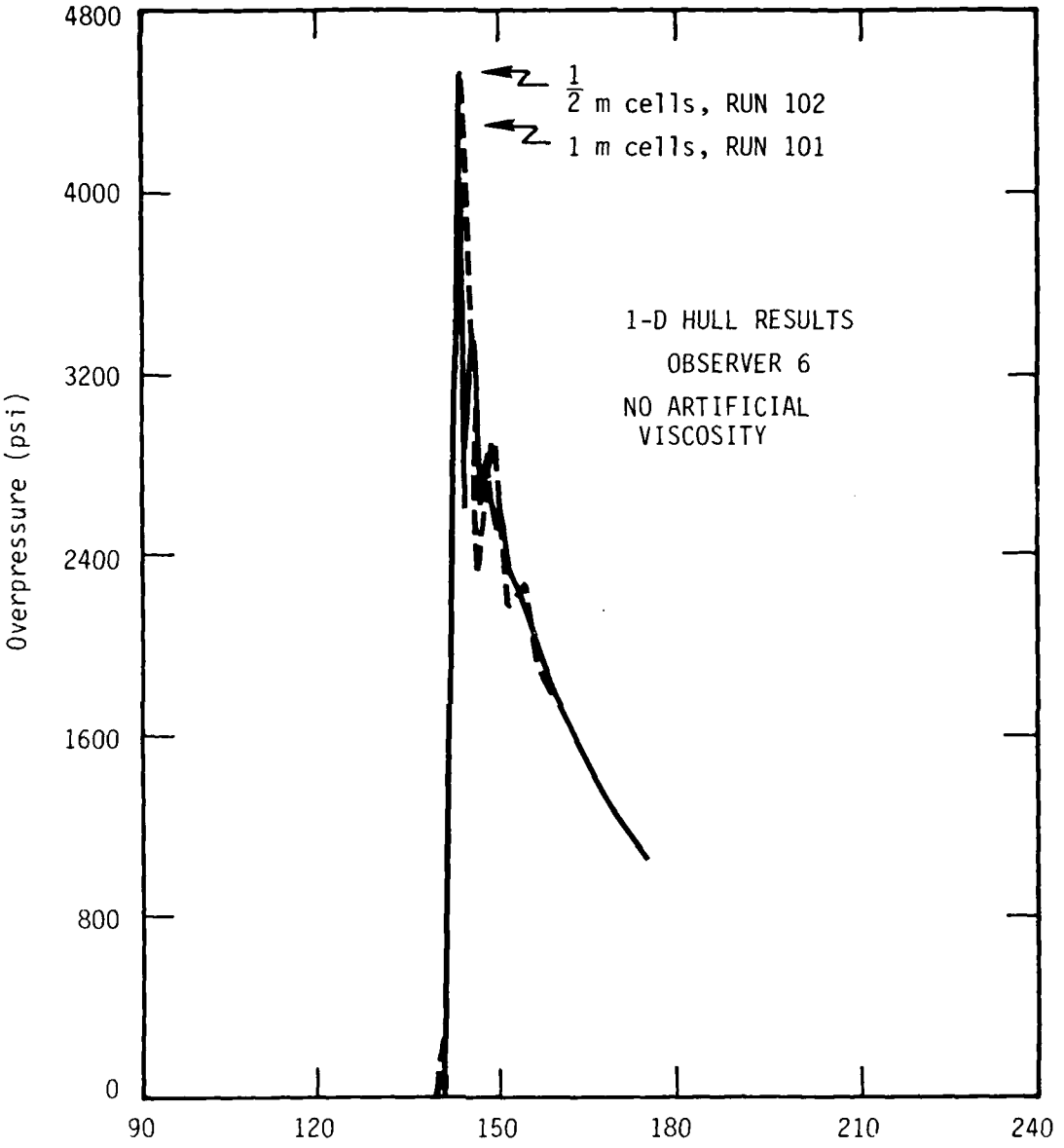

Figure 26. Comparison of reflected pressure for ½ m and 1 m zoning.

SECTION 6

CONCLUSIONS AND RECOMMENDATIONS

The principal conclusions of this effort relating to the implementation of FCT in HULL are: FCT can be implemented in HULL in a reasonable fashion; as currently configured, FCT costs more than merely halving HULL zone size; FCT cost can be reduced to a more competitive level, but coding becomes very complex and difficult to modify; and more work apparently needs to be done on the FCT technique utilized at the AFWL.

Our recommendation relevant to including FCT in HULL as formulated at AFWL is that the effort not be pursued further since it is too risky, benefits seem to be minimal, and considerable development is still required. Instead, we recommend that FCT be implemented in HULL as formulated at NRL (reference 8). HULL is designed to allow easy modification to the difference technique while retaining the extensive software needed for producing large calculations (e.g., appropriate equation of state data bases, atmosphere models, sophisticated plotting routines, program tape libraries, and general problem data generators.

The principal conclusions of this effort relevant to improving rezone techniques are: use of a computational subgrid is desirable since coding modifications are straightforward and in several cases it will obviate the need for rezone; zone size variations using no artificial viscosity do not modify waveforms nearly as much as artificial viscosity variations for zone variations of 5-10% or even abrupt one-time factor-of-2 changes for high overpressure; and effects from changes in zone size depend on shock strength. Probably the most important observation has been that pulse dispersions introduced by propagation through coarse zoning will lead to reduction in peak overpressure and

may never recover to the correct value for low overpressures. Whereas for high overpressures, non-linear effects will tend to steepen any dispersed pulse. Whether the steepening thus obtained produces an accurate waveform remains to be demonstrated.

Our recommendations relevant to improving rezone techniques are: the SAI computational subgrid technique should be implemented and used with the AFWL HULL code; continue evaluation of effect of zone size variation on HULL one-dimensional results for decaying waveforms; and finally, in order to further refine rezone techniques, the effects introduced by use of artificial viscosity in HULL must be better understood, as well as the effects introduced by usage of current HULL rezones.

REFERENCES

1. Jay P. Boris and David L. Book, "Flux-Corrected Transport. I. SHASTA, A Fluid Transport Algorithm That Works," Journal of Computational Physics 11, 38-69 (1973).

2. D. L. Book, J. P. Boris, and K. Hain, "Flux-Corrected Transport II: Generalizations of the Method," Journal of Computational Physics 18, 248-283 (1975).

3. J. P. Boris and D. L. Book, "Flux-Corrected Transport. III. Minimal-Error FCT Algorithms," Journal of Computational Physics 20, 397-431 (1976).

4. M. A. Fry, et al, "The HULL Hydrodynamics Computer Code," Air Force Weapons Laboratory, TR-76-183, September 1976.

5. R. E. Durrett and D. A. Matuska, "The HULL Code; Finite Difference Solution to the Equations of Continuum Mechanics," Air Force Armament Laboratory, TR-78-125, November 1978.

6. Leon Chandler, "Remarks on Flux-Corrected Transport at AFWL," Air Force Weapons Laboratory, Kirtland AFB, N.M., AFWL-TR79-70, (to be published).

7. Reginald W. Clemens and Billie J. Thorne, "Conversion of a HULL Eulerian Code to the CRAY-1 Victor Computer," AFATL TR-78-11.

8. Steven T. Zalesak, "Fully Multidimensional Flux-Corrected Transport," Naval Research Laboratory, Washington, D.C., NRL Memorandum Report 3716, May 1978.

9. "HULL Computer Source Listings," Science Applications, Inc., May 1978.

10. C. Needham, L. Wittwer, et.al., "Air Force Weapons Laboratory Low Altitude Multiburst (LAMB) Model," AFWL TN-75-2 (unpublished).

11. Peter W. Lunn, et.al., "Development of an Artificial Viscosity Function," Air Force Weapons Laboratory, Kirtland AFB, N.M., AFWL-TR-77-53, September 1977.

12. Landau and Lifshitz, Fluid Mechanics, Pergamon Press, (1975), p. 380.

APPENDIX A

EXAMPLES OF COMPARISONS OF CALCULATIONS WITH EXPERIMENTAL DATA

Reference 4 describes comparisons of theoretical calculations made with HULL and its predecessor SHELL with various high explosive (HE) experimental data. Some of the figures from that reference have been extracted and included in this appendix for convenience. Comparisons of the theoretical calculations with high explosive (HE) experimental data have been performed at the AFWL as a result of their theoretical support of many large scale instrumented HE detonations (from DISTANT PLAIN through DICE THROW).

Predictions of overpressure with SHELL are shown in Figure 27 along with data obtained on a 500 ton sphere of TNT detonated at the ground. Although SHELL results fall below the experimental data below pressures of 10 psi, HULL results were considerably better due to the improved difference scheme found in HULL. Experimental results are plotted from PRAIRIE FLAT and DIAL PACK which were both detonated at Suffield, Canada.

A comparison has also been made for MINE UNDER, which was a 100 ton TNT sphere detonated 1 diameter above the ground. The agreement in peak overpressure between calculations and data was similar to that shown for the tangent sphere explosions. The positive phase duration (Figure 28), which is more difficult to measure than peak overpressure, and hence, has larger experimental error is also shown to be well represented by calculations.

Figures 29 through 30 present data, taken by BRL and AFWL during MIXED COMPANY (a 500 ton tangent sphere of TNT), compared with AFWL calculations. Peak overpressure agrees well as does the overpressure impulse (Figure 30).

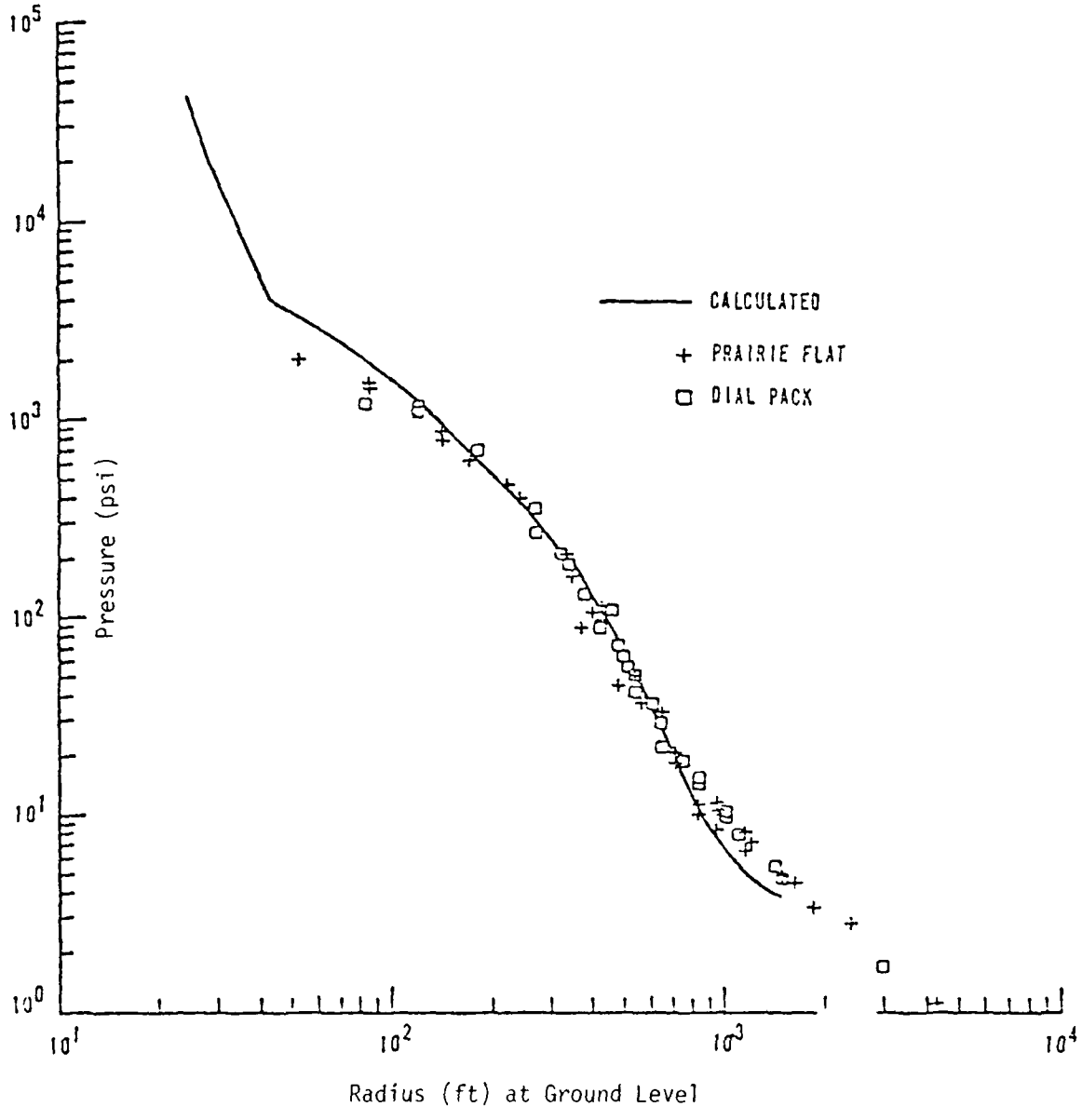

Figure 27. DIAL PACK (overpressure versus radius).

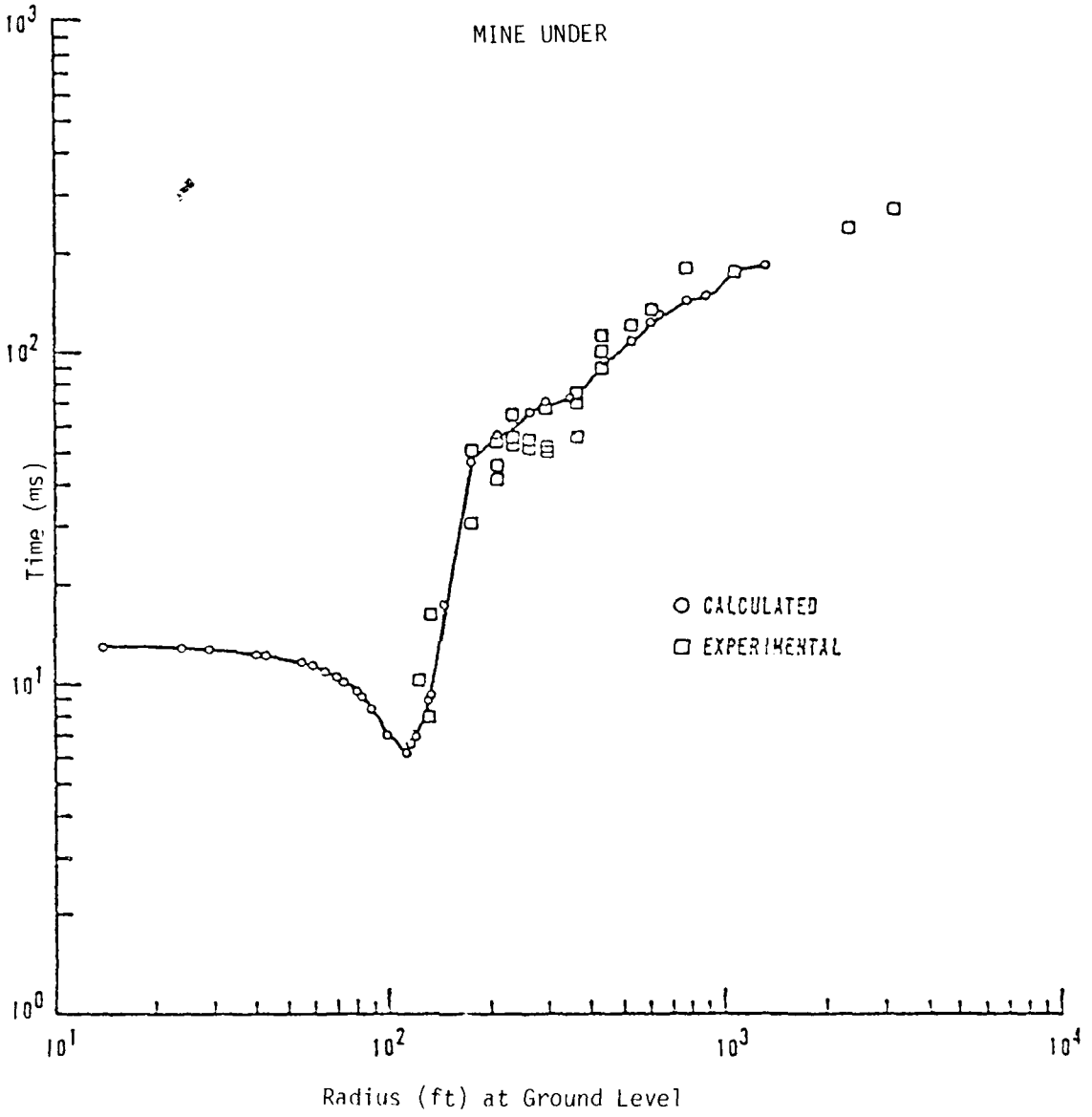

Figure 28. Positive phase duration versus radius.

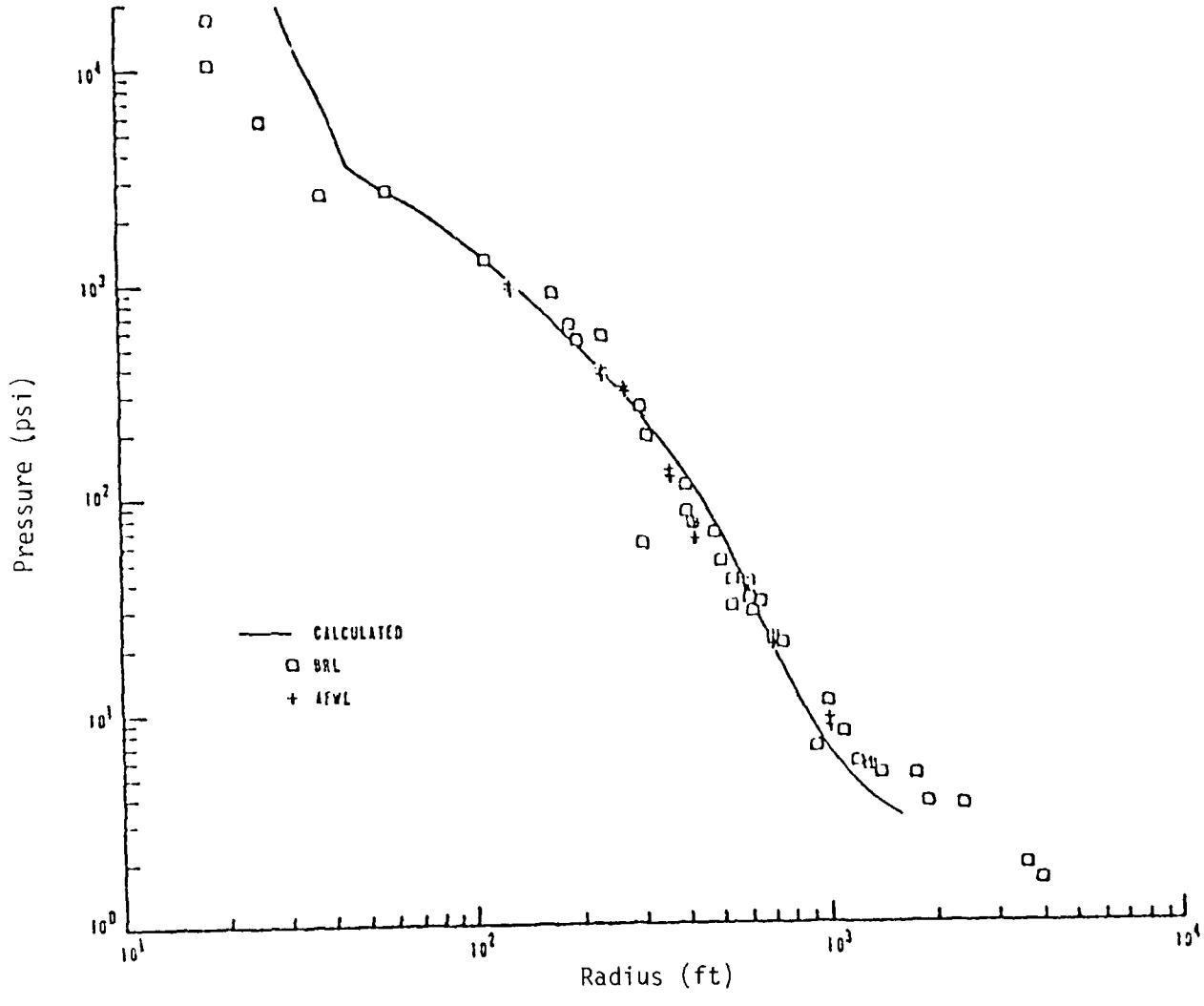

Figure 29. AFWL-MIXED COMPANY (overpressure versus radius).

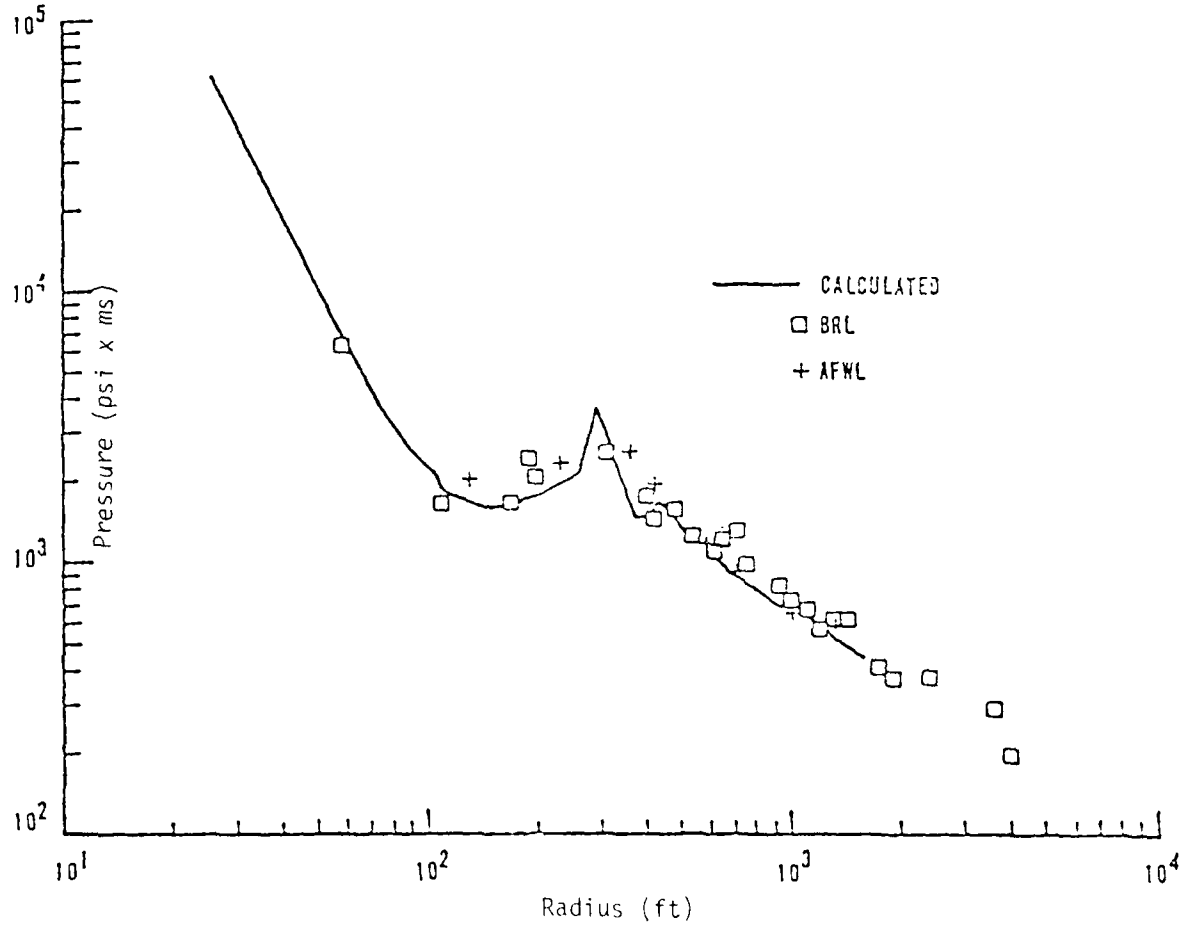

Figure 30. AFWL-MIXED COMPANY (overpressure impulse versus radius).

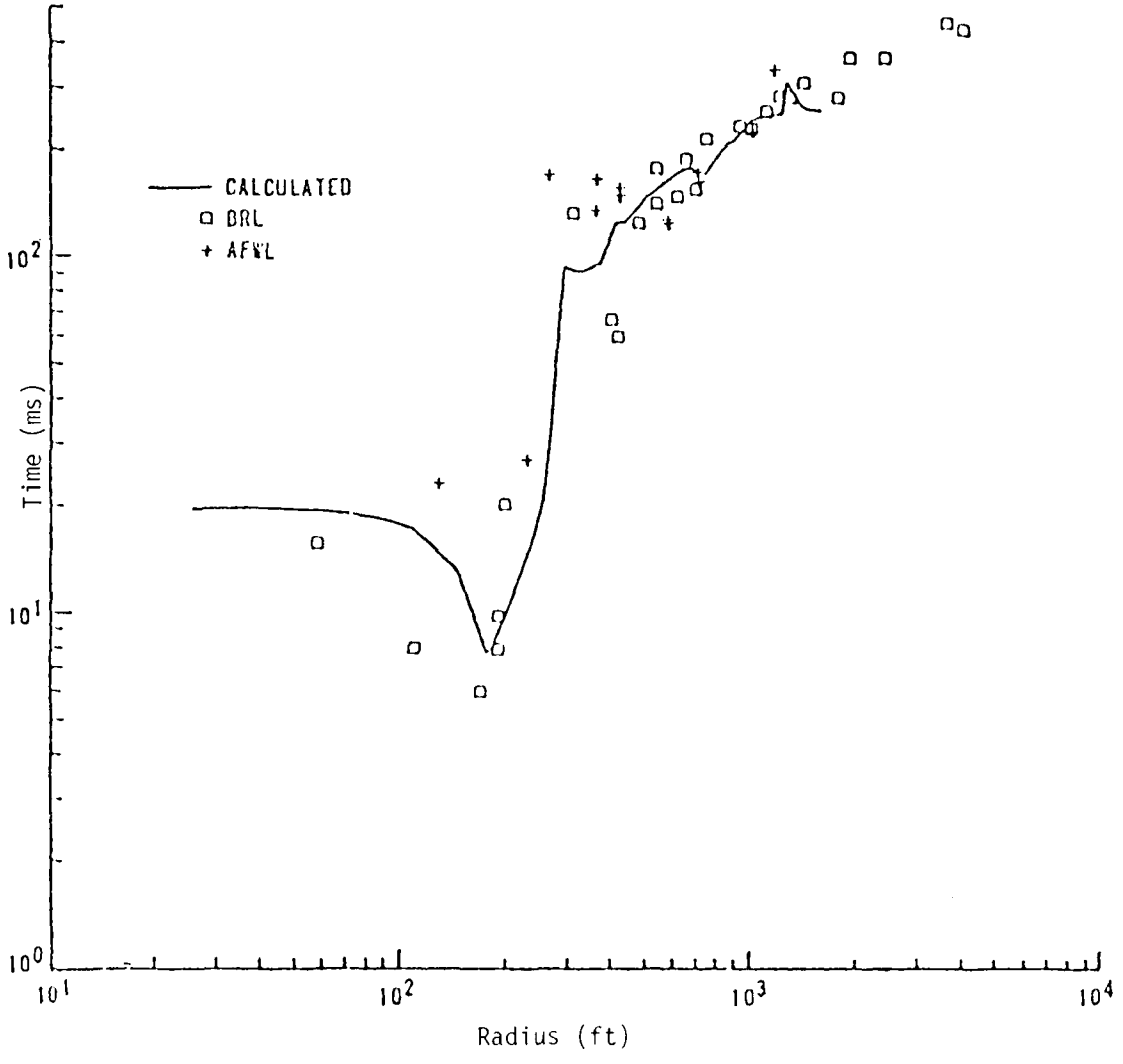

Figure 31. AFWL MIXED COMPANY (positive phase duration).

Dynamic pressure has not been measured directly in the past. The normal method used is to infer the dynamic pressure from measurements of the total pressure and the overpressure at the same point. Several smoothing techniques are used in an attempt to reduce any accentuated differences which appear as high frequency oscillations. The inference of dynamic pressure "data" for MIXED COMPANY is further complicated by the fact that total pressure gages were not at the same locations as the overpressure gages. The former were 3 feet above ground, whereas the latter were at ground level. The HULL calculations predict significant pressure gradients between ground level and 3 feet, which if they exist would tend to lower the inferred dynamic pressure. This may be responsible for the disagreement between the calculations and inferred data shown in Figure 32.

Reference 4 also presents comparisons with data taken for Dipole West, shots 8 and 11. Those experiments used two charges detonated one above the other such that the distance between charges was twice that of the lower charge above the ground, thus enabling direct comparisons between real, ideal surfaces, and calculations. Figure 33 provides an example of the excellent agreement attained. From this figure one can infer that the calculations seem to be providing the flow field accurately, not just near the ground.

Some of the most carefully performed experiments in recent years were made by Carpenter at TRW. A large number of triply redundant detonations of PBX-9404 spheres were exploded over a polished concrete slab. HULL calculations were performed by the AFWL in support of this project. Figures 34 and 35 show although HULL is missing the abs peaks the integrated waveforms (impulse) show excellent agreement.

Finally, for PRE DICE THROW Event 2 (a 6 ton detonation of a capped cylinder of AN/FO) a HULL calculation was performed for a geometry never before done and for a relatively unknown explosive. Figure 36 compares the experimental and calculated overpressure peaks. Agreement was excellent; the calculated waveforms were virtually the same as those measured.

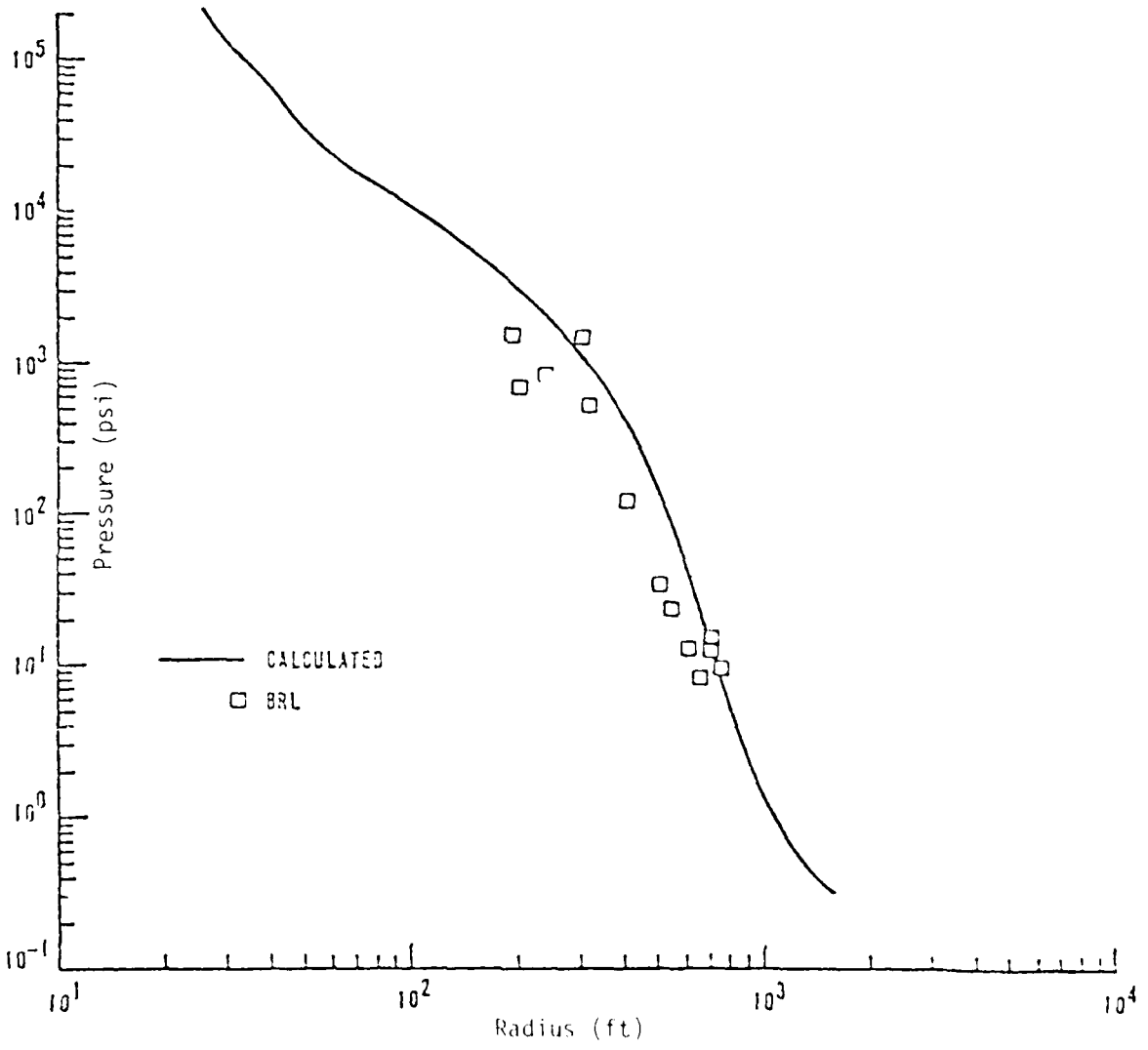

Figure 32. AFWL MIXED COMPANY (horizontal dynamic pressure).

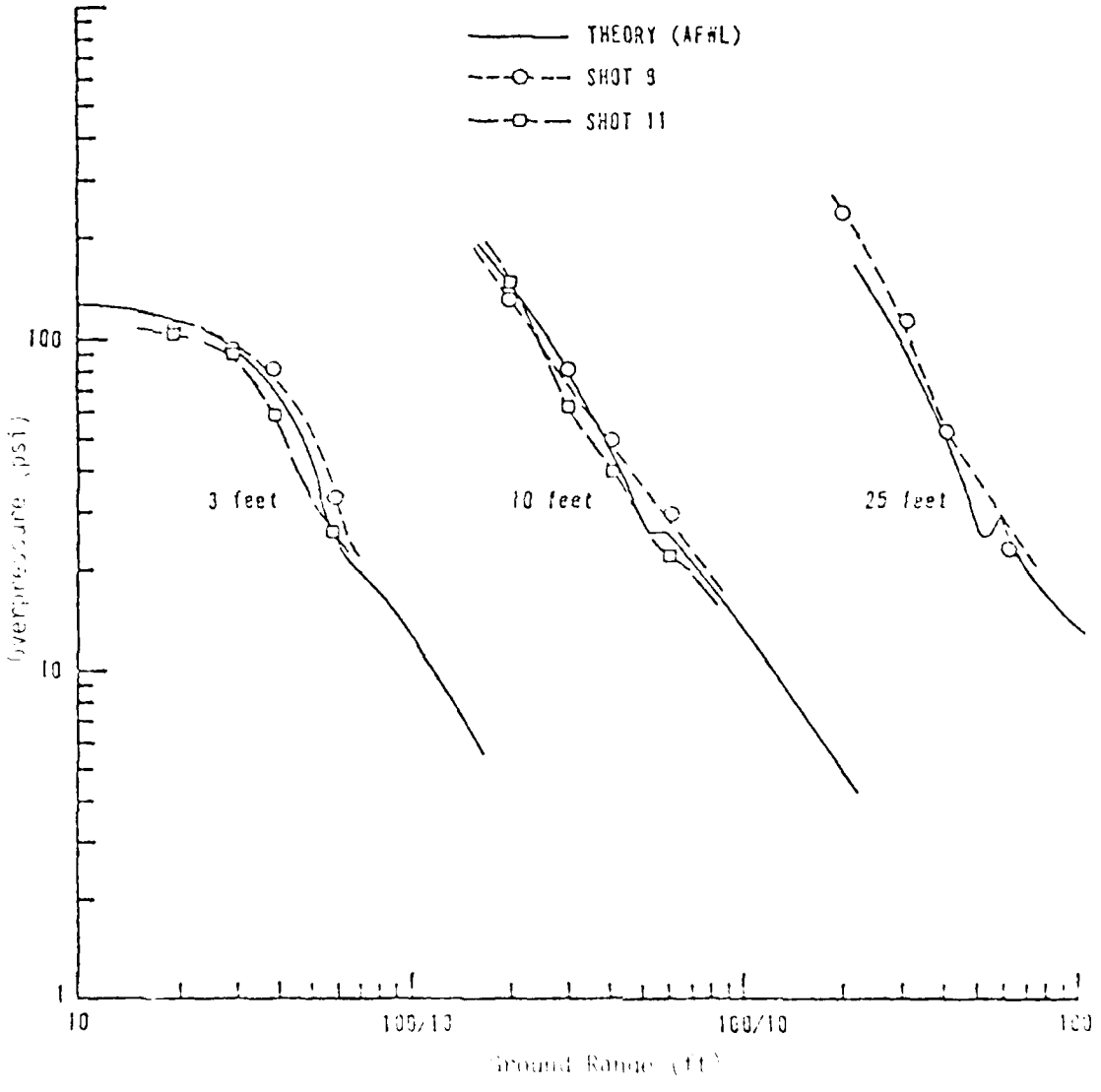

Figure 33. Comparison of calculated and experimental maximum overpressures at 3, 10, and 25 feet; Shots 9 and 11, Dipole West.

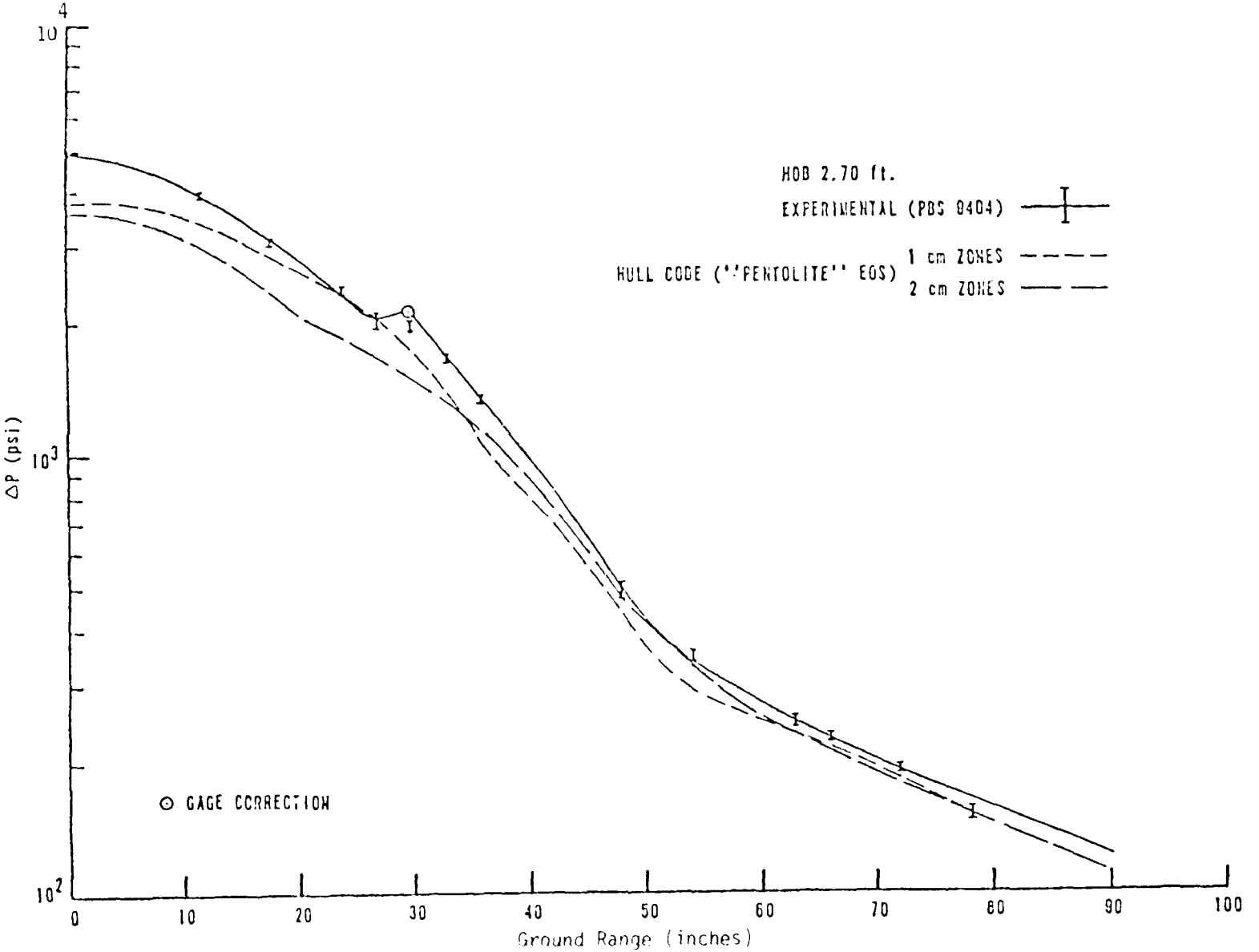

Figure 34. Surface overpressure versus ground range for 8 pound HE spheres.

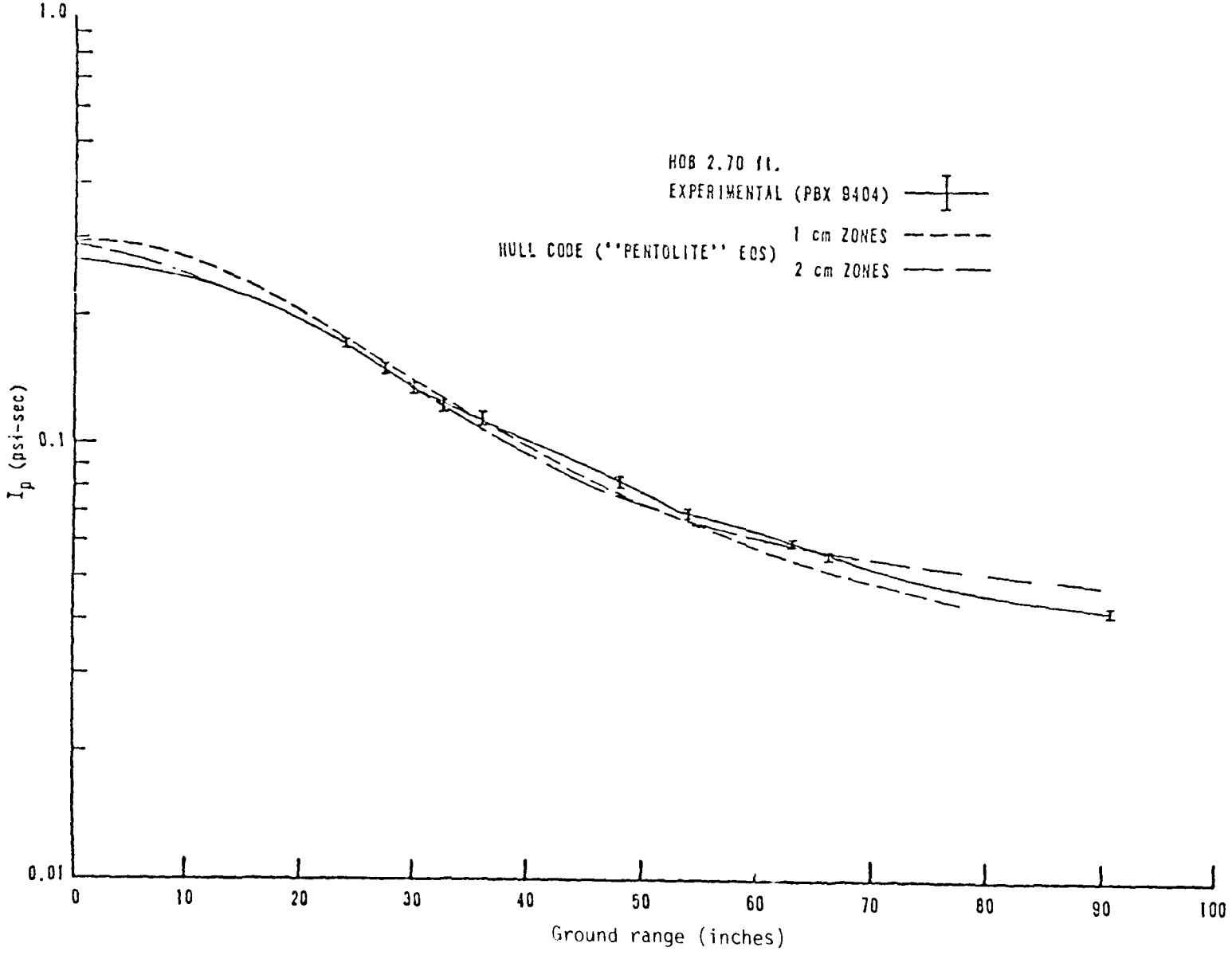

Figure 35. Positive phase impulse versus ground range for 8 pound HE spheres.

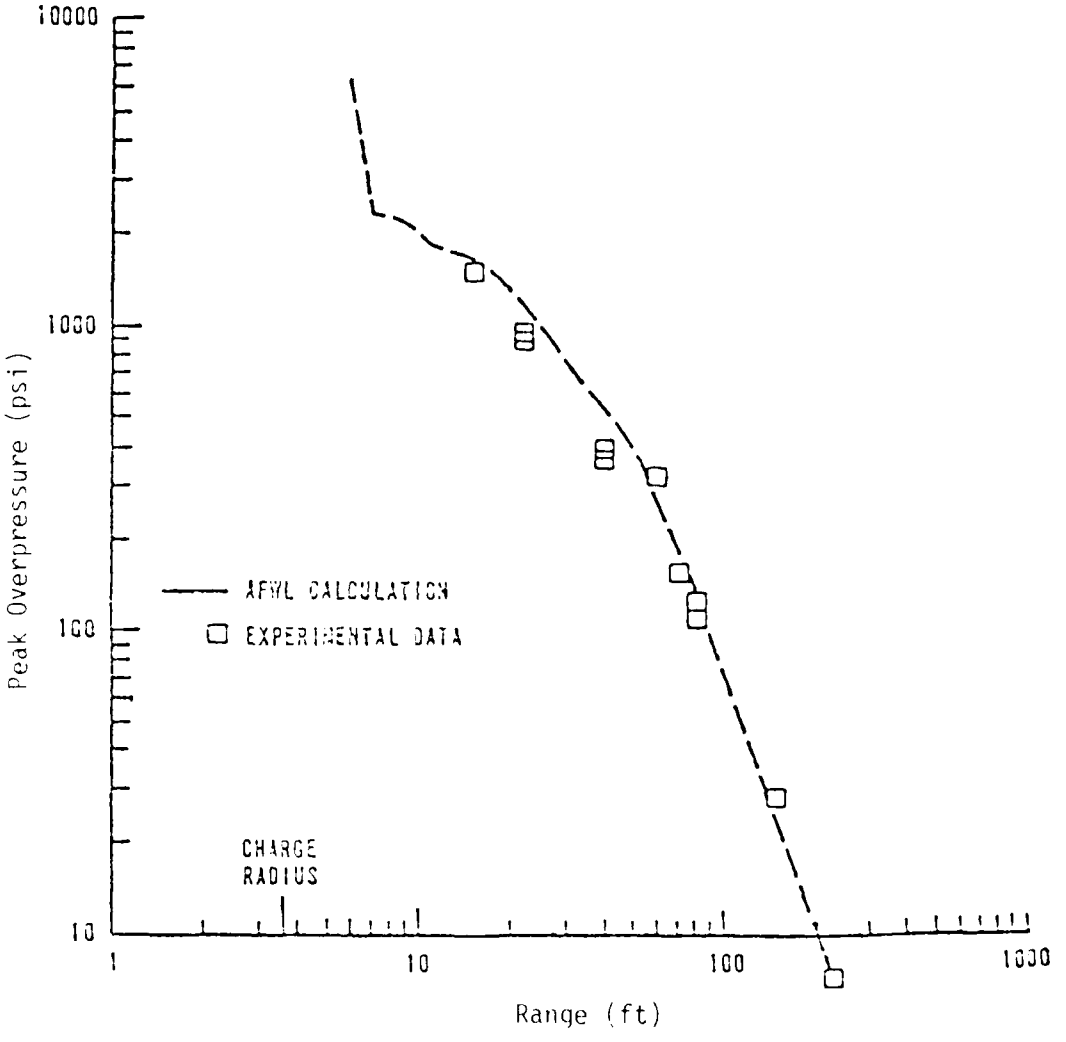

Figure 36. Pre DICE THROW 1 calculation (Event 2).

APPENDIX B

RESULTS FOR FCT IN HULL

This appendix contains some of the results of calculations performed for the initial evaluation of the effects of the Flux Corrected Transport (FCT) algorithm which has been incorporated into the self-contained in-core version of HULL. This algorithm and its implementation in HULL were described in Section 3.

An isothermal sphere was selected as the test calculation, and was performed three times with the conditions that follow:

Calculation Number	Description
1.0010	HULL without FCT; DX=DY=10. cm
1.0005	HULL without FCT; DX=DY=5. cm
2.0010	HULL with FCT; DX=DY=10. cm

In each calculation the initial conditions were the same, and are the following: (c.f. Figure 13).

Ambient Conditions:

Air Mass Density - 1.22×10^{-3} gm-cm^{-3}

Air Internal Energy - 2.06×10^{9} erg-gm^{-1}

Isothermal Sphere:

Air Internal Energy - 2.00×10^{10} erg-gm^{-1}

Sphere Radius - 2.00×10^{2} cm.

During each calculation, the mesh variables in column I = 1, Row J = 1, and diagonal I = J were obtained at a set of standard times, at intervals of 10^{-3} second. Figures 37 through 43 contain histograms of the pressure in the column of cells adjacent to the Y-axis (I = 1, J), c.f. Figure 13. Figures 44 through 50 contain histograms of the mass

density in this same column of cells. In all histograms the solid line represents data from calculation 1.0010 (without FCT); the data represented by points are data from calculation 2.0010 (with FCT). The FCT algorithm was operative from the start of calculation 2.0010; thus, these results reflect FCT throughout the duration of the calculation, and do not represent adjustment of calculation 1.0010, at the standard times in the figures.

Investigation of the effects of FCT in one-dimensional calculations were continuing at AFWL. The results presented in Figures 37 through 50 for the two-dimensional isothermal sphere, exhibit behavior similar to that in the one-dimensional calculations. That is, some clipping of the shock peak (of Figures 37 through 43), and a plateau effect are observed in both kinds of calculations (reference 6).

In its current form, the FCT coding results in an overhead factor of twenty-five times the cost of the same calculation without FCT. This form of the FCT coding is however readily modified. Some work on reducing this overhead was conducted, and an efficient form of the FCT anti-diffusion phase can be constructed. The drawback to implementing a more efficient form is that the indexing is many levels deep and the code is in a form such that almost any change requires a significant rewrite and may require another storage structure and access method. It was concluded that until the final form of the algorithm is decided, the current FCT coding is adequate for FCT evaluation.

Pressure and density results along the x-axis were compared with those along the y-axis. There were no significant differences between the results along the two axes, and therefore those along J=1 are not shown.

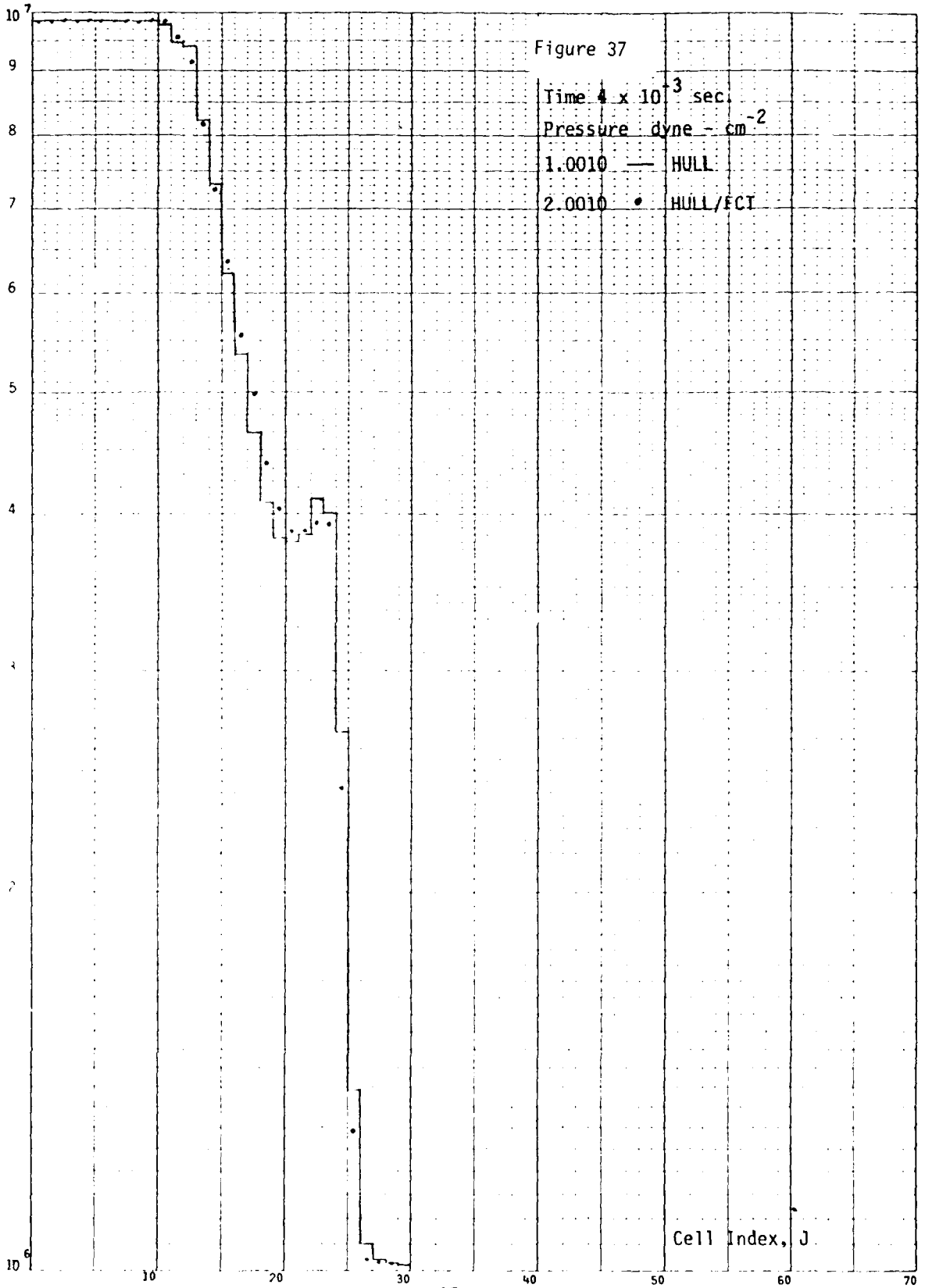
Figure 37
Time 4 x 10^-3 sec.
Pressure dyne - cm^-2
1.0010 — HULL
2.0010 • HULL/FCT
10^7
9
8
7
6
5
4
10^6
10
20
30
40
50
60
70
Cell Index, J

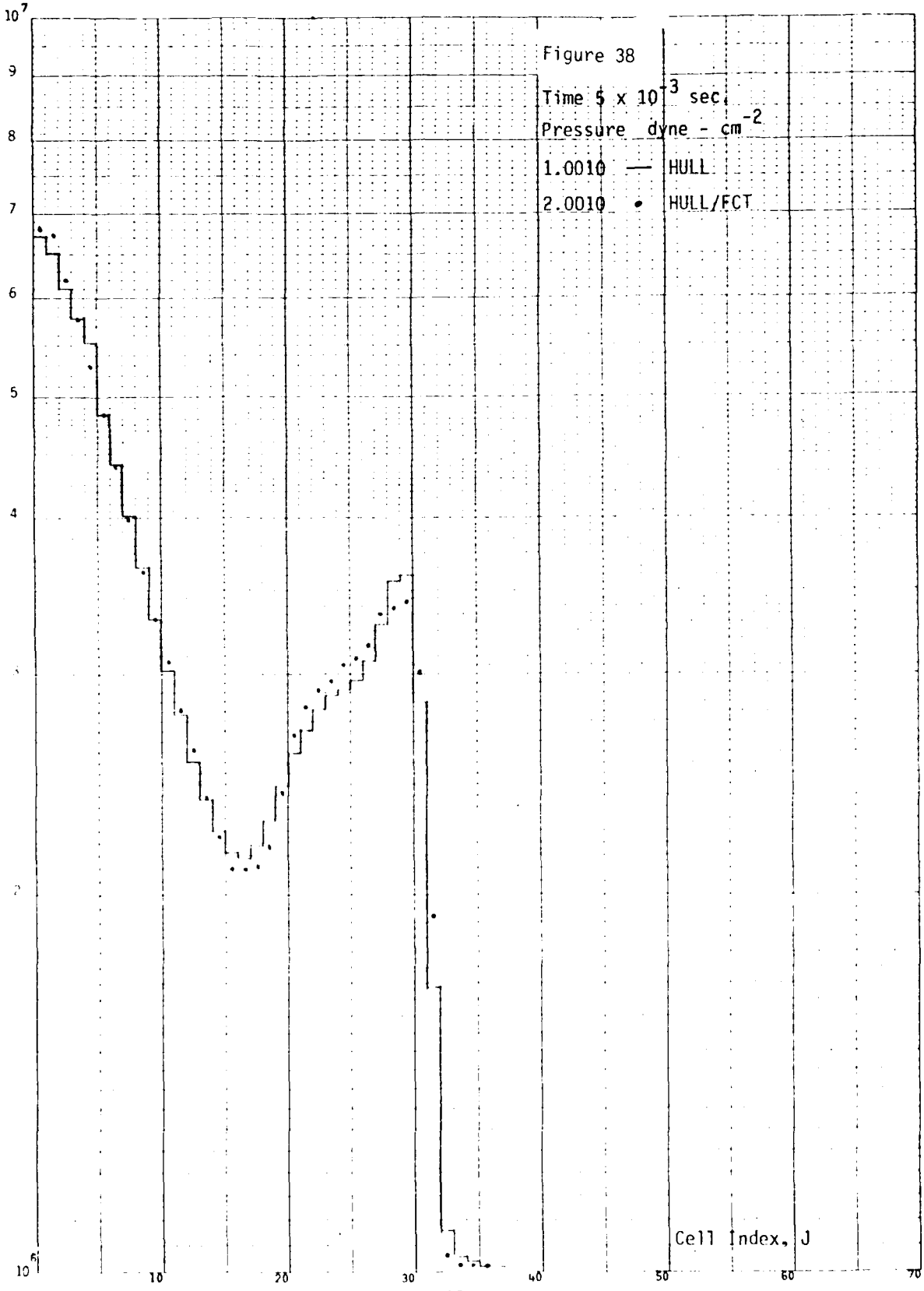
Figure 38
Time 5 x 10^-3 sec.
Pressure dyne - cm^-2
1.0010 — HULL
2.0010 • HULL/FCT
10^7
9
8
7
6
5
4
10^6
10
20
30
40
50
60
70
Cell Index, J

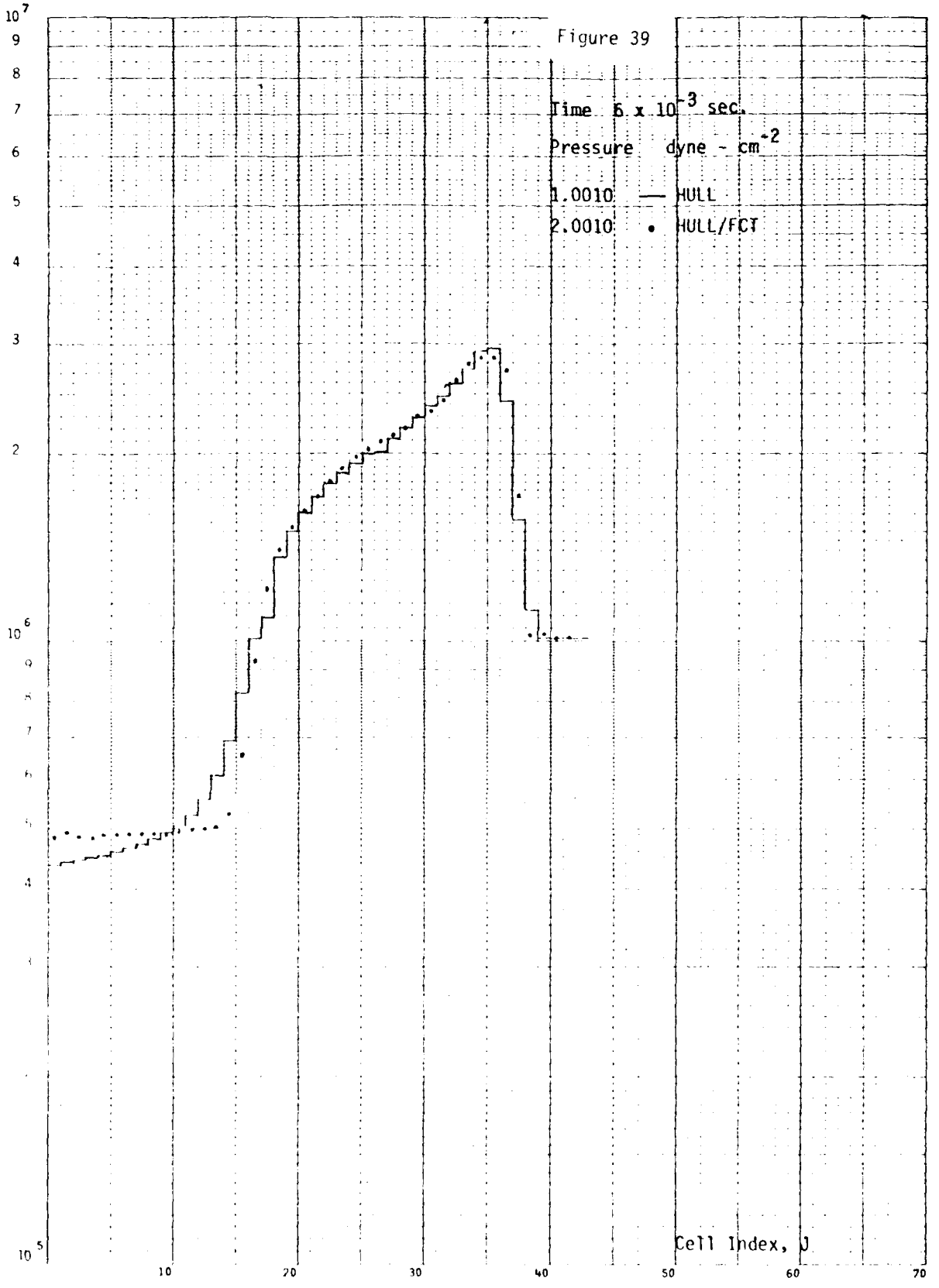
Figure 39
Time 6 x 10^-3 sec.
Pressure dyne - cm^-2
1.0010 — HULL
2.0010 • HULL/FCT
10^7
9
8
7
6
5
4
3
2
10^6
10^5
10
20
30
40
50
60
70
Cell Index, J

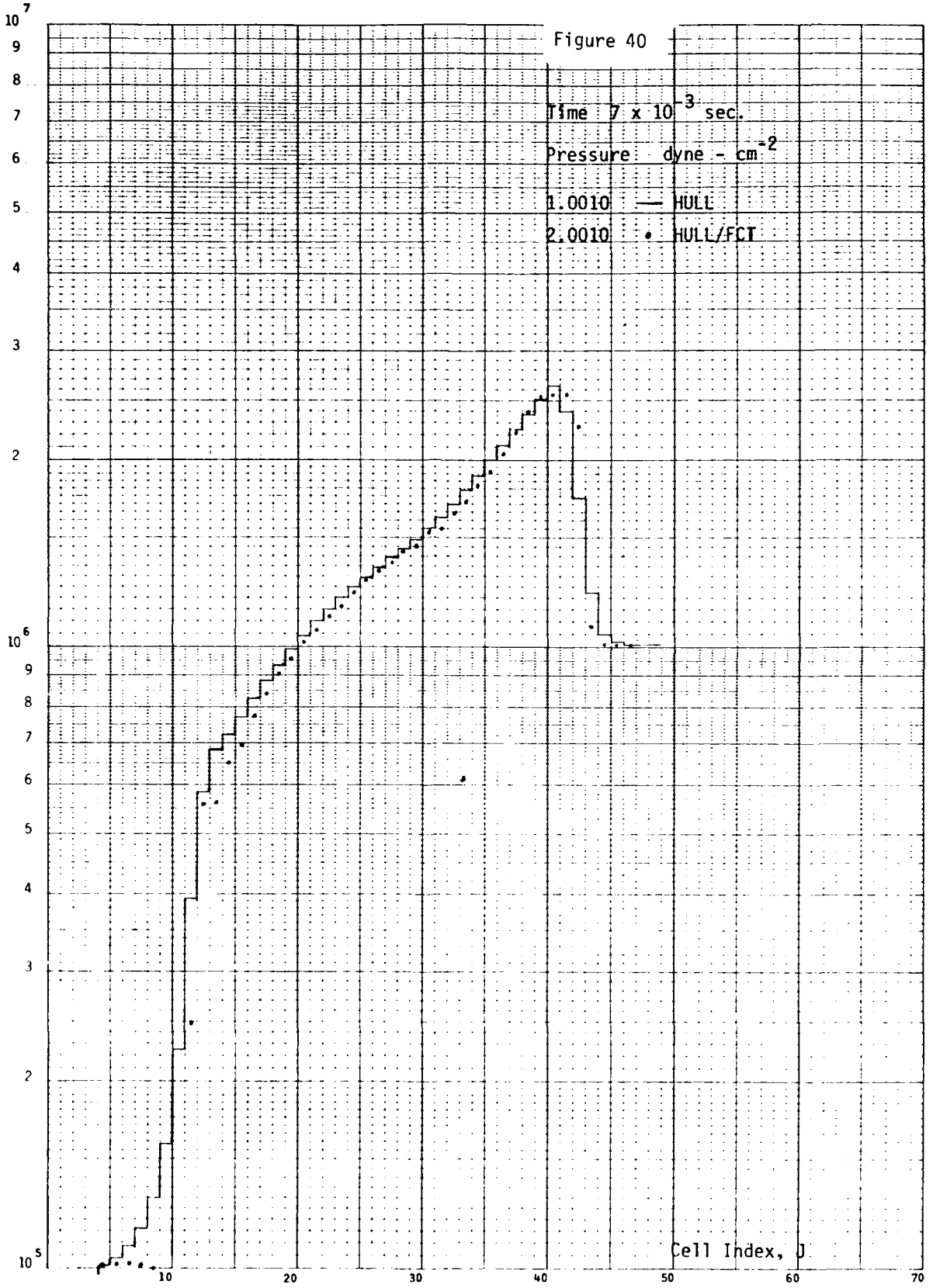
Figure 40
Time 7 x 10^-3 sec.
Pressure dyne - cm^-2
1.0010 — HULL
2.0010 • HULL/FCT
10^7
9
8
7
6
5
4
3
2
10^6
9
8
7
6
5
4
3
2
10^5
10
20
30
40
50
60
70
Cell Index, J

Figure 41

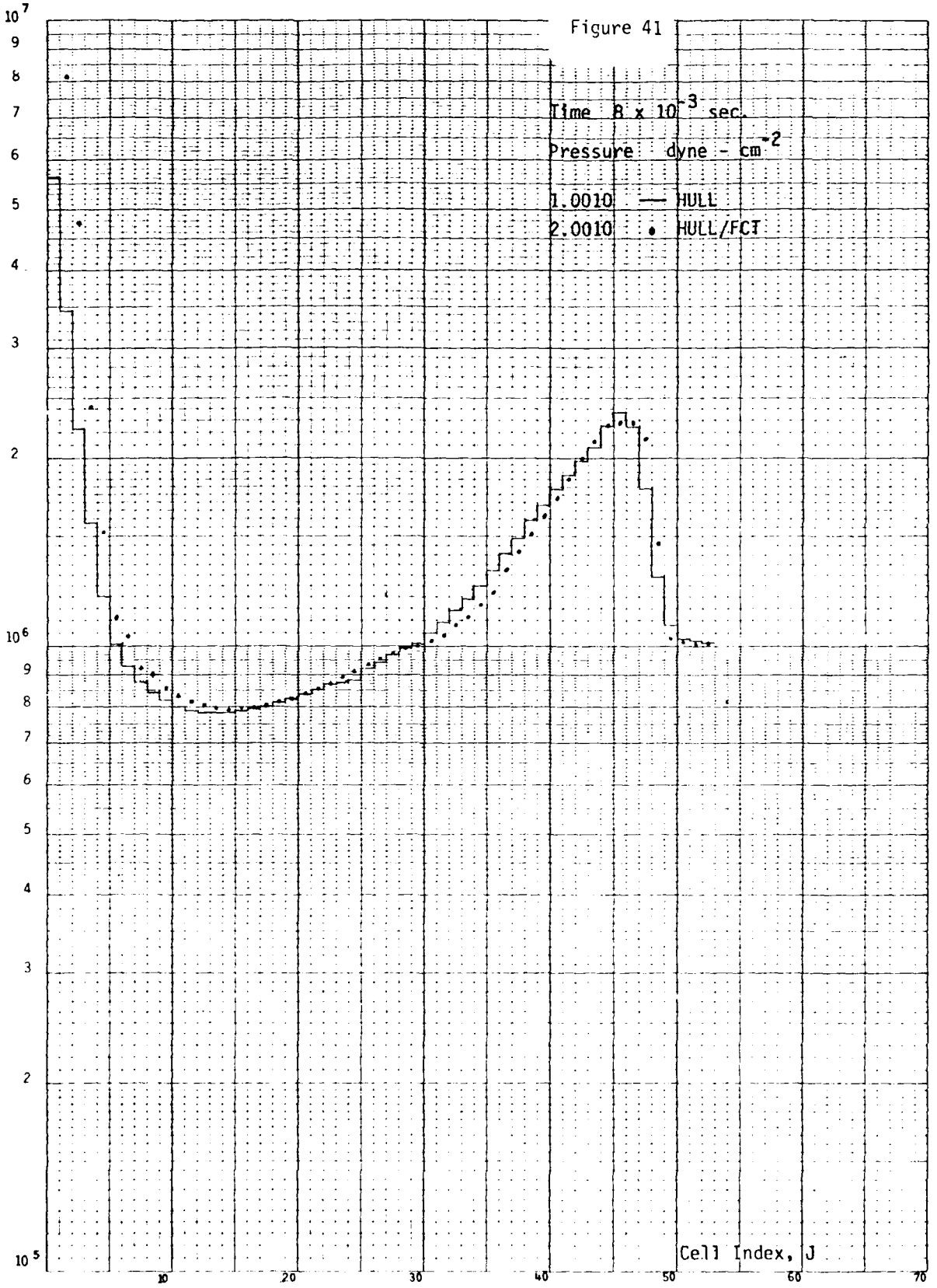
Time 8 x 10^-3 sec.
Pressure dyne - cm^-2
1.0010 — HULL
2.0010 • HULL/FCT
10^7
9
8
7
6
5
4
3
2
10^6
9
8
7
6
5
4
3
2
10^5
10
20
30
40
50
60
70
Cell Index, J


Figure 42
Time 9 x 10^-3 sec.
Pressure dyne - cm^-2
1.0010 — HULL
2.0010 • HULL/FCI
10^7
9
8
7
6
5
4
3
2
10^6
9
8
7
6
5
4
3
2
10^5
10

AD-A100 108 SCIENCE APPLICATIONS INC MCLEAN VA F/G 9/2
IMPROVEMENTS TO THE AFWL HULL CODE.(U)
JUN 79 B S CHAMBERS, J A HASDAL, W R THOMAS DNA001-78-C-0383
UNCLASSIFIED SAI-79-103-AQ DNA-5035F NL

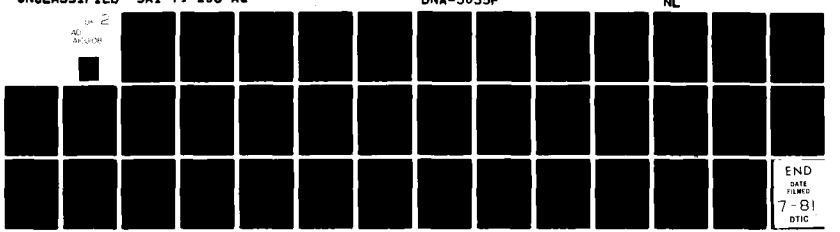

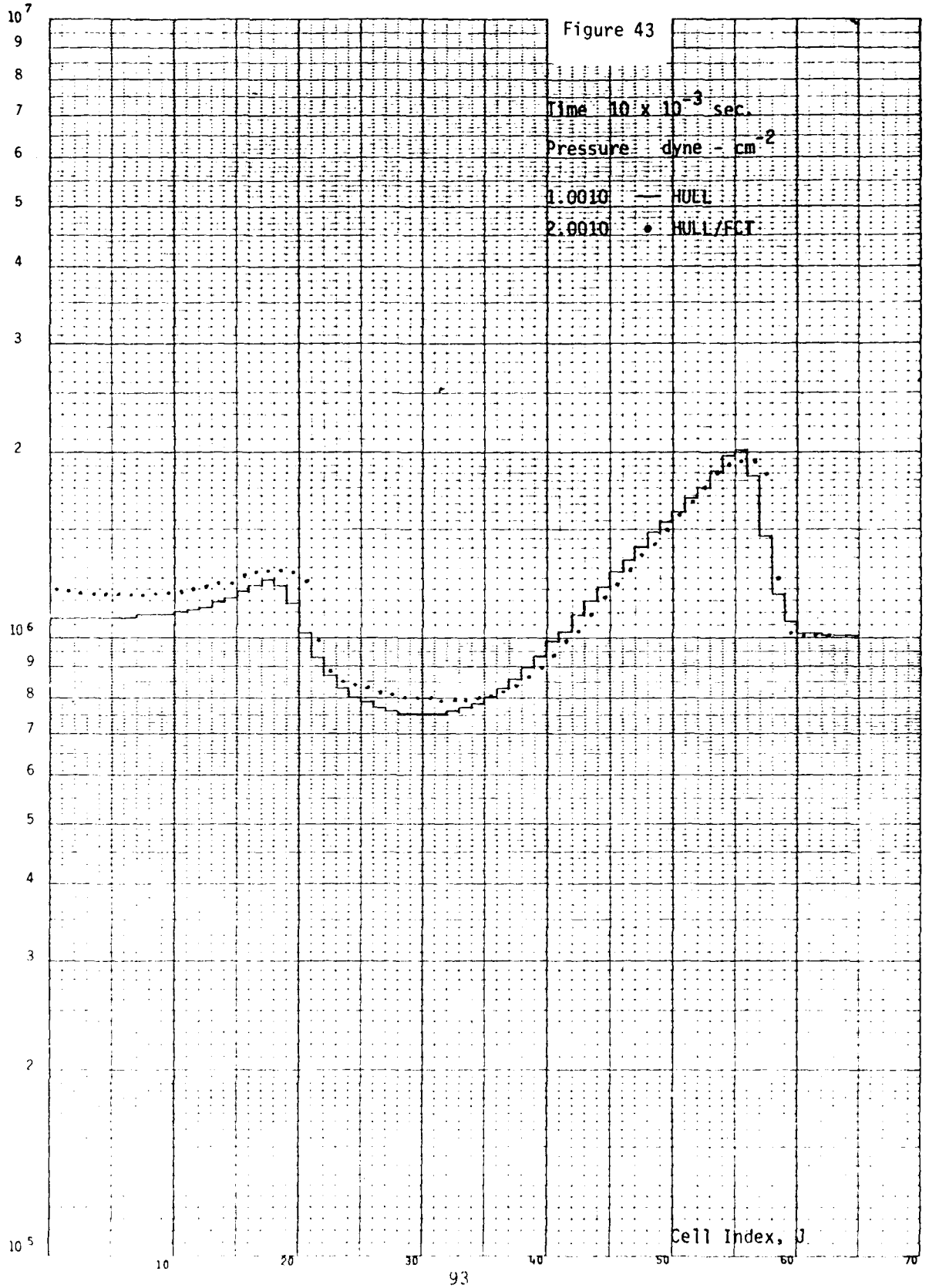
Figure 43
Time 10 x 10^-3 sec.
Pressure dyne - cm^-2
1.0010 — HULL
2.0010 • HULL/FCI
10^7
9
8
7
6
5
4
3
2
10^6
9
8
7
6
5
4
3
2
10^5
10
20
30
40
50
60
70
Cell Index, J

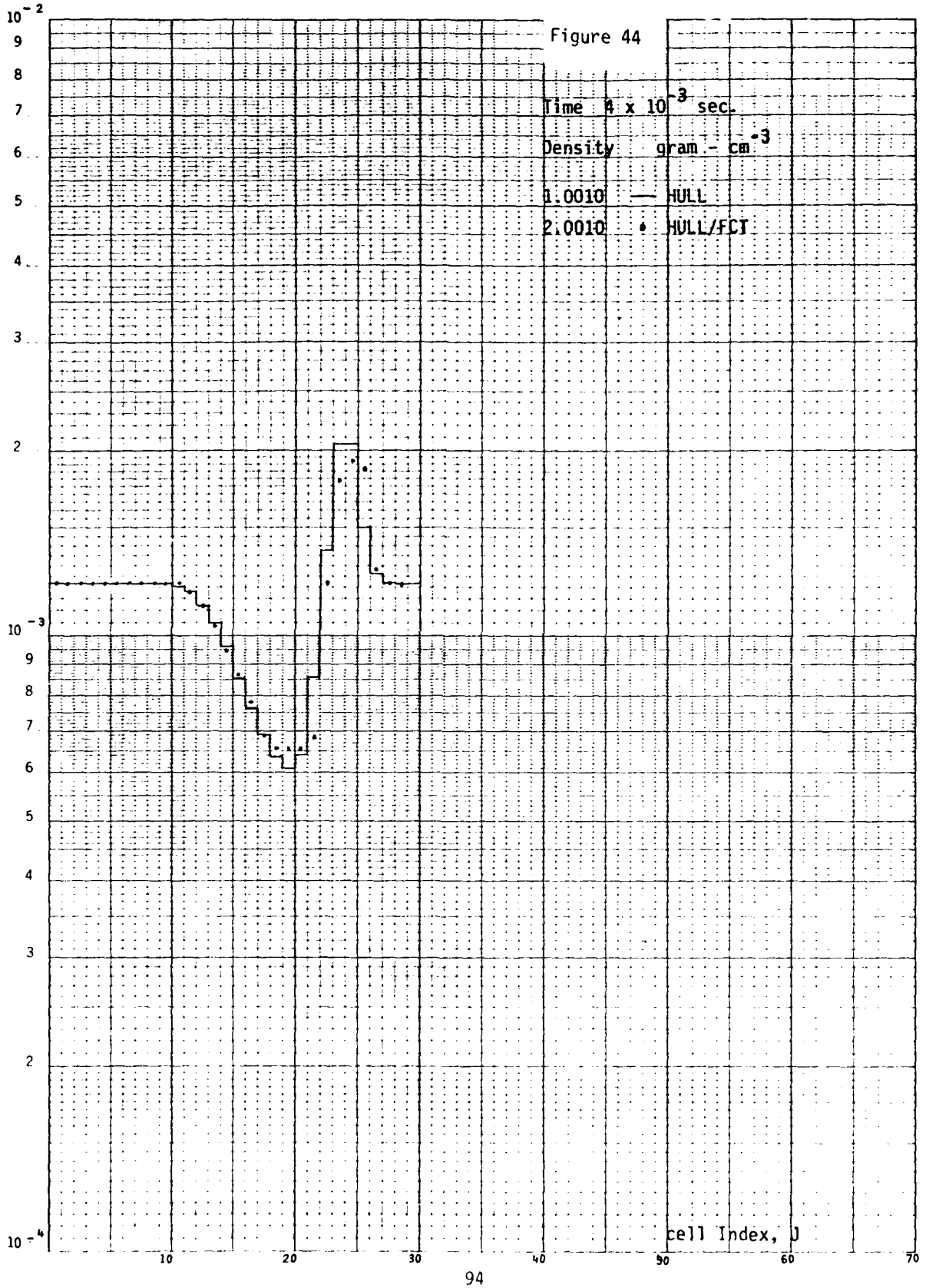
Figure 44
Time 4 x 10^-3 sec.
Density gram - cm^-3
1.0010 — HULL
2.0010 • HULL/FCT
10^-2
9
8
7
6
5
4
3
2
10^-3
9
8
7
6
5
4
3
2
10^-4
10
20
30
40
50
60
70
cell Index, J

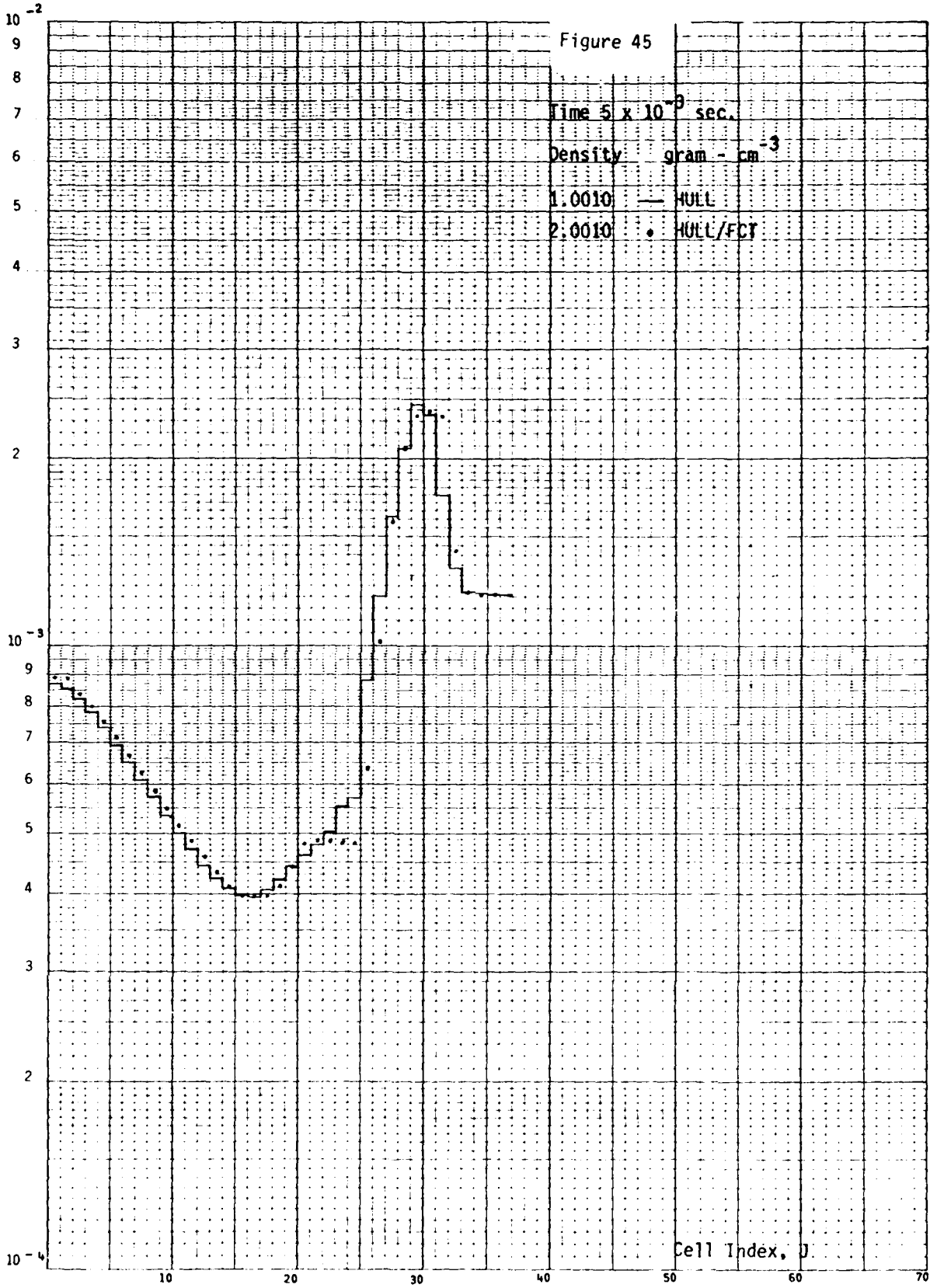
Figure 45
Time 5 x 10^-9 sec.
Density gram - cm^-3
1.0010 — HULL
2.0010 • HULL/FCT
10^-2
9
8
7
6
5
4
3
2
10^-3
9
8
7
6
5
4
3
2
10^-4
10
20
30
40
50
60
70
Cell Index, J

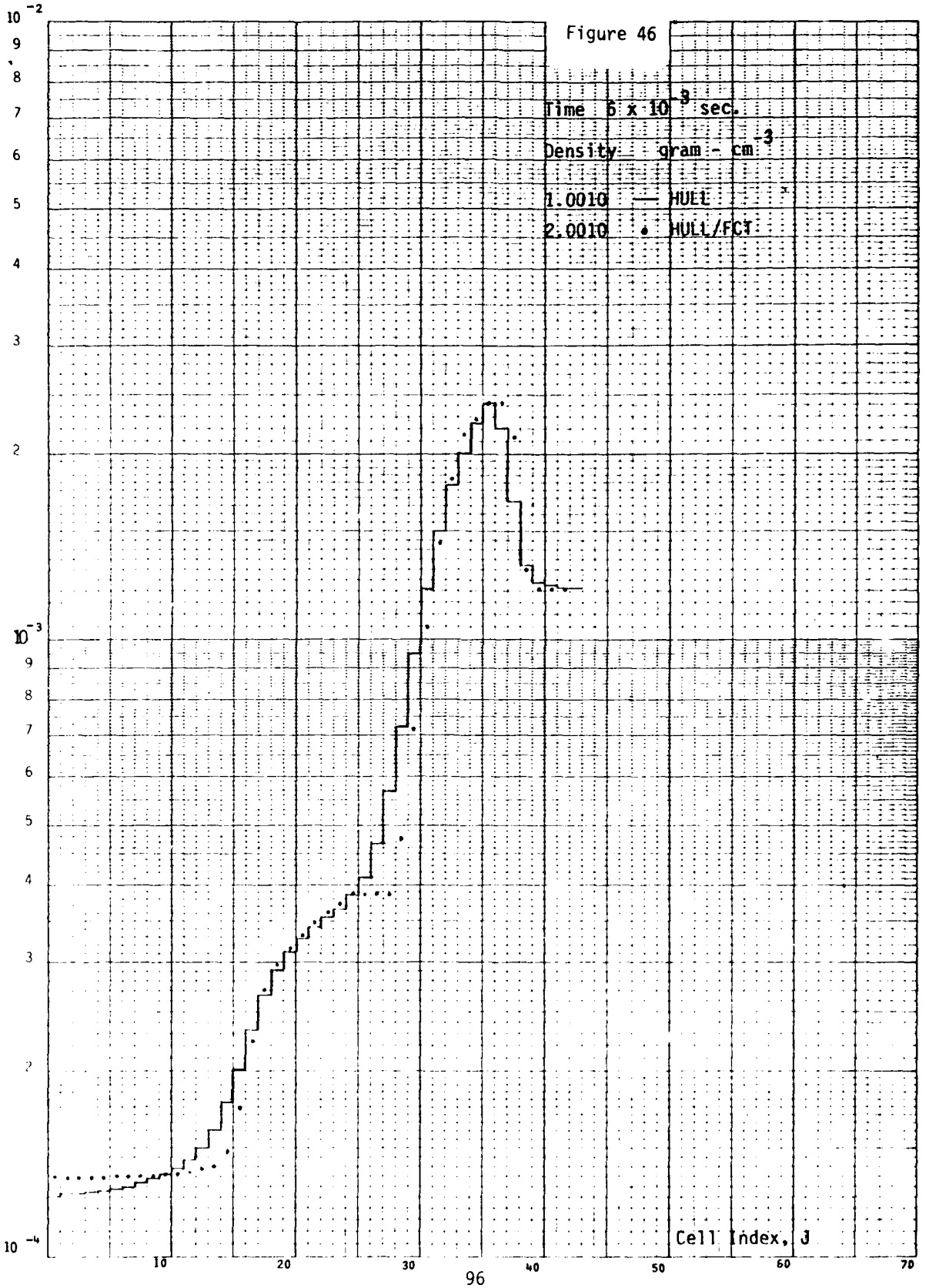
Figure 46
Time 6 x 10^-3 sec.
Density gram - cm^-3
1.0010 — HULL
2.0010 • HULL/FCT
10^-2
9
8
7
6
5
4
3
2
10^-3
9
8
7
6
5
4
3
2
10^-4
10
20
30
40
50
60
70
Cell Index, J

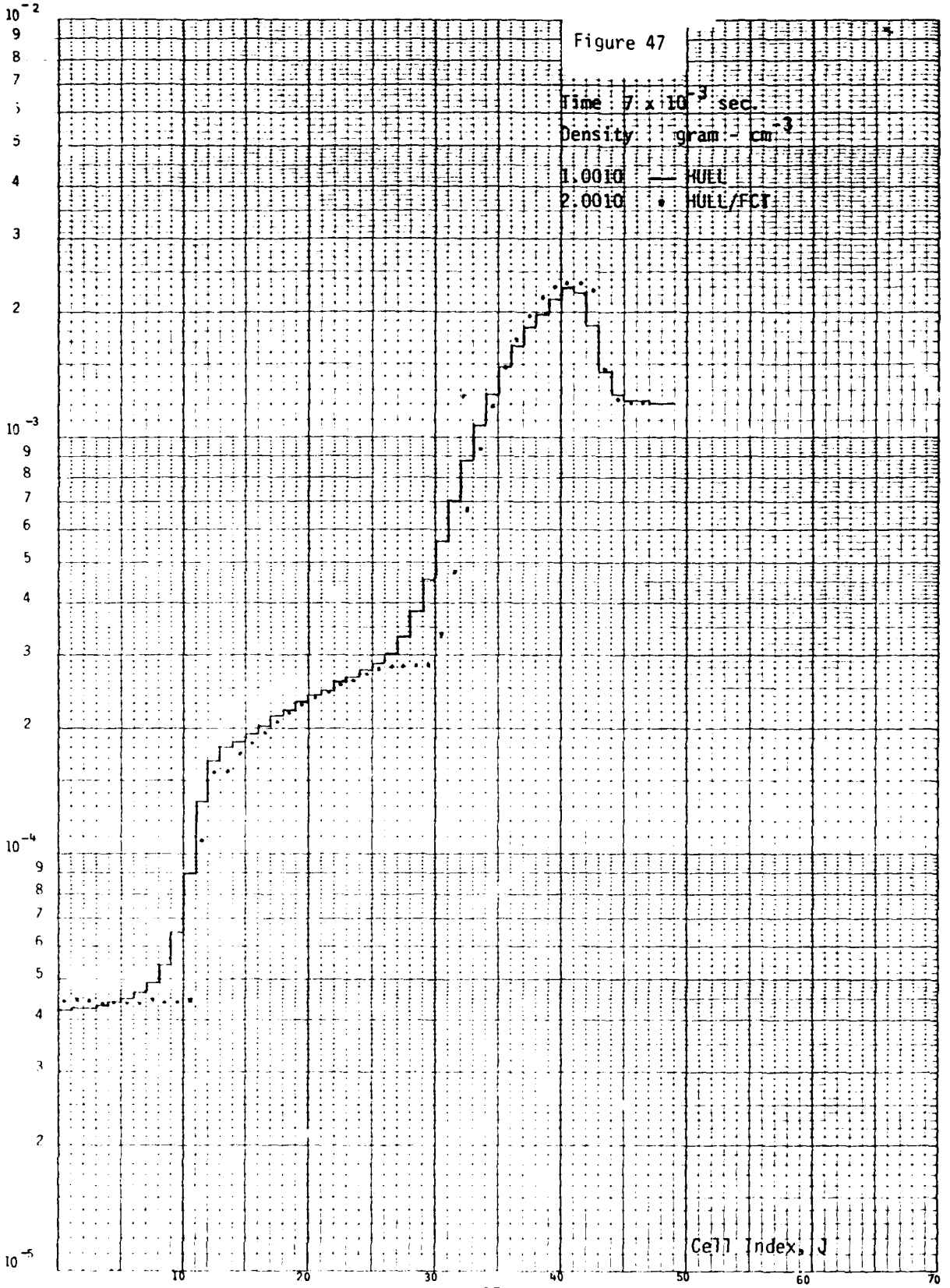
Figure 47
Time 7 x 10^-3 sec.
Density gram - cm^-3
1.0010 — HULL
2.0010 • HULL/FCT
10^-2
9
8
7
6
5
4
3
2
10^-3
9
8
7
6
5
4
3
2
10^-4
9
8
7
6
5
4
3
2
10^-5
10
20
30
40
50
60
70
Cell Index, J

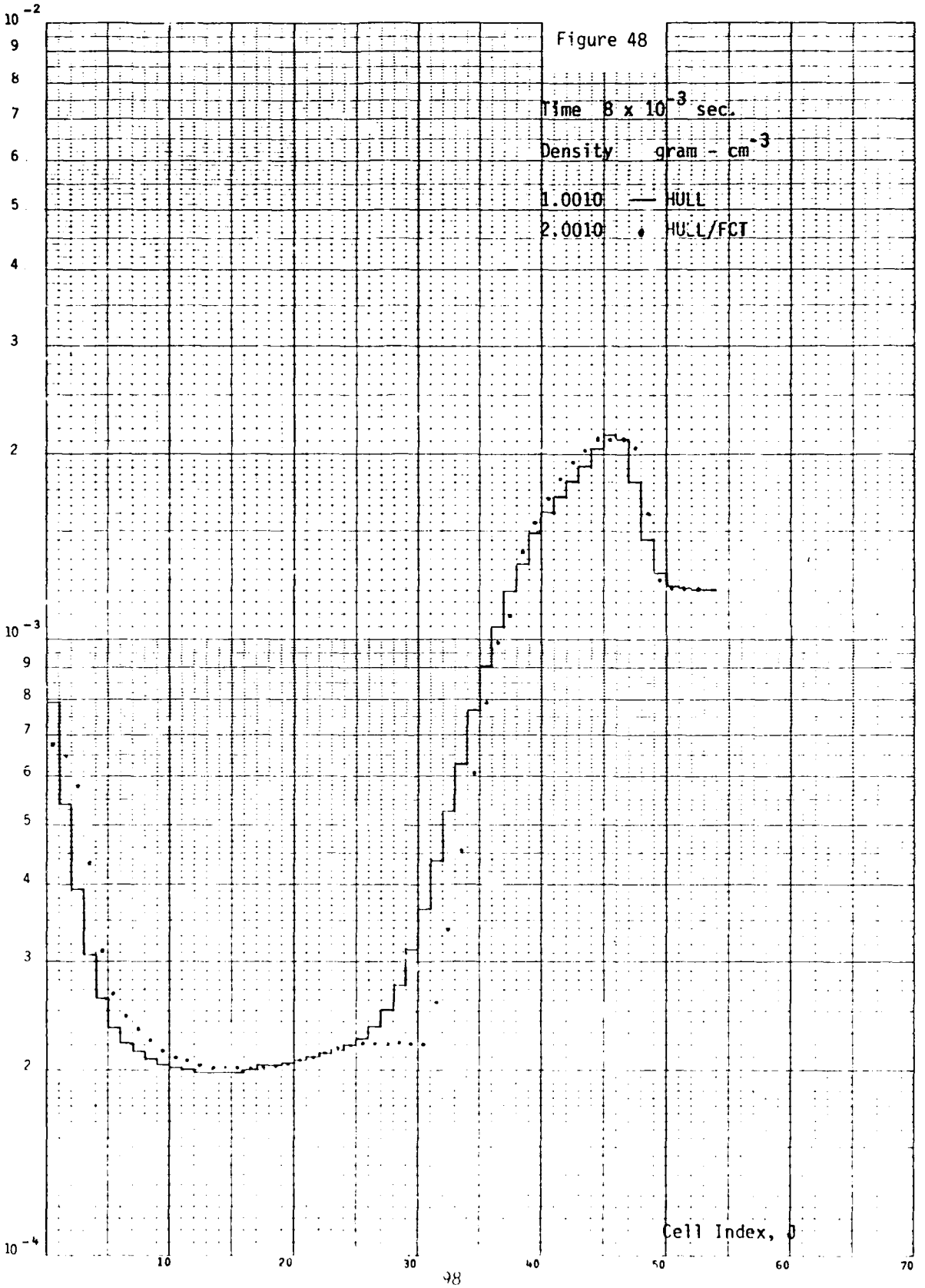
Figure 48
Time 8 x 10^-3 sec.
Density gram - cm^-3
1.0010 — HULL
2.0010 • HULL/FCT
10^-2
9
8
7
6
5
4
3
2
10^-3
9
8
7
6
5
4
3
2
10^-4
10
20
30
40
50
60
70
Cell Index, J

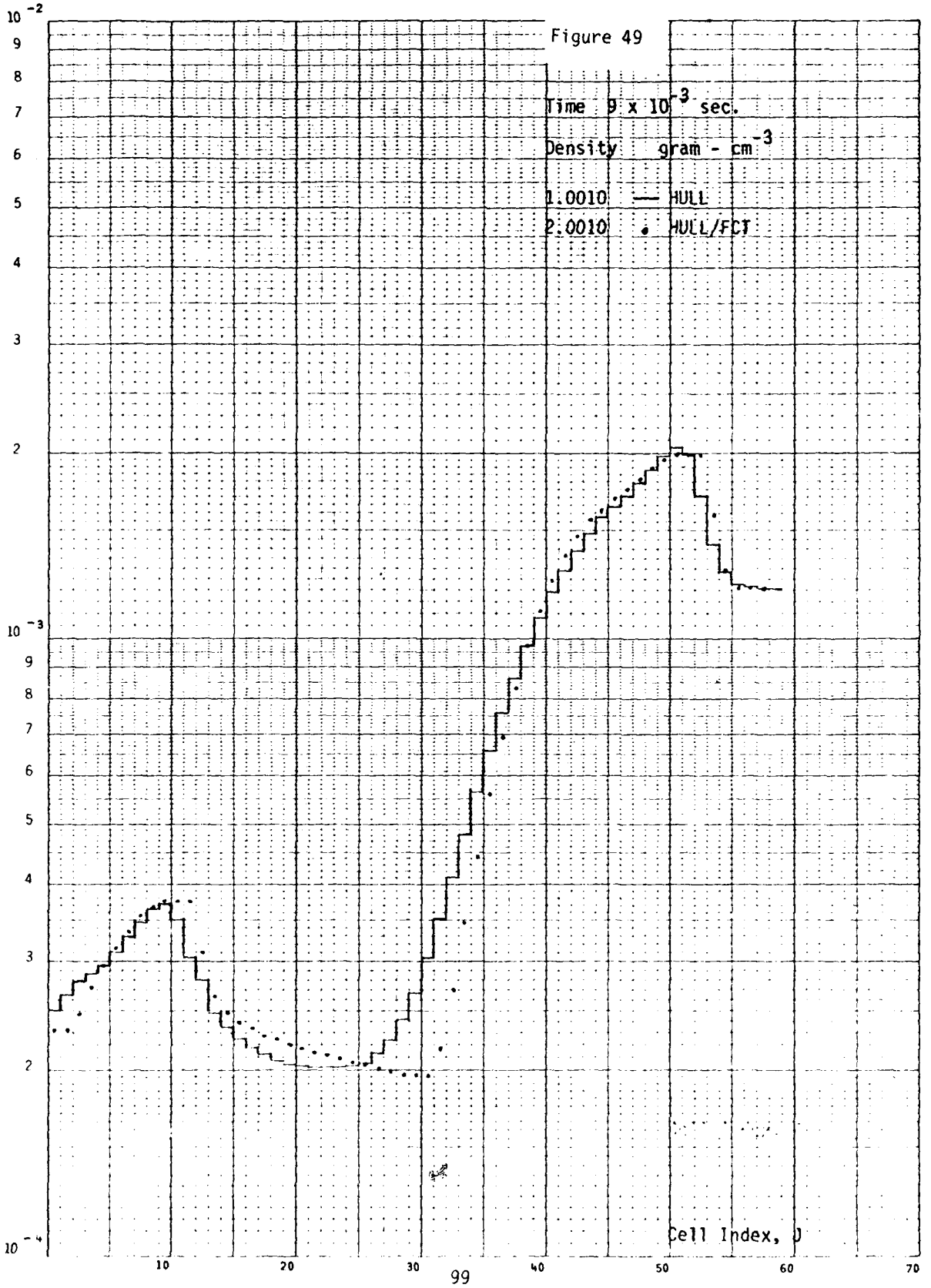
Figure 49
Time 9 x 10^-3 sec.
Density gram - cm^-3
1.0010 — HULL
2.0010 • HULL/FCT
10^-2
9
8
7
6
5
4
3
2
10^-3
9
8
7
6
5
4
3
2
10^-4
10
20
30
40
50
60
70
Cell Index, J

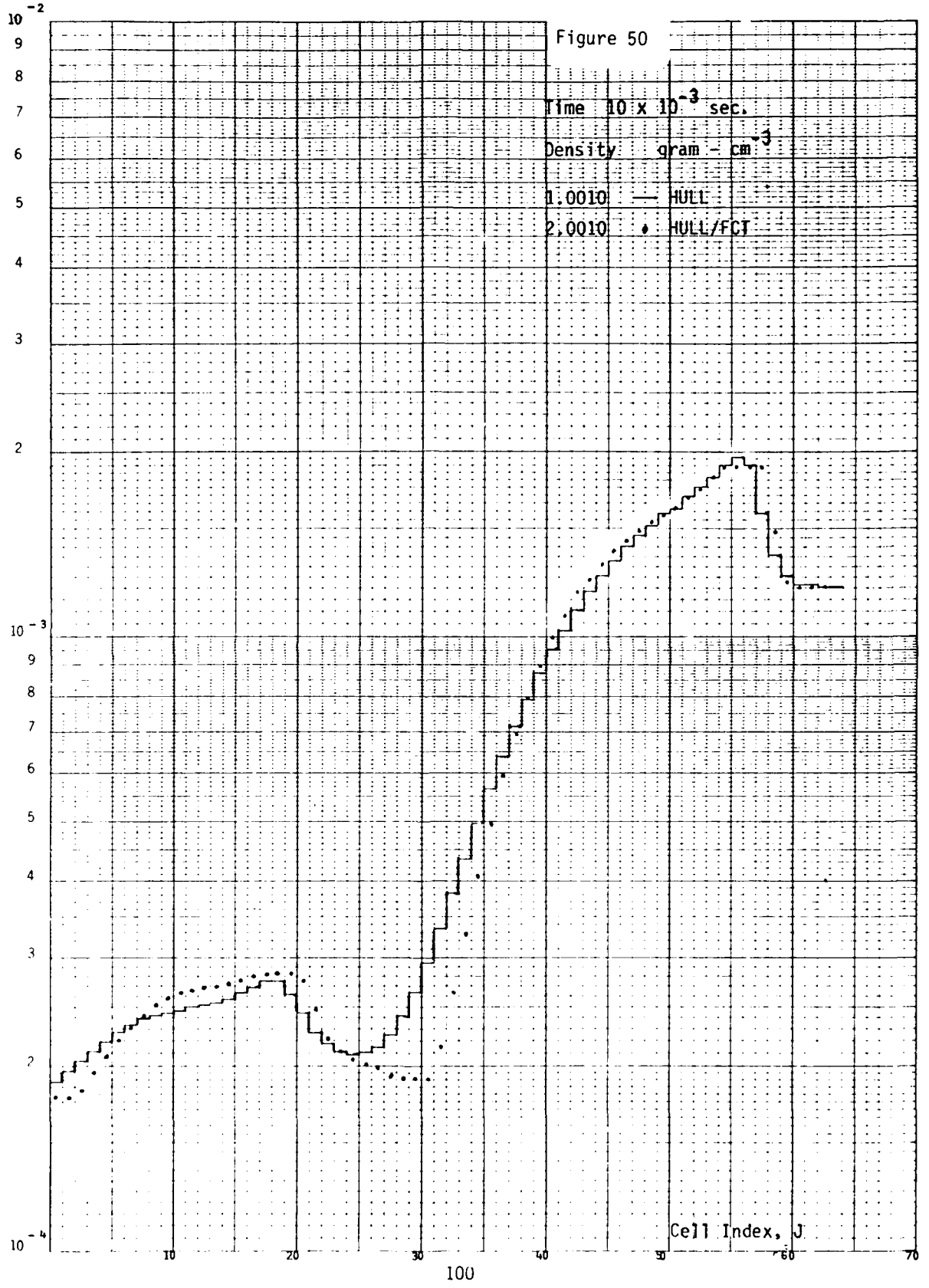
Figure 50
Time 10 x 10^-3 sec.
Density gram - cm^-3
1.0010 — HULL
2.0010 • HULL/FCT
10^-2
9
8
7
6
5
4
3
2
10^-3
9
8
7
6
5
4
3
2
10^-4
10
20
30
40
50
60
70
Cell Index, J

Figures 51 through 53 contain plots of pressure at three selected problem times. These plots extend through the mesh along the radial line defined by the cells with cell indexes I = J. The distances between cell centers in this direction is $\sqrt{2}$ times greater than that of either the I = 1 (column) or J = 1 (row) directions, and therefore these figures have been plotted to the same scale as the row and column plots by multiplying the cell index, I or J, by $\sqrt{2}$. These are seen to be comparable to those along I = 1.

Figures 54 through 59 contain the pressure and density profiles through the I = 1 column for calculation 1.0005 at times of 4, 5, and 6×10^{-3} seconds. The following observations result from comparisons with the corresponding data shown for the larger zoned calculations. Calculation 1.0005 contains more detailed structure in the vicinity of the shock front. The local extreme values are sometimes 5% to 10% different in magnitude when comparing the 5 cm and 10 cm zone calculations without FCT. The 10 cm zone calculation with FCT does not preferentially correct at 10 cm zone calculation toward the values of the 5 cm zone calculation.

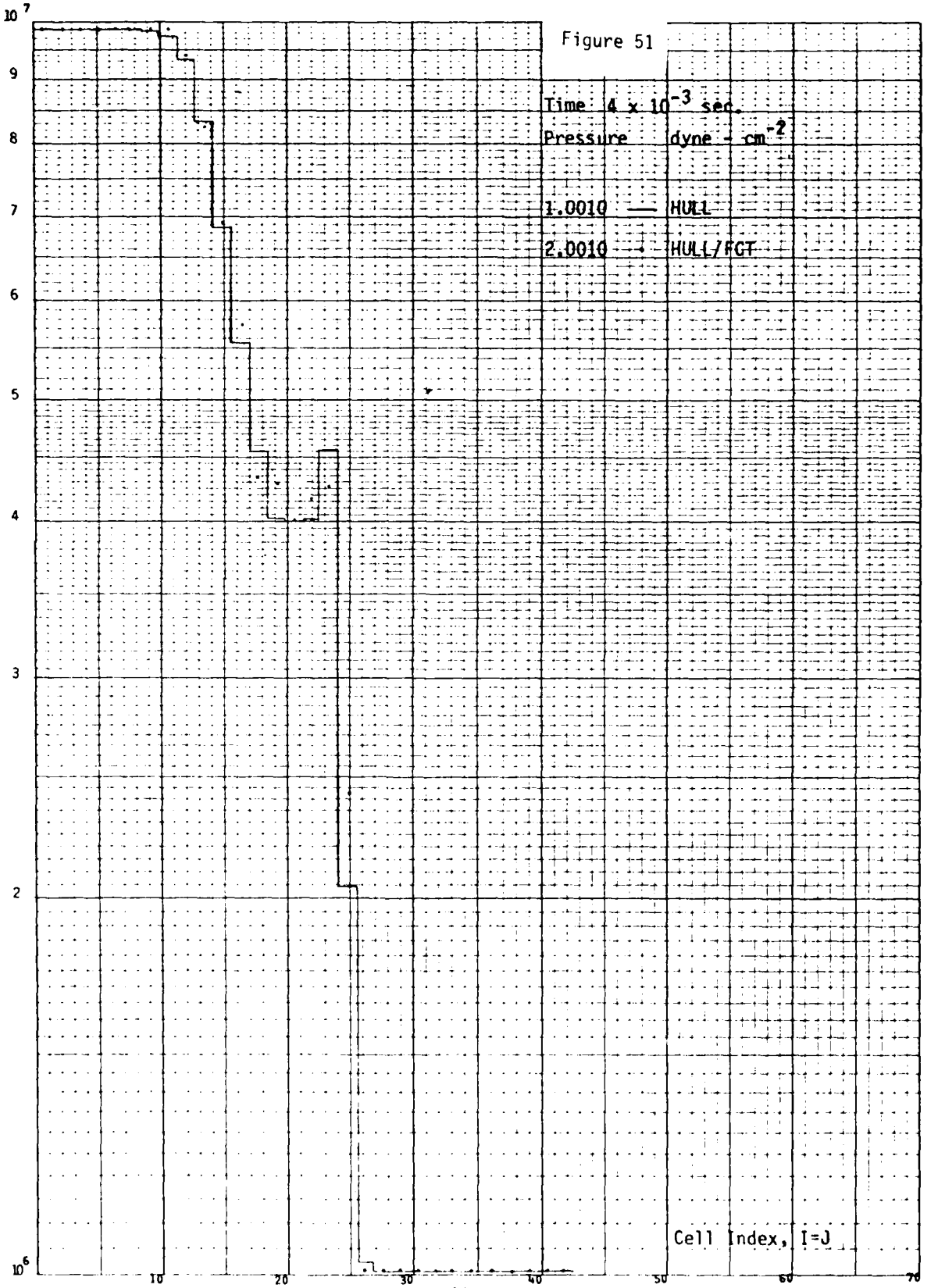
Figure 51
Time 4 x 10^-3 sec.
Pressure dyne - cm^-2
1.0010 — HULL
2.0010 - HULL/FCT
10^7
9
8
7
6
5
4
3
2
10^6
10
20
30
40
50
60
70
Cell Index, I=J

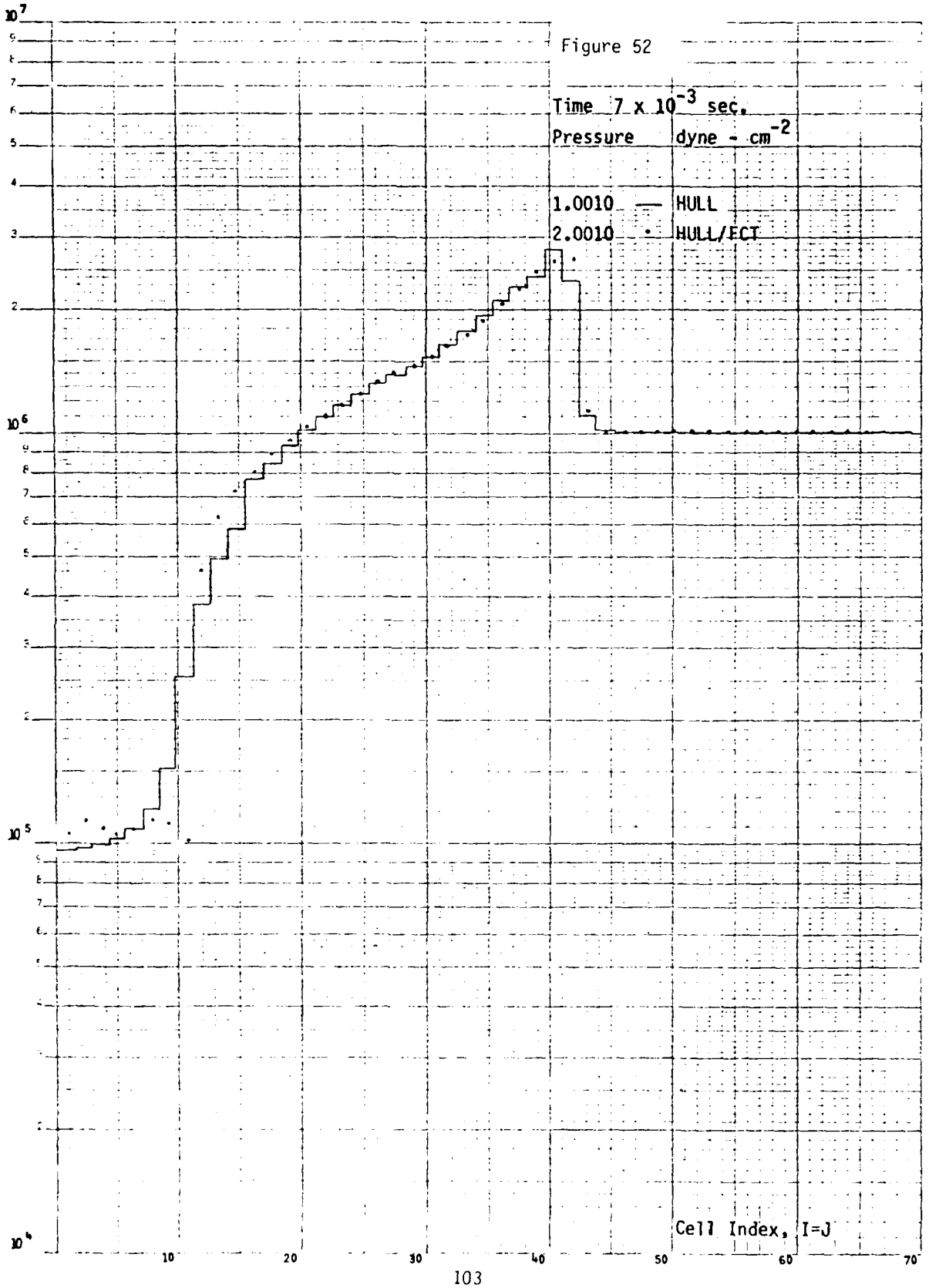
Figure 52
Time 7 x 10^-3 sec.
Pressure dyne - cm^-2
1.0010 — HULL
2.0010 · HULL/ECT
10^7
10^6
10^5
10^4
10
20
30
40
50
60
70
Cell Index, I=J

Figure 53

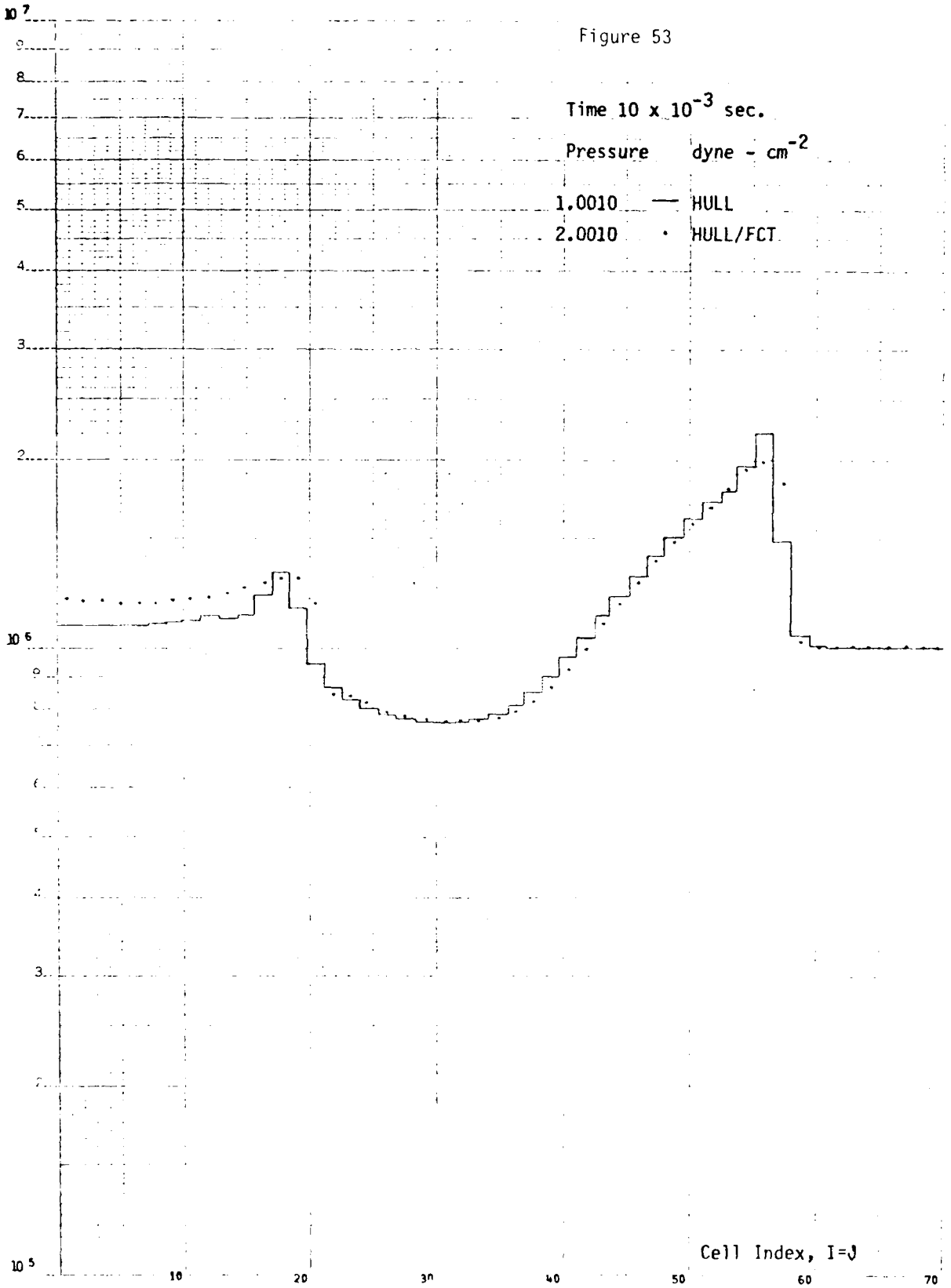
Time 10 x 10^{-3} sec.
Pressure dyne - cm^{-2}
1.0010 — HULL
2.0010 · HULL/FCT
10^7
8
7
6
5
4
3
2
10^6
3
10^5
10
20
30
40
50
60
70
Cell Index, I=J

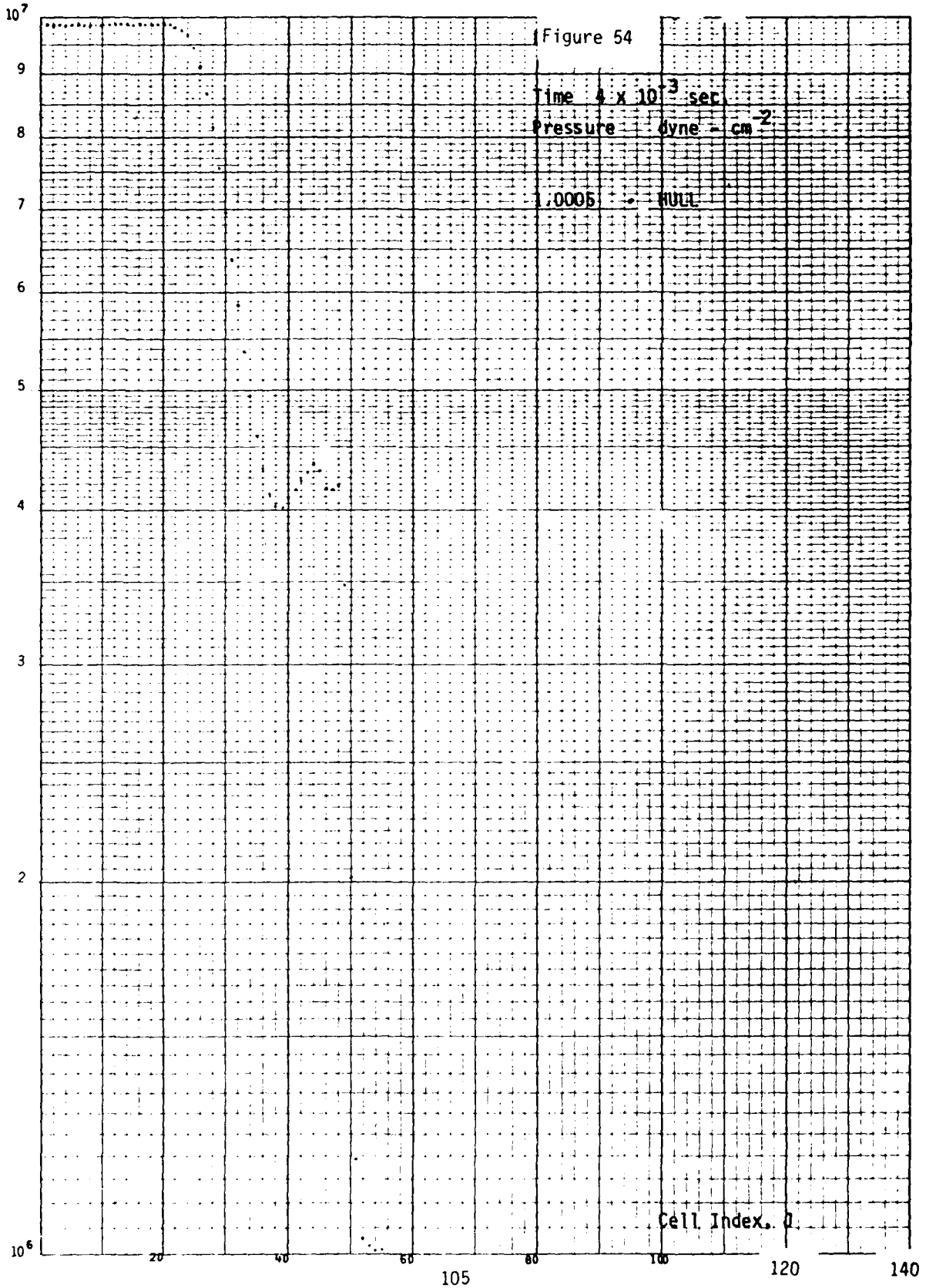
Figure 54
Time 4 x 10^-3 sec
Pressure - dyne - cm^-2
1.0005 - HULL
Cell Index. J.
10^7
9
8
7
6
5
4
3
2
10^6
20
40
60
80
100
120
140

Figure 55

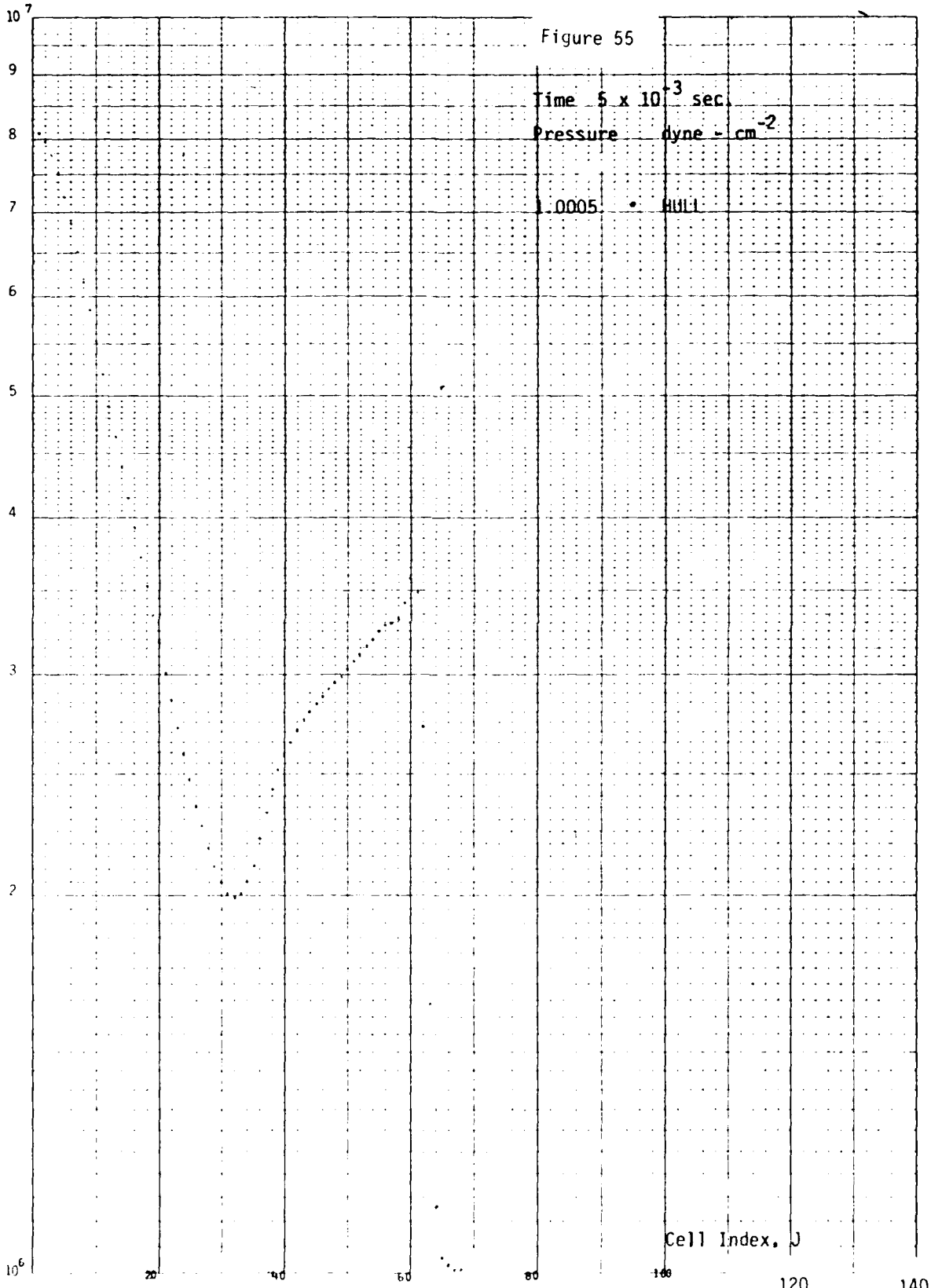
Time 5 x 10^-3 sec.
Pressure dyne - cm^-2
1.0005 • HULL
10^7
9
8
7
6
5
4
3
2
10^6
20
40
60
80
100
120
140
Cell Index, J

Figure 56

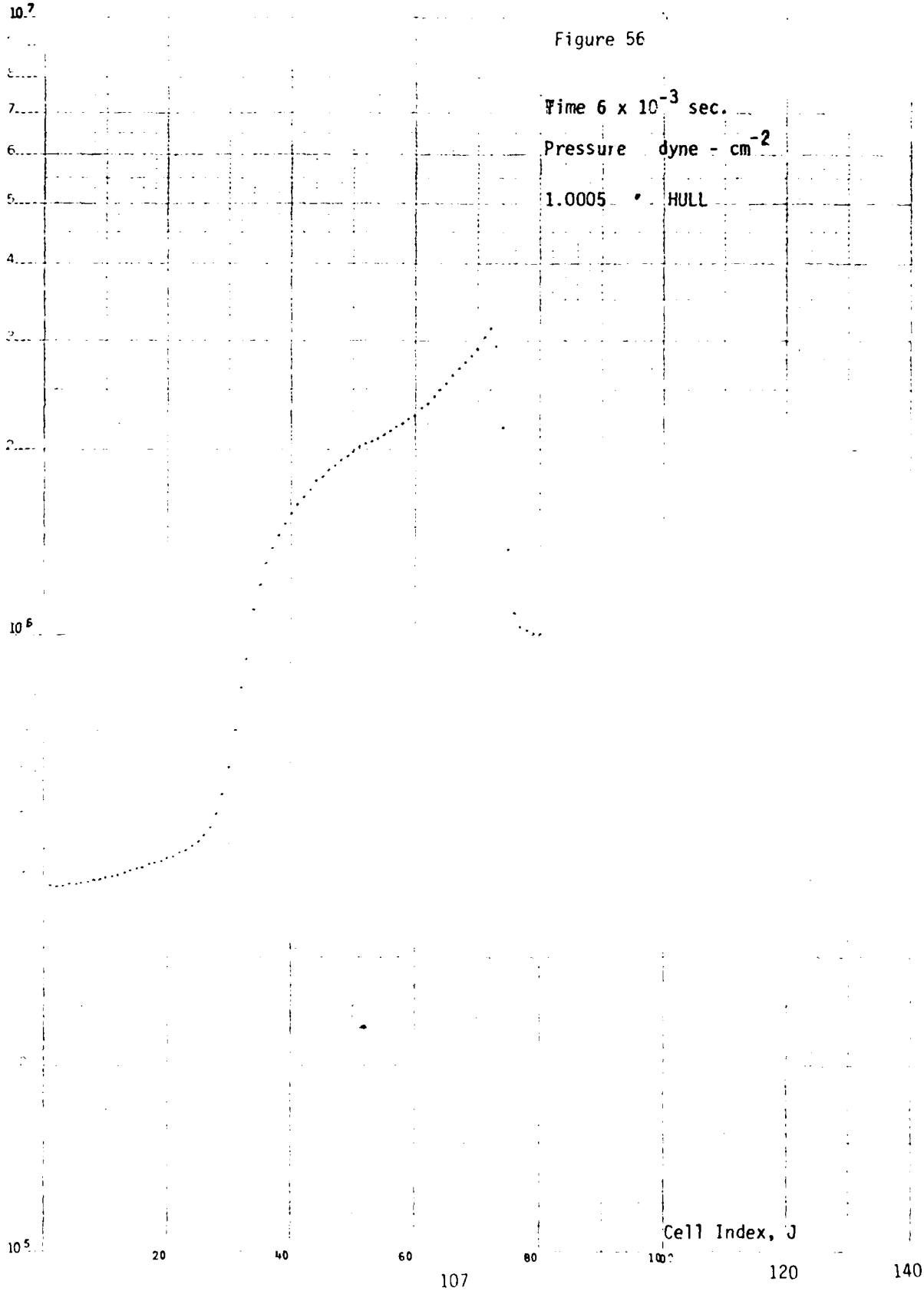
Time 6 x 10^-3 sec.
Pressure dyne - cm^-2
1.0005 • HULL
10^7
7
6
5
4
10^6
10^5
20
40
60
80
100
120
140
Cell Index, J

Figure 57

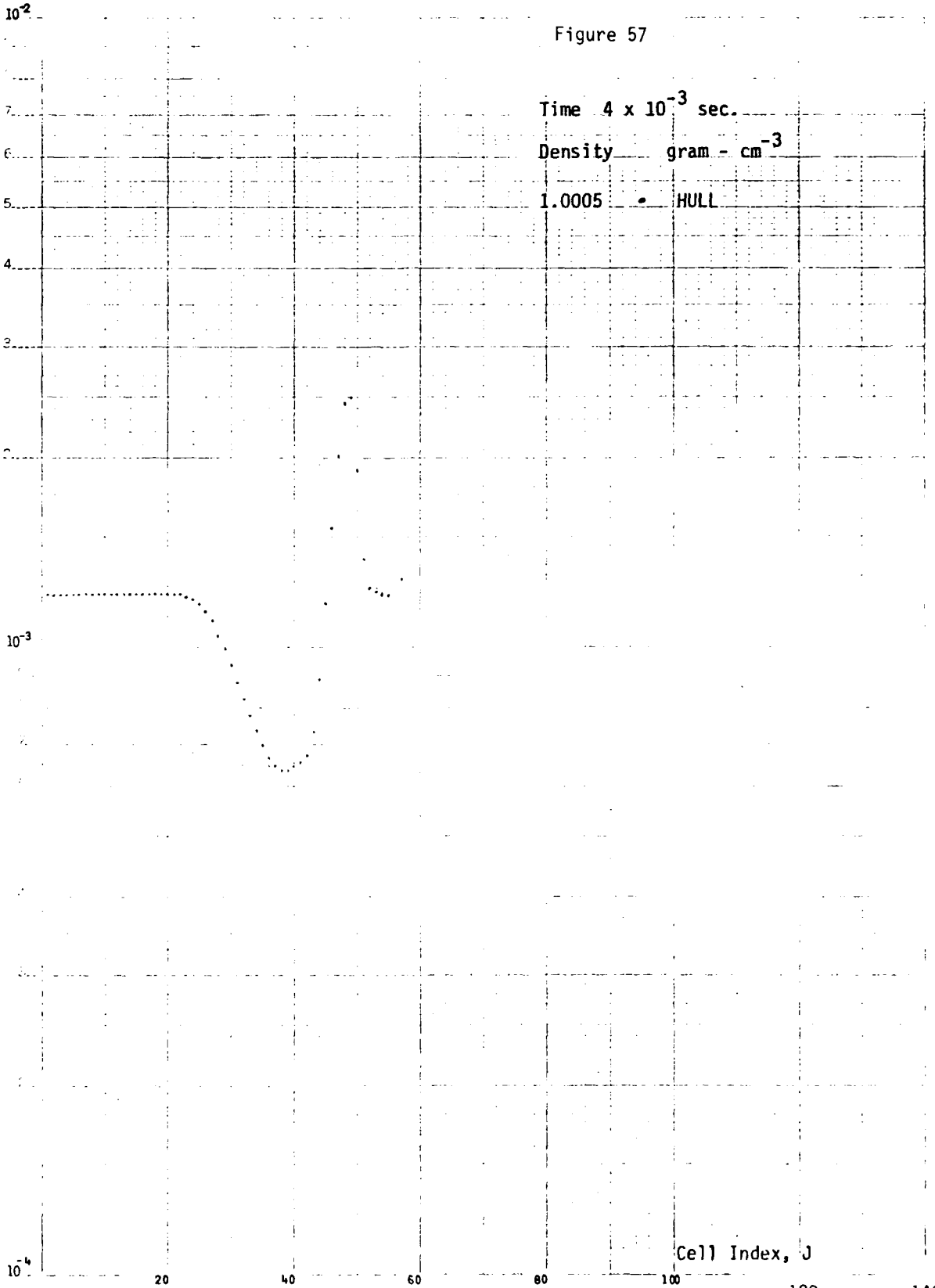
Time 4 x 10^-3 sec.
Density gram - cm^-3
1.0005 • HULL
10^-2
7
6
5
4
3
2
10^-3
10^-4
20
40
60
80
100
120
140
Cell Index, J

Figure 58

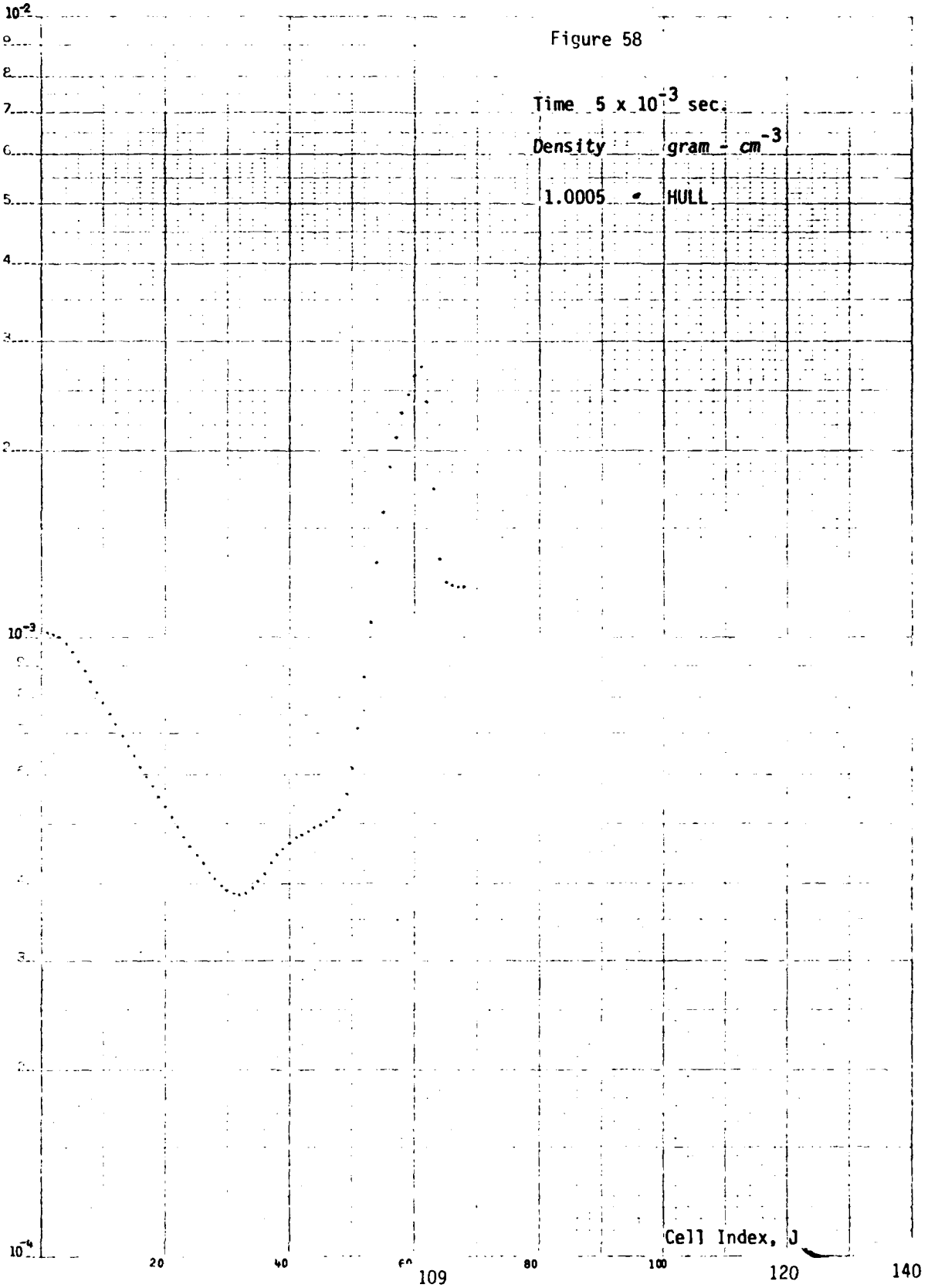
Time 5 x 10^-3 sec.
Density gram - cm^-3
1.0005 • HULL
10^-2
10^-3
10^-4
20
40
60
80
100
120
140
Cell Index, J

Figure 59

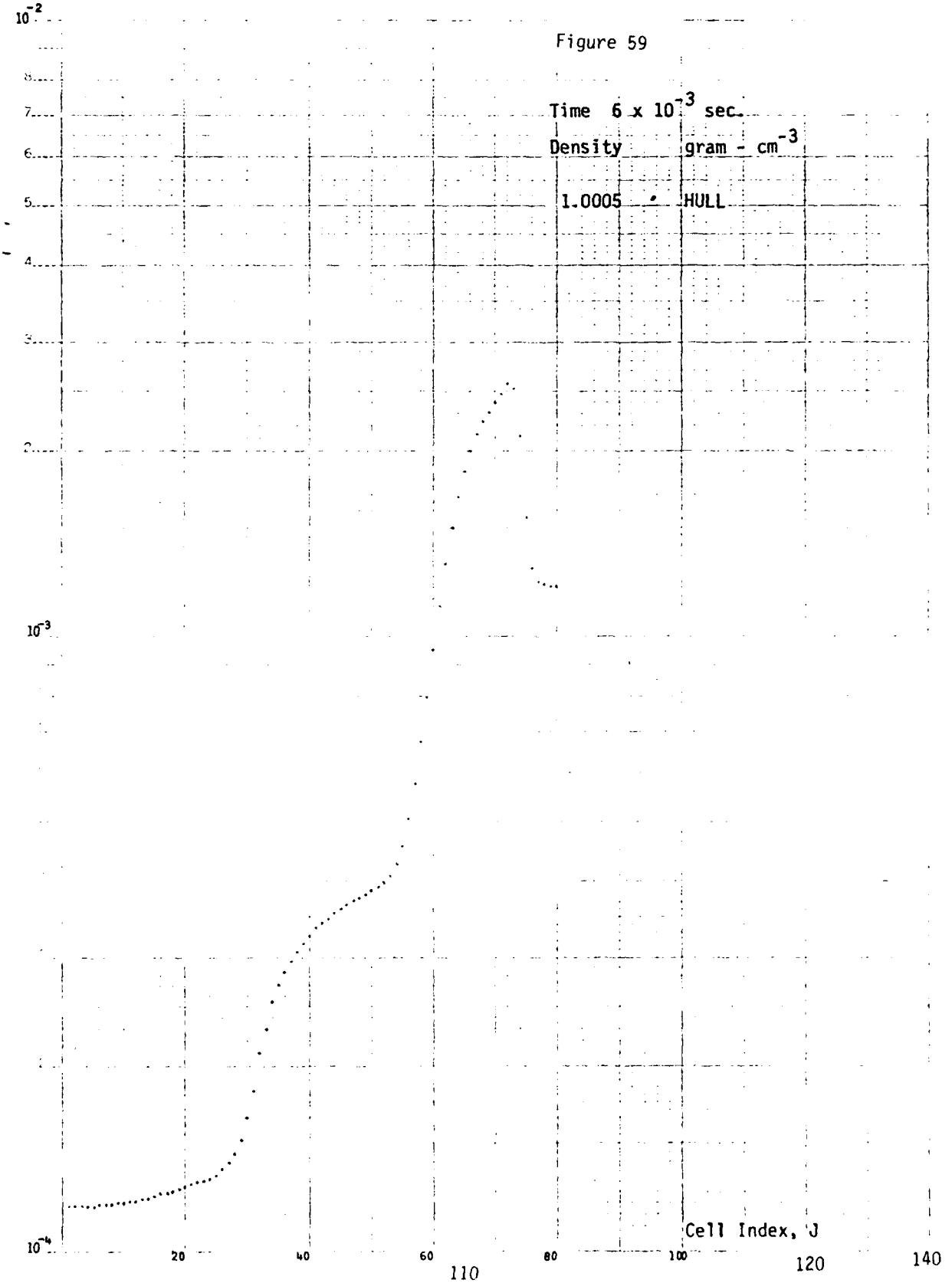
Time 6 x 10^-3 sec.
Density gram - cm^-3
1.0005 • HULL
10^-2
8
7
6
5
4
3
2
10^-3
10^-4
20
40
60
80
100
120
140
Cell Index, J

APPENDIX C

HULL 1-D RESULTS

This appendix presents the overpressure histories for three observers 1, 5, and 6 as defined in Section 5. All runs shown here were with artificial viscosity. Two sets have been included, the first set (Figures 59 through 67) are for the low overpressure and the second (Figures 68 through 76) are for the high overpressure. Figure 21 in Section 5 shows the zoning for each run. Individuals that desire the waveforms for the other observers can request same from any of the authors.

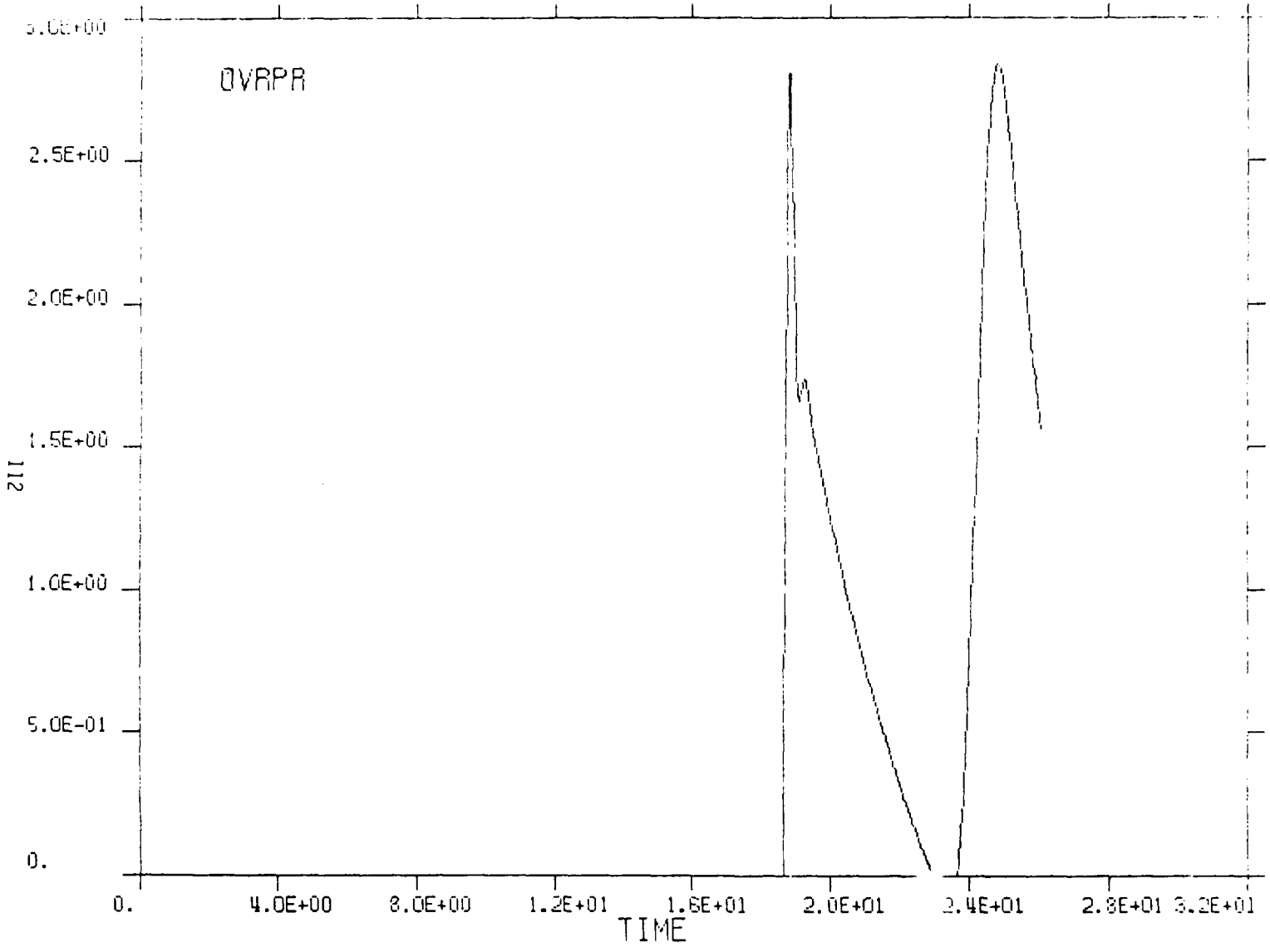

Figure 60. Overpressure run 153 observer 1.

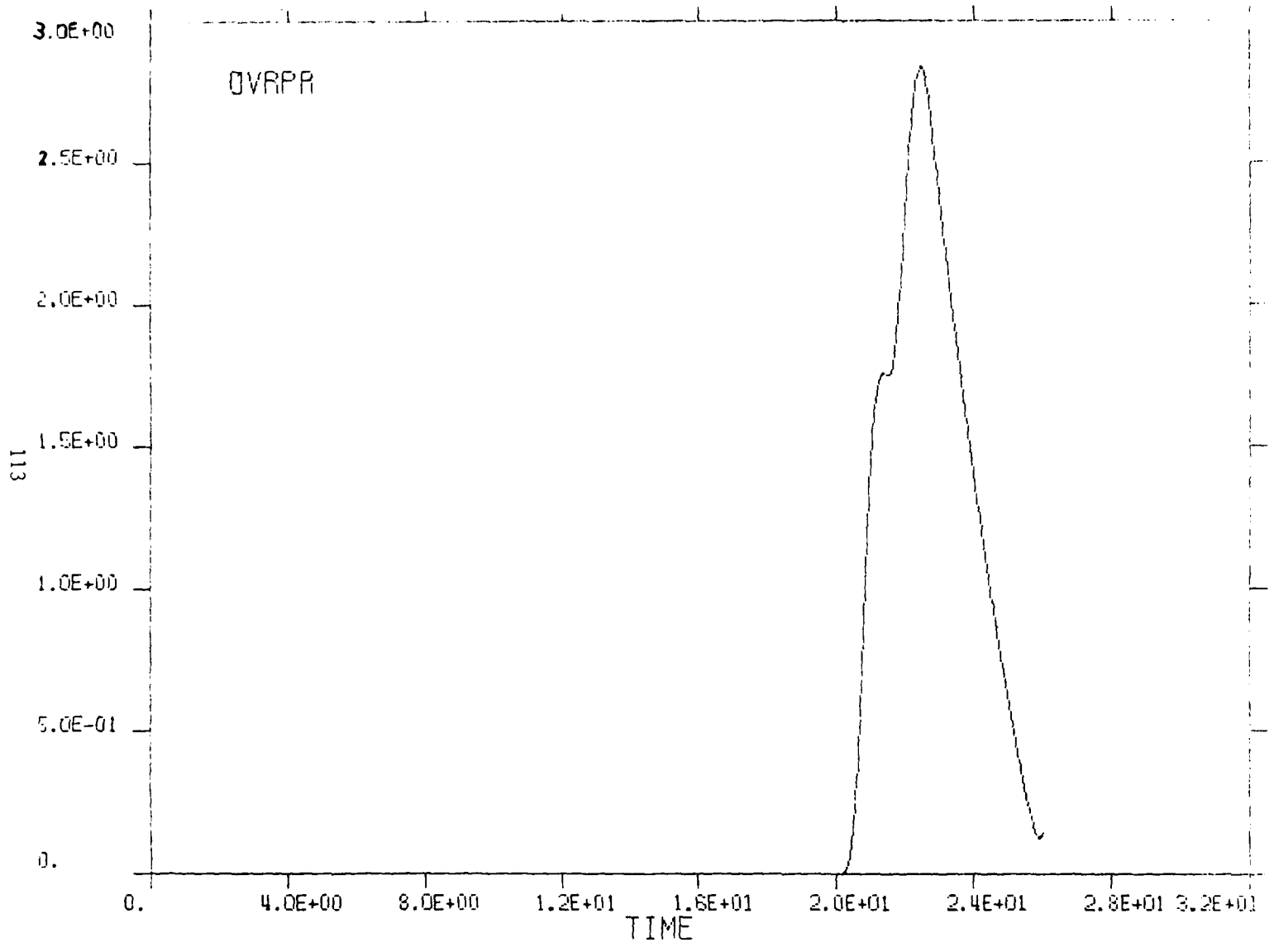

Figure 61. Overpressure run 153 observer 5.

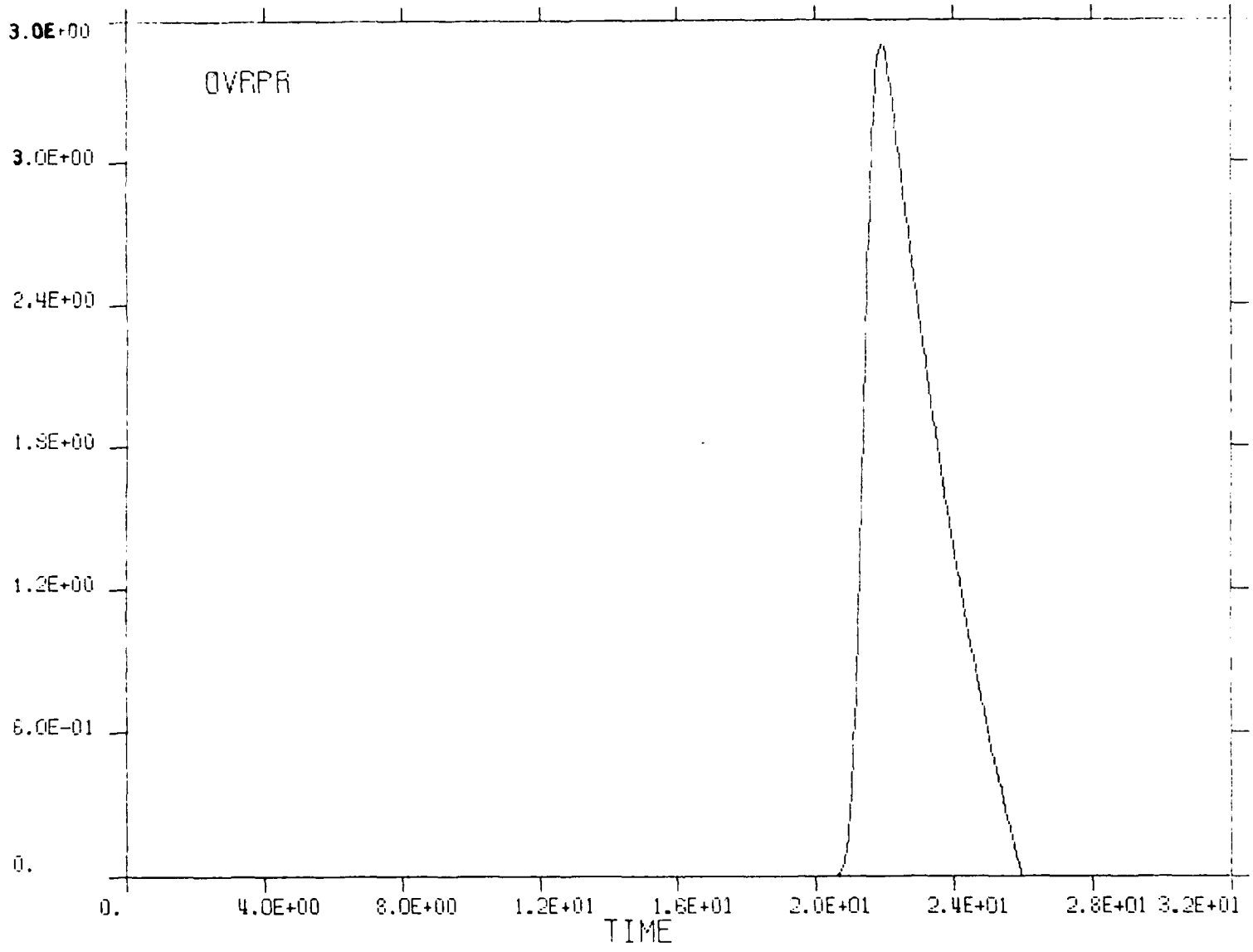

Figure 62. Overpressure run 153 observer number 6.

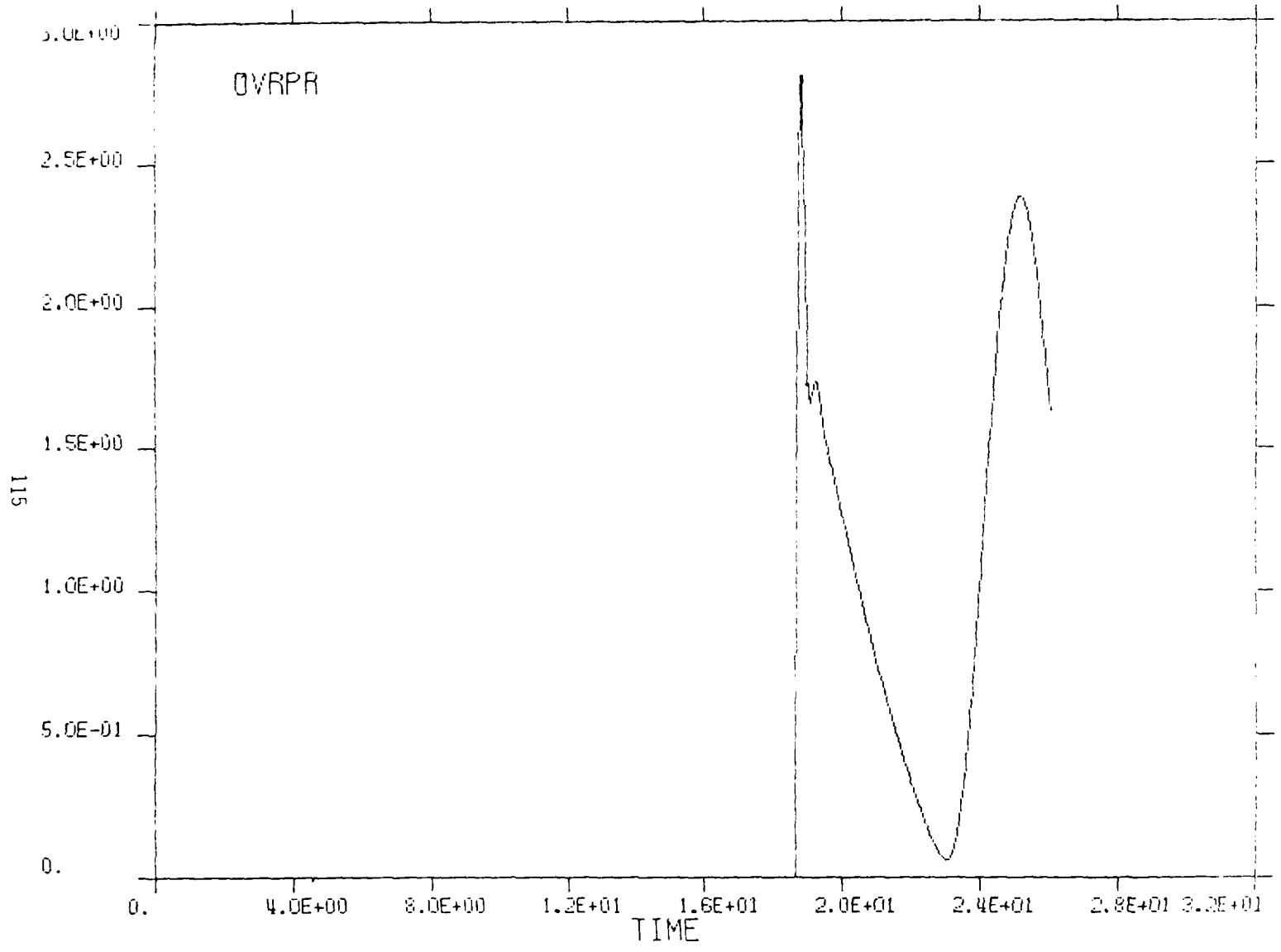

Figure 63. Overpressure run 133 observer number 1.

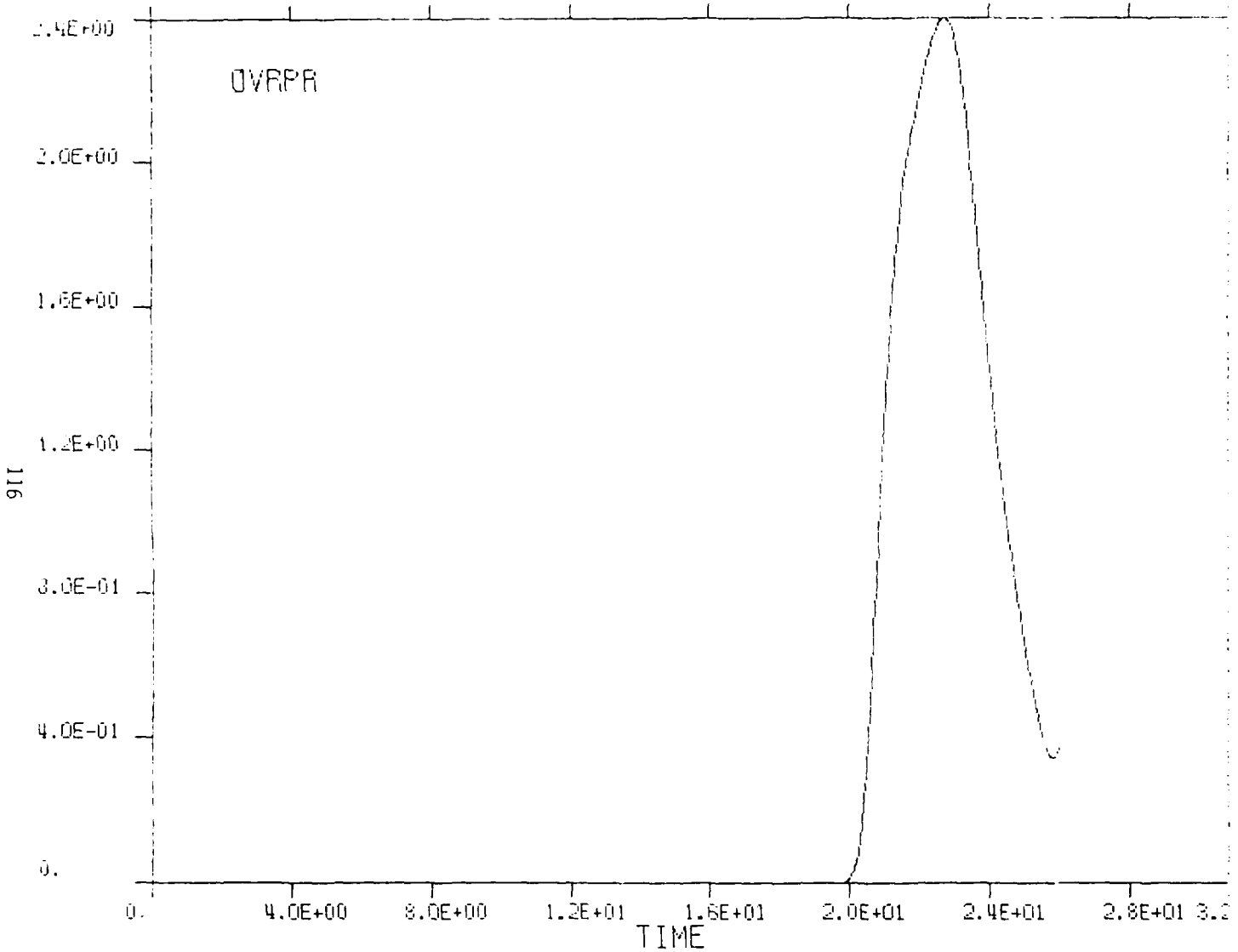

Figure 64. Overpressure run number 133 observer number 5.

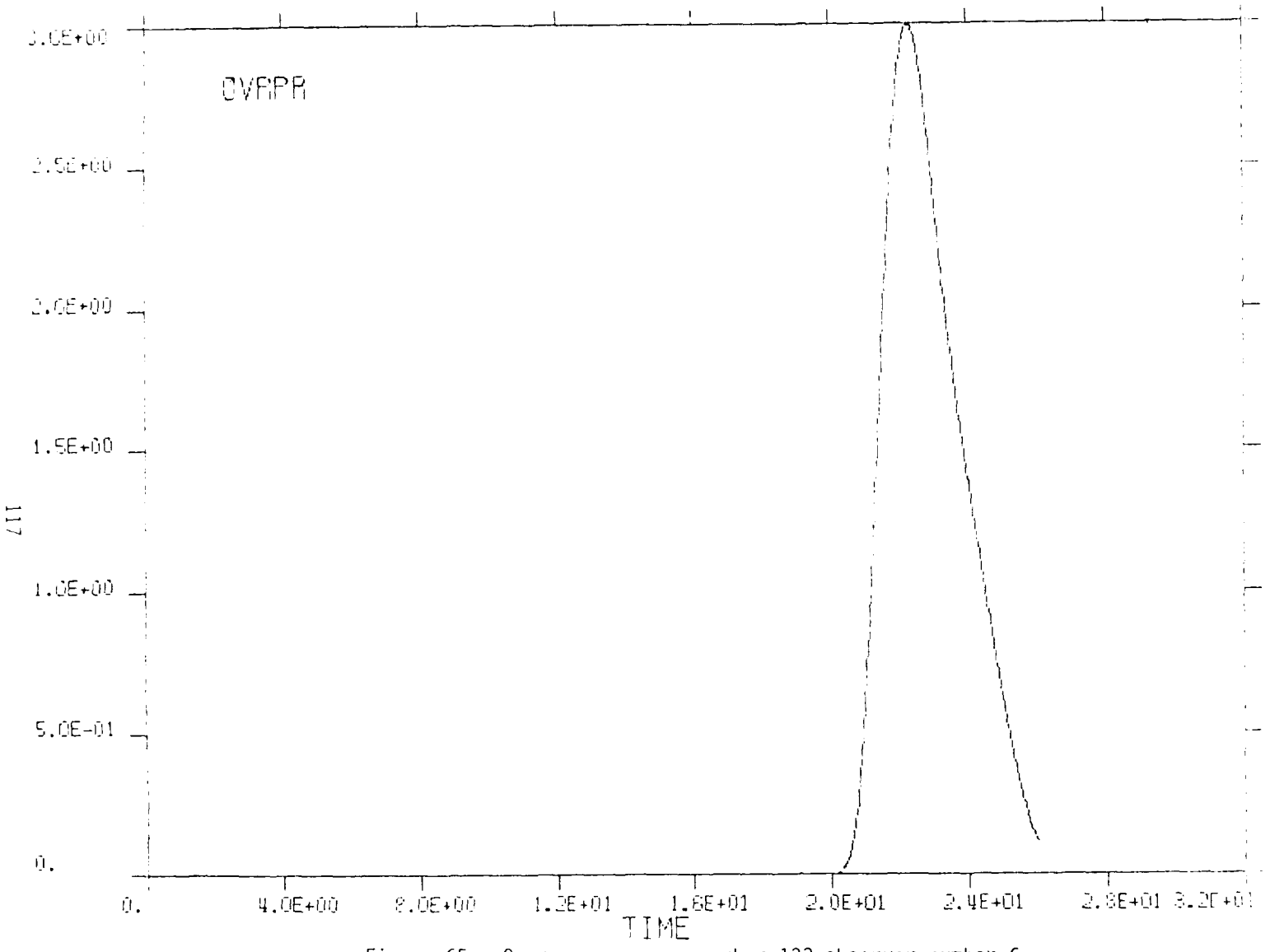

Figure 65. Overpressure run number 133 observer number 6.

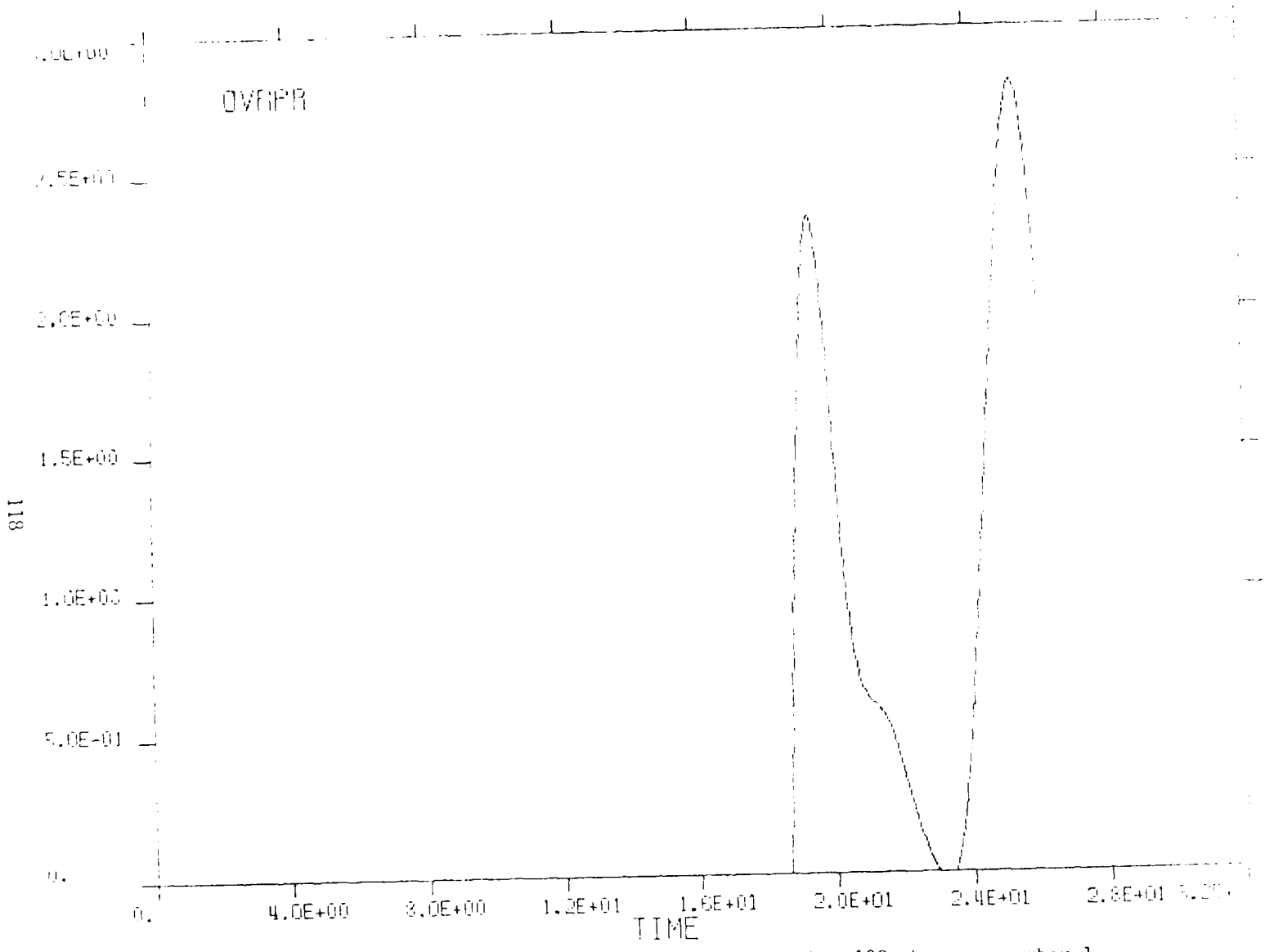

Figure 66. Overpressure run number 138 observer number 1.

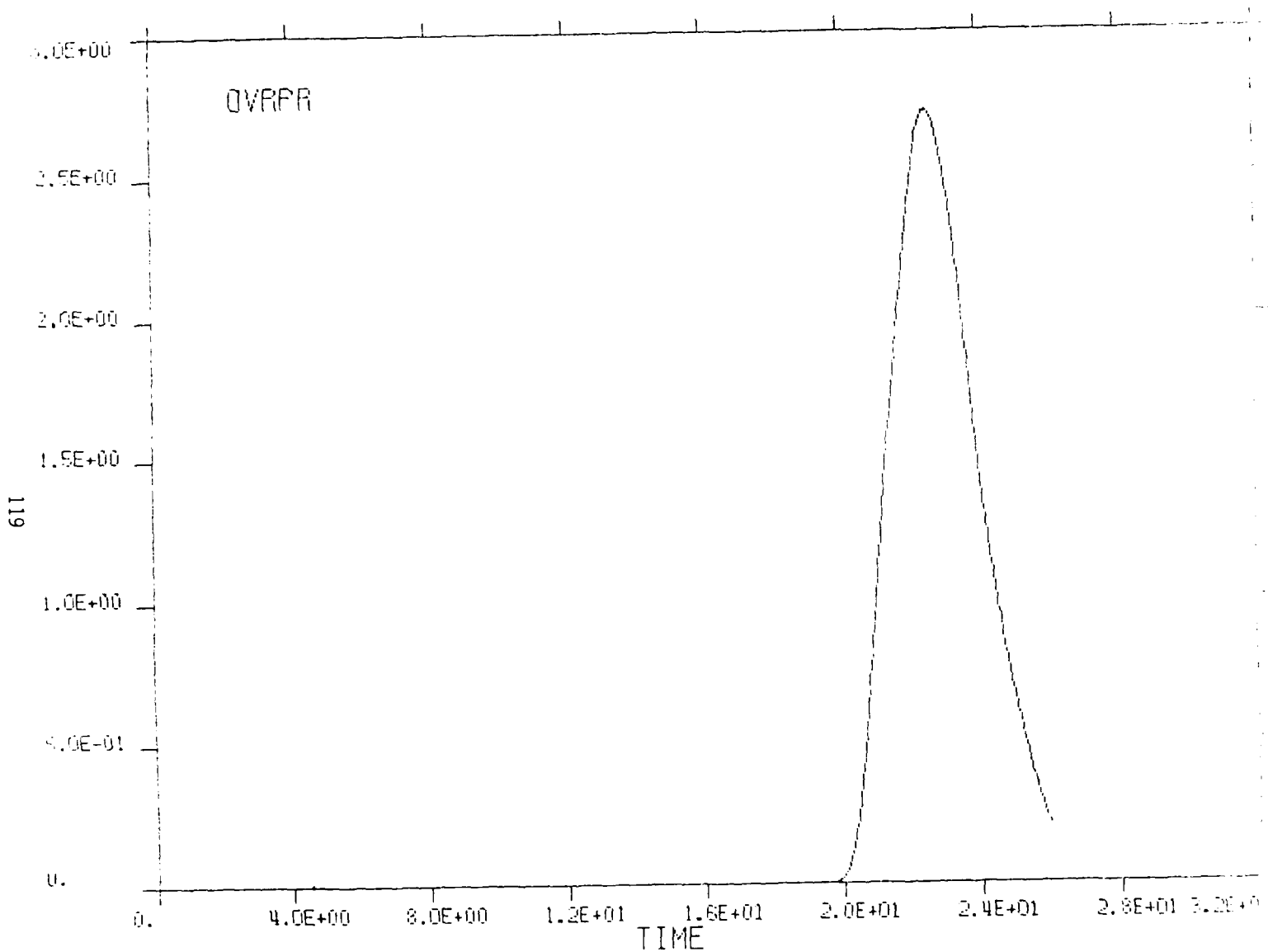

Figure 67. Overpressure run number 138 observer number 5.

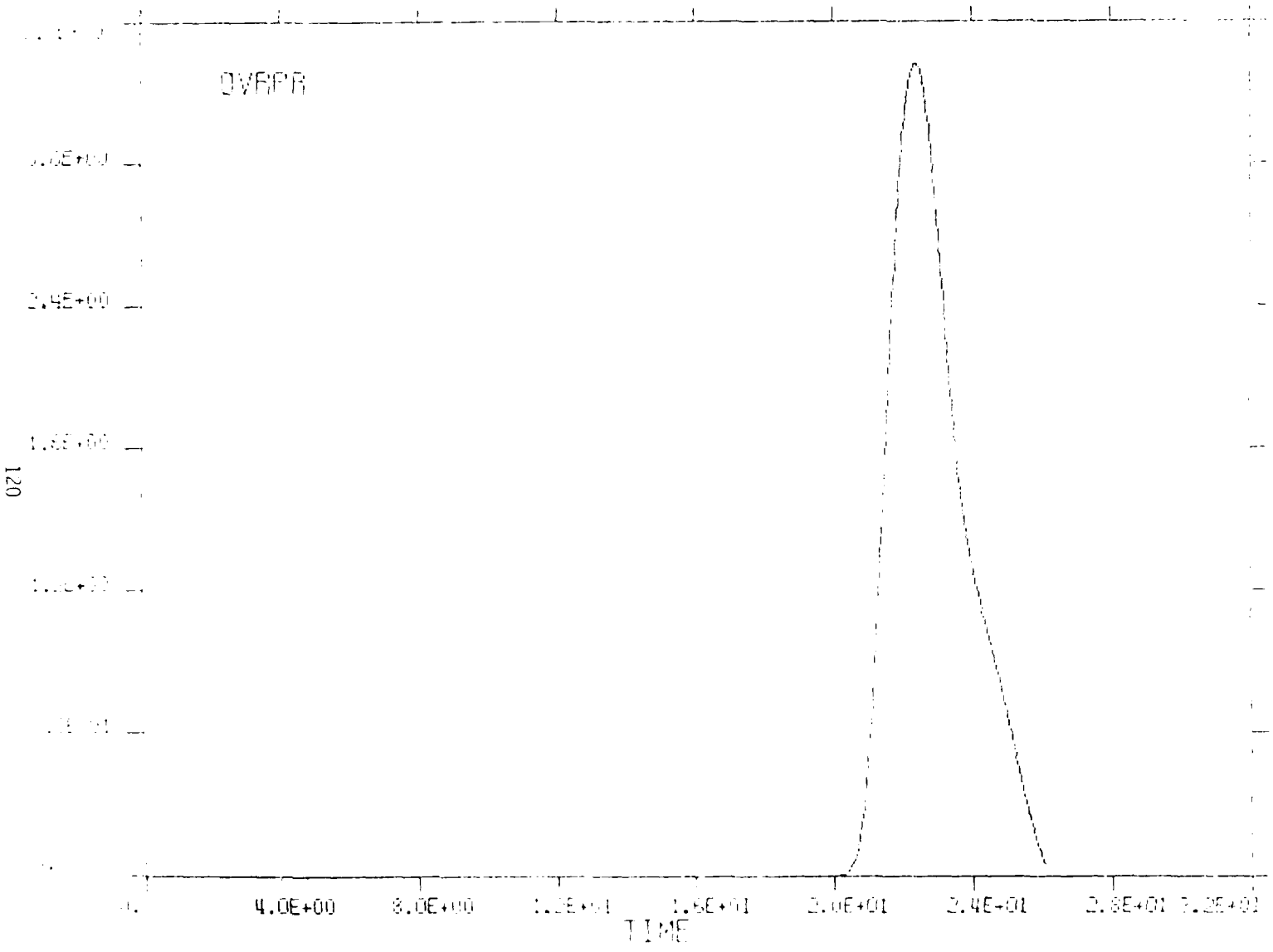

Figure 68. Overpressure run number 138 observer number 6.

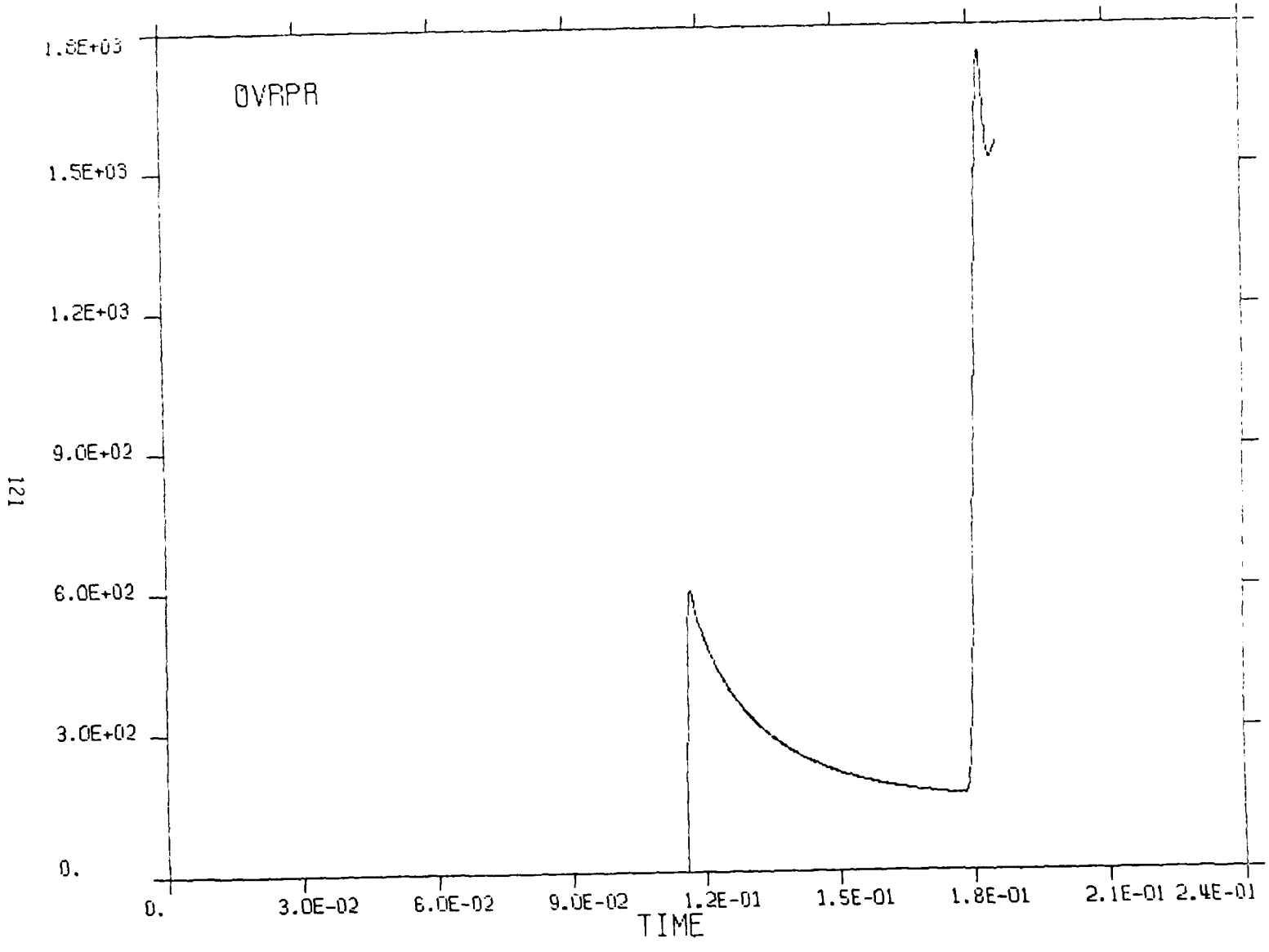

Figure 69. Overpressure run number 151 observer number 1

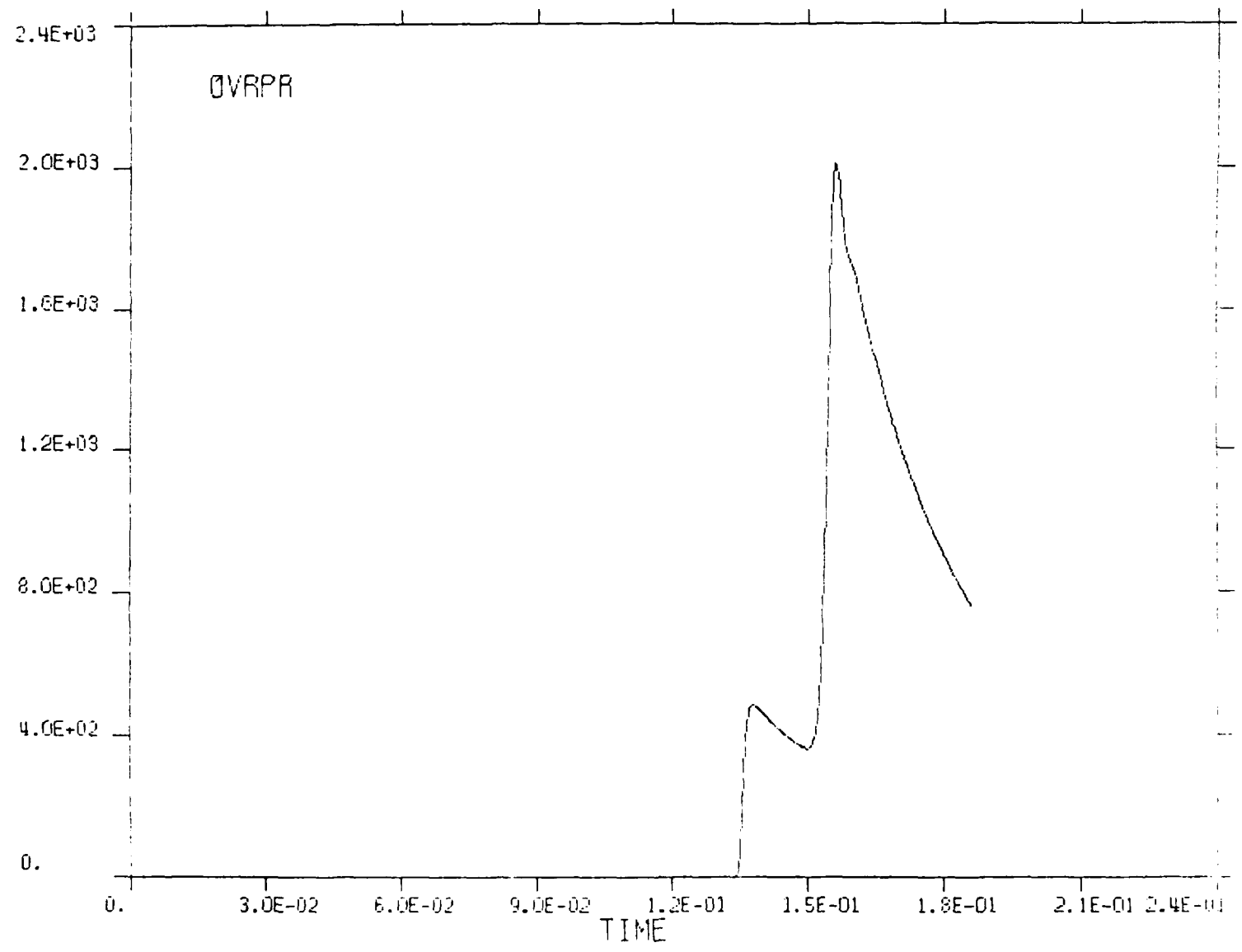

Figure 70. Overpressure run number 151 observer number 5

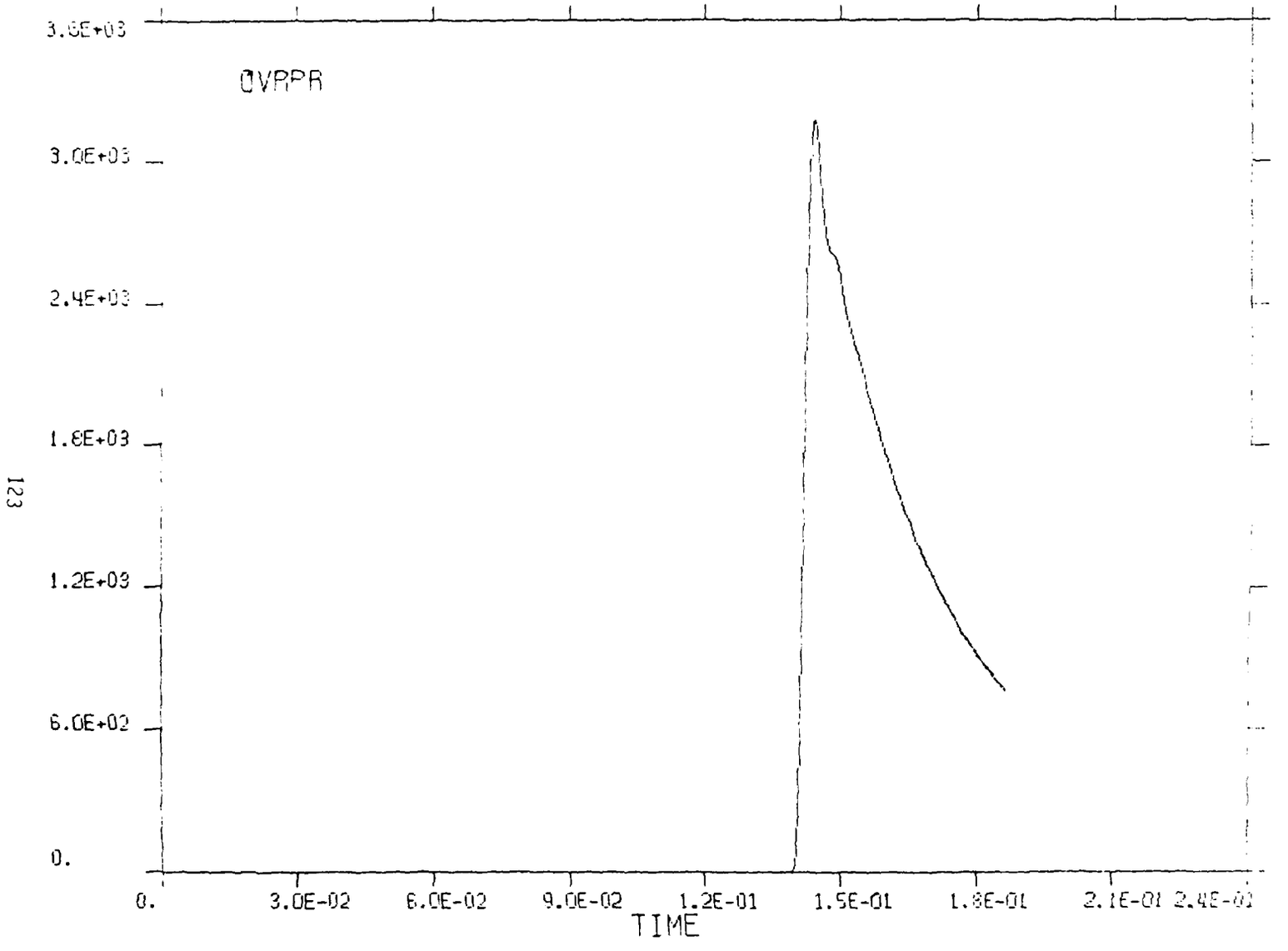

Figure 71. Overpressure run number 151 observer number 6.

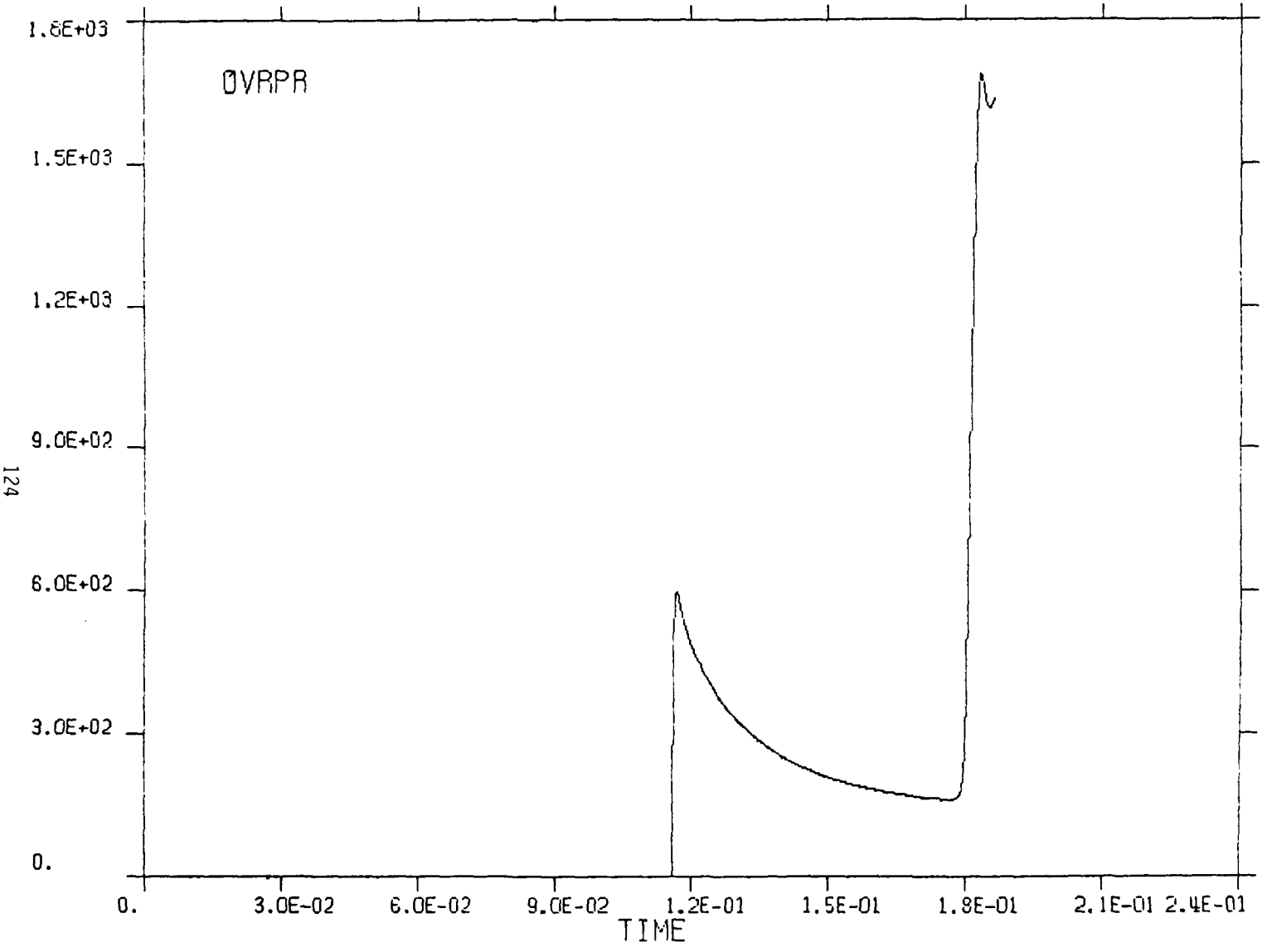

Figure 72. Overpressure run number 131 observer number 1

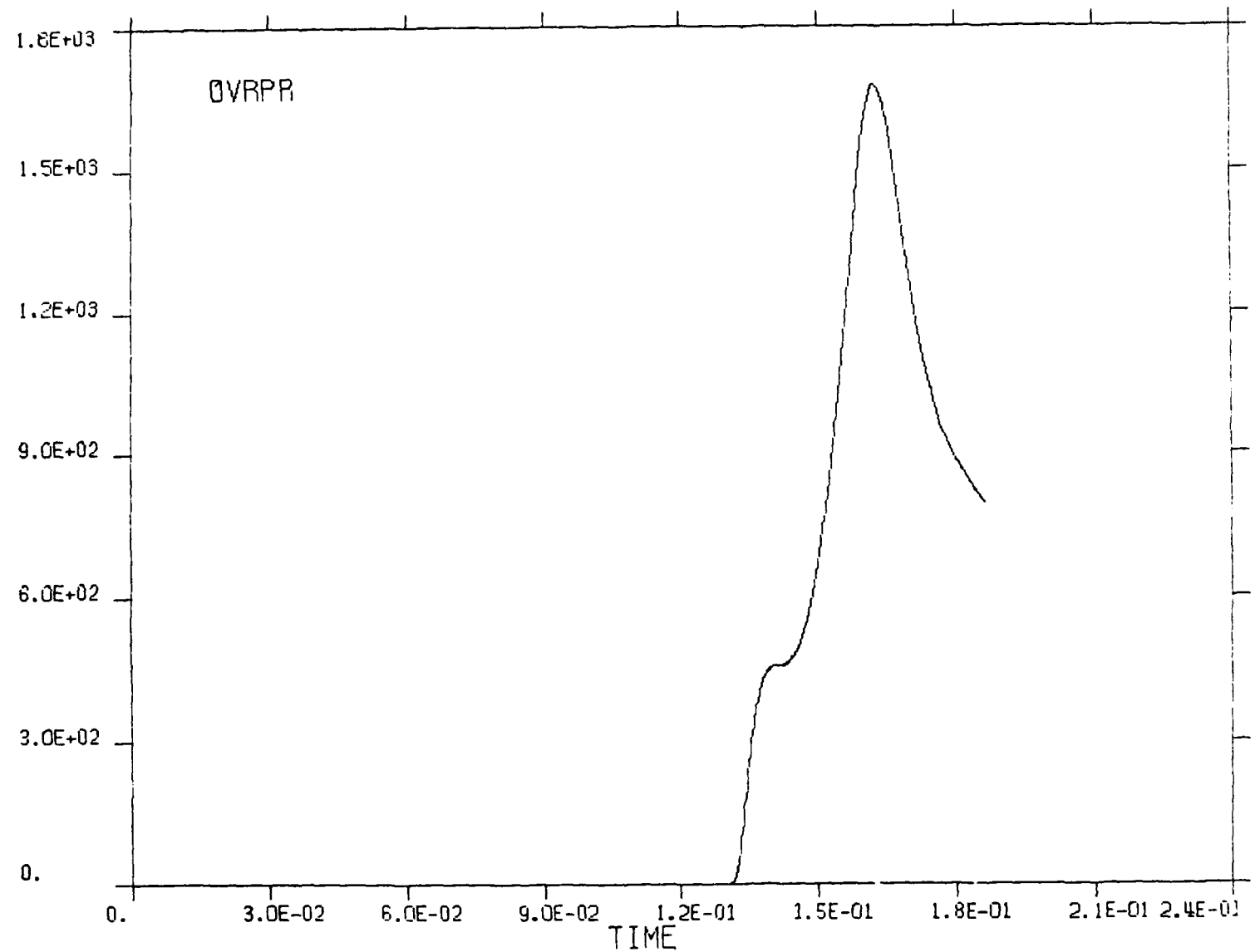

Figure 73. Overpressure run number 131 observer number 5

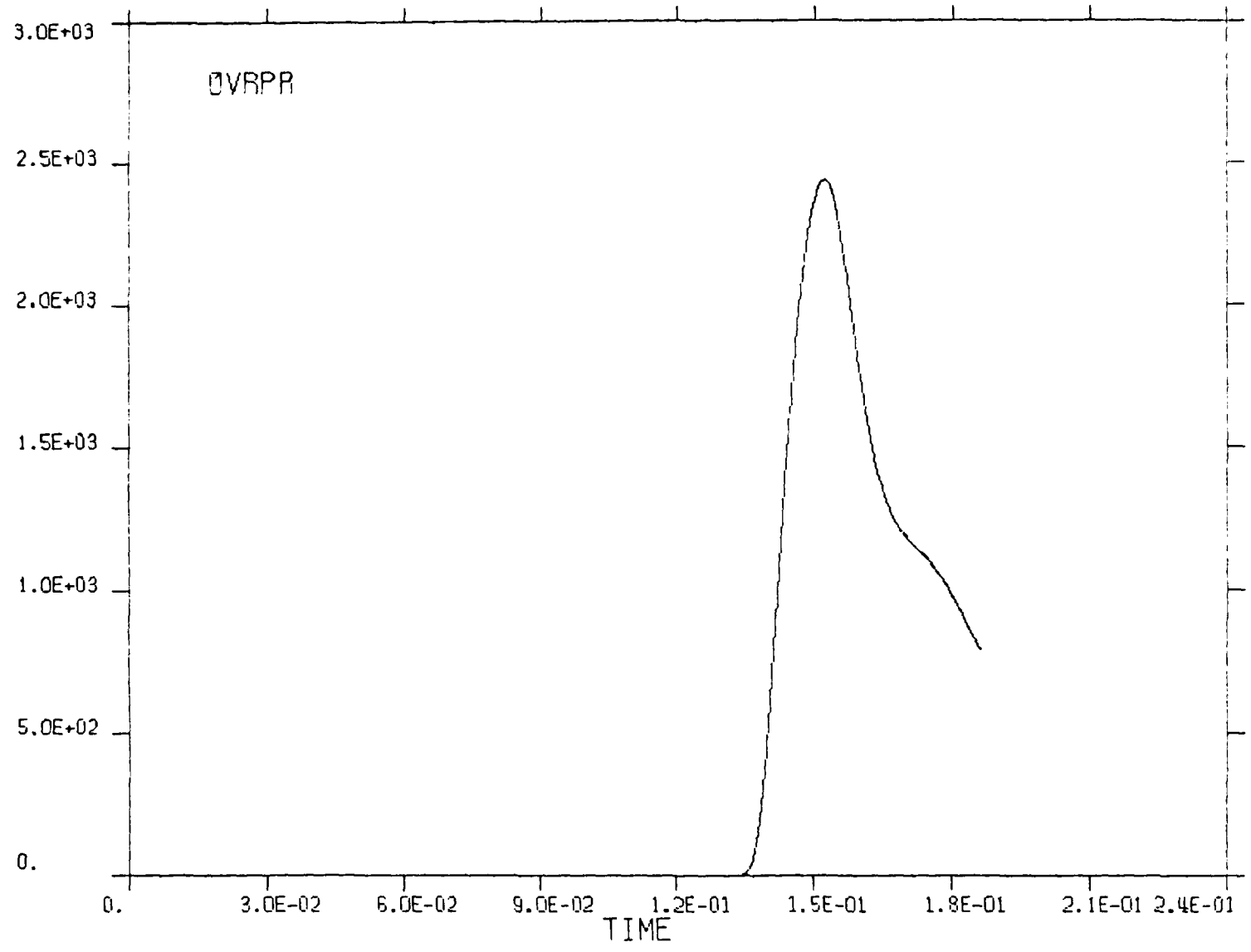

Figure 74. Overpressure run number 131 observer number 6.

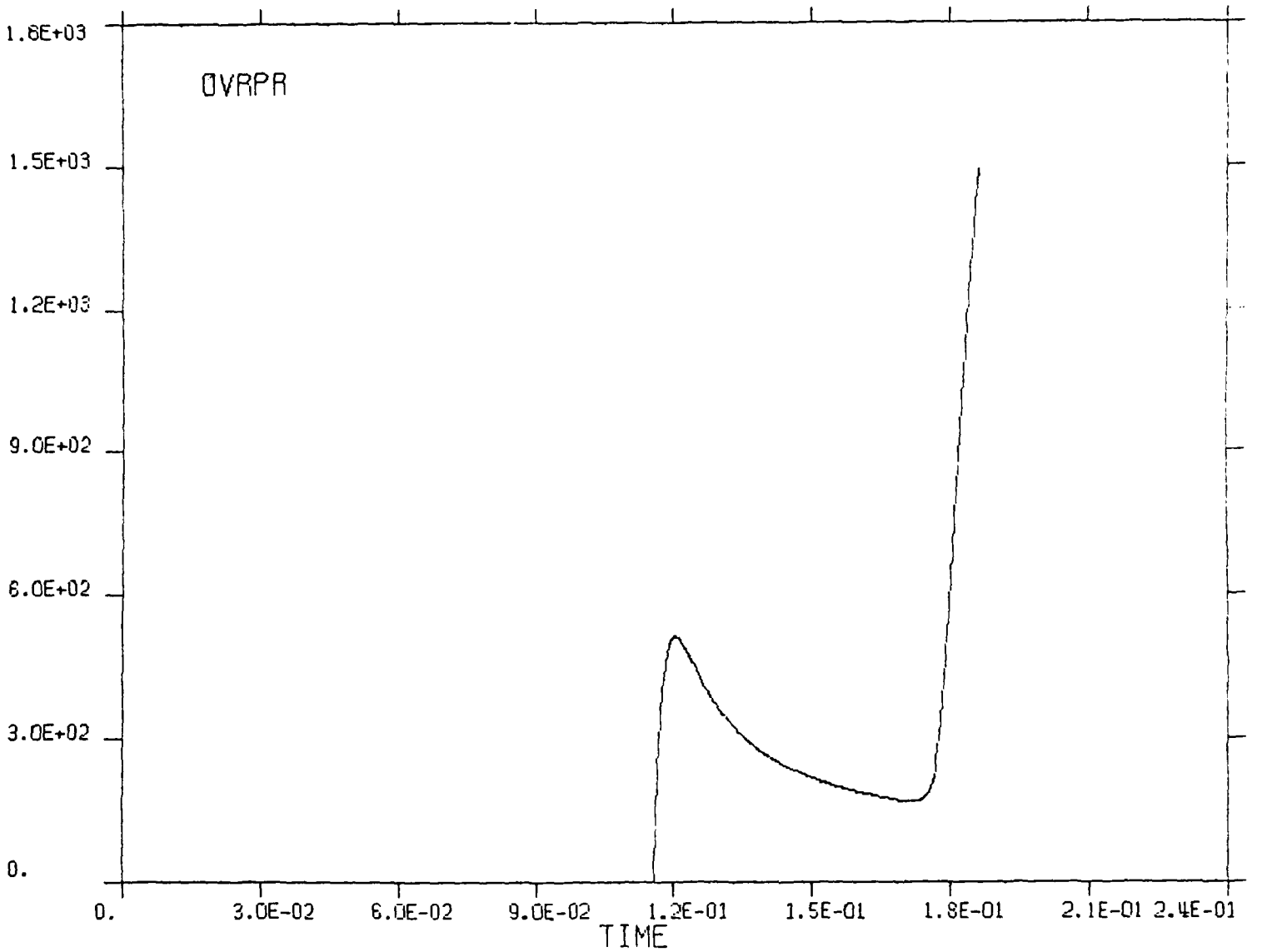

Figure 75. Overpressure run number 136 observer number 1

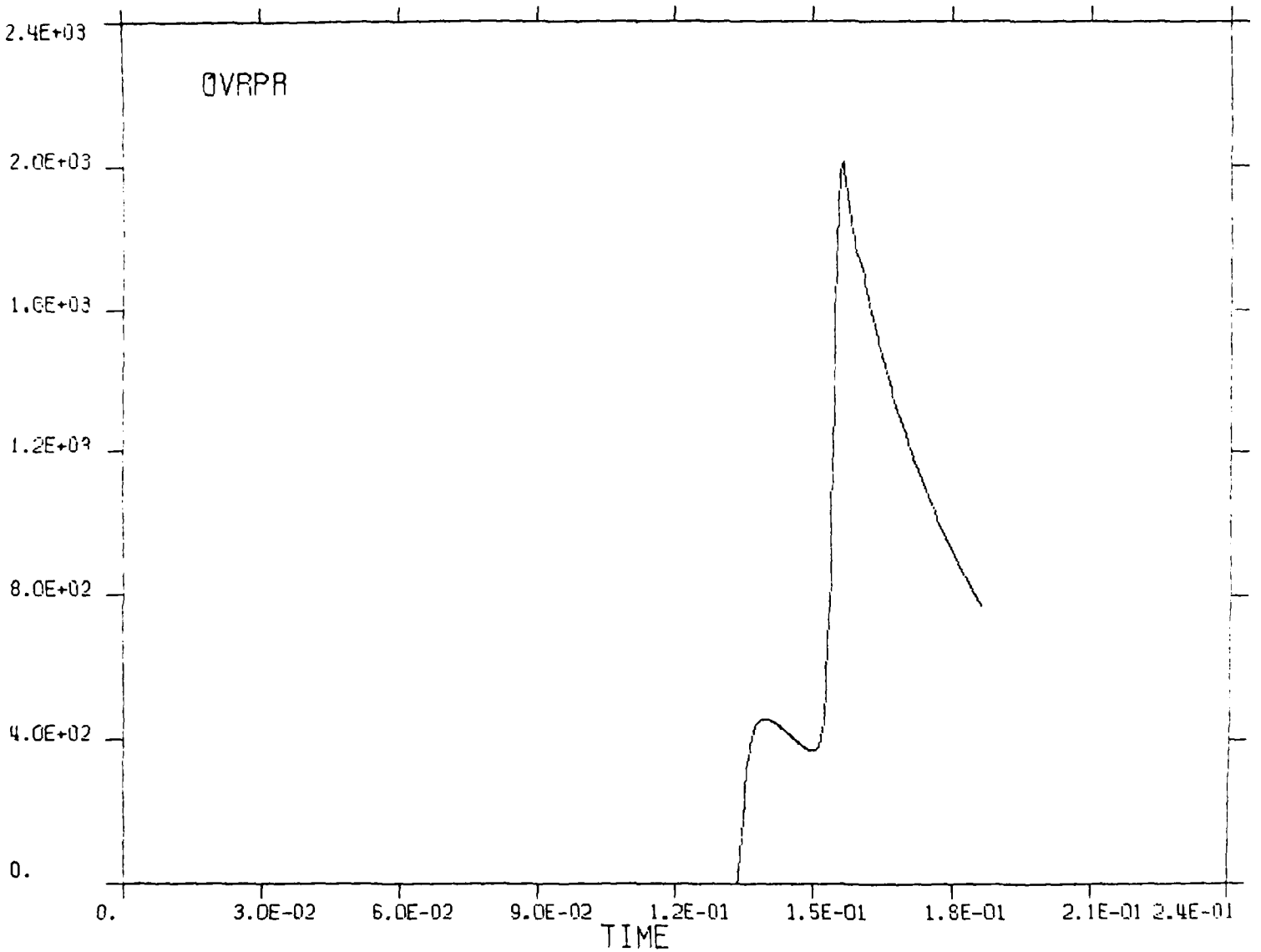

Figure 76. Overpressure run number 136 observer number 5

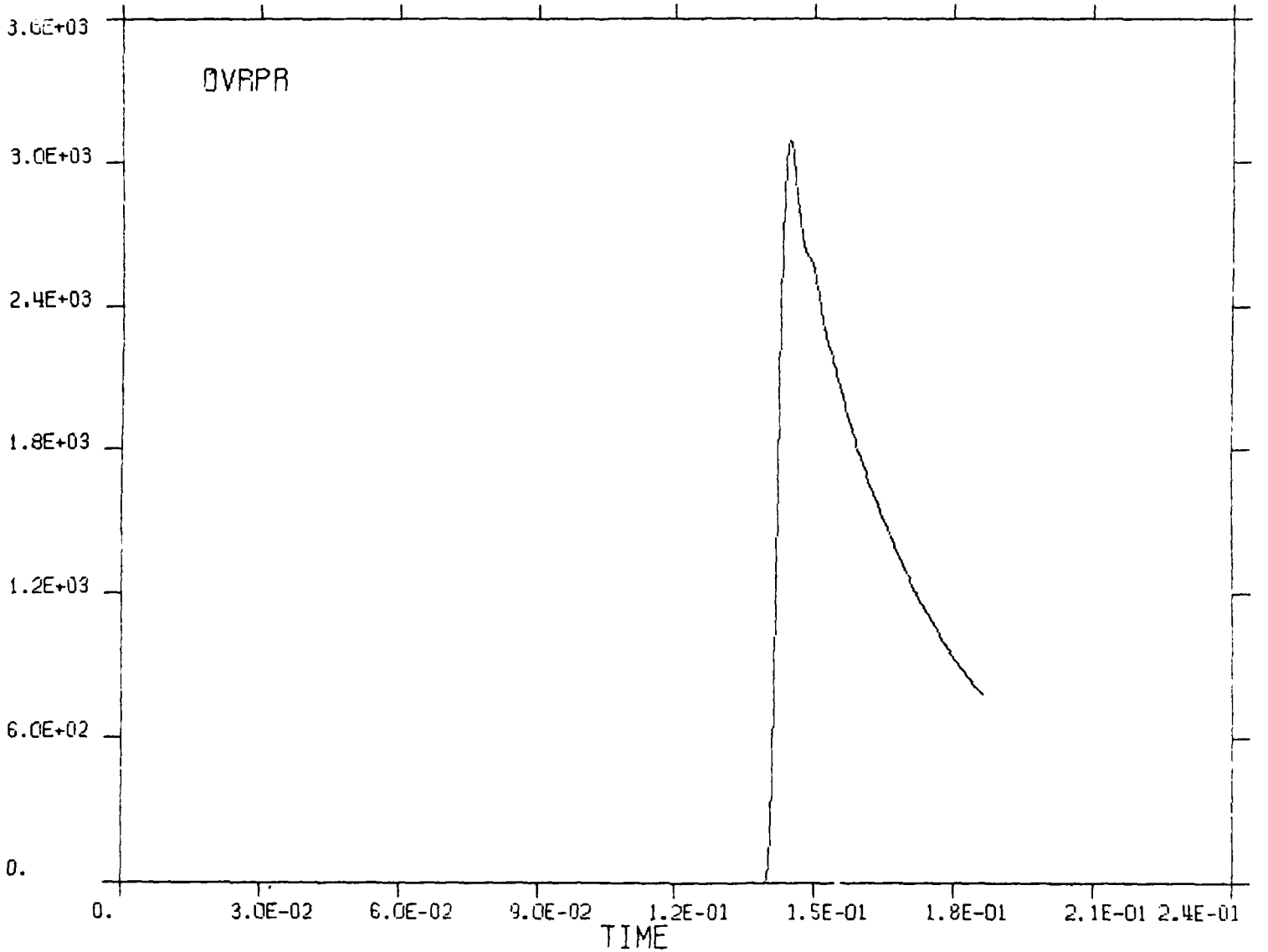

Figure 77. Overpressure run number 136 observer number 6.

DISTRIBUTION LIST

DEPARTMENT OF DEFENSE

Defense Communications Agency
ATTN: CCTC

Defense Nuclear Agency
ATTN: SPSS
ATTN: RAAE
3 cy ATTN: SPAS
4 cy ATTN: TITL

Defense Technical Information Center
Cameron Station
12 cy ATTN: DD

Joint Strat Tgt Planning Staff
ATTN: JLTW-2
ATTN: JLA
ATTN: JPST, G. Burton
ATTN: JPST
ATTN: JPTM

DEPARTMENT OF THE ARMY

BMD Advanced Technology Center
Department of the Army
ATTN: ATC-T, M. Capps

BMD Systems Command
Department of the Army
ATTN: BMDSC, R. Dekalb

DEPARTMENT OF THE NAVY

Naval Surface Weapons Center
White Oak Laboratory
ATTN: Code K06, C. Lyons

Office of Naval Research
ATTN: Code 465

Office of the Chief of Naval Operations
ATTN: OP 654E14, R. Blaise

Strategic Systems Project Office
Department of the Navy
ATTN: NSP-2722, F. Wimberly

DEPARTMENT OF THE AIR FORCE

Aeronautical Systems Division
Air Force Systems Command
2 cy ATTN: ASD/ENFTV, D. Ward

Air Force Flight Dynamics Laboratory
ATTN: FXG
ATTN: FBAC, D. Roselius

Air Force Weapons Laboratory
Air Force Systems Command
ATTN: NTES, K. Filippelli
ATTN: NTYV, A. Sharp
ATTN: DYV
ATTN: SUL
ATTN: HO, W. Minge
ATTN: DYV, E. Copus
2 cy ATTN: NTO

DEPARTMENT OF THE AIR FORCE (Continued)

Ballistic Missile Office
Air Force Systems Command
2 cy ATTN: MNRTE
3 cy ATTN: MNNX, J. Allen

Foreign Technology Division
Air Force Systems Command
ATTN: SDBG
ATTN: TQTD
ATTN: SDBS, J. Pumphrey

Strategic Air Command
Department of the Air Force
ATTN: XQBM
ATTN: DOXT
ATTN: XPFS
ATTN: XPQM

DEPARTMENT OF ENERGY CONTRACTORS

Lawrence Livermore National Lab
ATTN: L-125, J. Keller
ATTN: L-262, J. Knox
ATTN: L-24, G. Staihle
ATTN: L-92, C. Taylor

Los Alamos National Scientific Lab
ATTN: R. Thirston
ATTN: J. Taylor
ATTN: D. Kerr
ATTN: J. McQueen
ATTN: R. Dingus
ATTN: MS 670, J. Hopkins

DEPARTMENT OF DEFENSE CONTRACTORS

Acurex Corp
ATTN: R. Rindal
ATTN: C. Nardo
ATTN: C. Powars

California Research & Technology, Inc
ATTN: M. Rosenblatt
ATTN: K. Kreyenhagen

Harold Rosenbaum Associates, Inc
ATTN: G. Weber

Kaman Sciences Corp
ATTN: F. Shelton
ATTN: J. Keith
ATTN: J. Harper
ATTN: J. Hoffman
ATTN: D. Sachs

Kaman TEMPO
ATTN: DASIAC
ATTN: B. Gambill

DEPARTMENT OF DEFENSE CONTRACTORS (Continued)

McDonnell Douglas Corp
ATTN: J. Garibotti
ATTN: R. Reck
ATTN: L. Cohen
ATTN: H. Berkowitz
ATTN: D. Dean
ATTN: E. Fitzgerald
ATTN: P. Lewis, Jr
ATTN: G. Johnson
ATTN: H. Hurwicz

Pacific-Sierra Research Corp
ATTN: H. Brode

R & D Associates
ATTN: P. Rausch
ATTN: W. Graham
ATTN: F. Field
ATTN: J. Carpenter
ATTN: P. Haas

Science Applicaitons, Inc
ATTN: W. Plows
ATTN: W. Yengst
ATTN: J. Stoddard
ATTN: C. Lee
ATTN: J. Manship
ATTN: J. Warner

Science Applications, Inc
ATTN: J. Cockayne
ATTN: W. Layson
ATTN: W. Seebaugh
ATTN: B. Chambers
ATTN: J. Hasdal
ATTN: W. Thomas

DEPARTMENT OF DEFENSE CONTRACTORS (Continued)

Science Applicaitons, Inc
ATTN: A. Martellucci

Systems Planning Corp
ATTN: F. Adelman

Systems, Science & Software, Inc
ATTN: G. Gurtman
ATTN: R. Duff

TRW Defense & Space Sys Group
ATTN: R. Plebuch
ATTN: T. Mazzola
ATTN: P. Brandt
ATTN: N. Lipner
ATTN: A. Zimmerman
ATTN: D. Baer
ATTN: M. King
ATTN: A. Ambrosio
ATTN: W. Wood
ATTN: G. Arenguren
ATTN: R. Bacharach
ATTN: T. Williams
ATTN: M. Seizew
2 cy ATTN: I. Alber

TRW Defense & Space Sys Group
ATTN: L. Berger
ATTN: E. Wong
ATTN: E. Allen
ATTN: D. Kennedy
ATTN: D. Glenn
ATTN: W. Polich
ATTN: N. Guiles
ATTN: V. Blankinship
ATTN: P. Dai